Detection and characterization of in-service damage in lattice structures using ultrasonics

Thesis submitted to the University of Nottingham for the degree of
Doctor of Philosophy, Jan 2025

Hasan Tarar
20263603

Supervised by

Ian Maskery
Ian Ashcroft

Signature <u>Hasan Tarar</u>

Date <u>08</u> / <u>January</u> / <u>2025</u>

Declaration

I hereby declare that this thesis and the work presented herein are the results of my own original research, except where explicitly stated otherwise. This thesis has not been submitted in whole or in part for consideration for any other degree or qualification at this or any other institution.

All sources of information, ideas, and contributions from others have been fully acknowledged and referenced.

I take full responsibility for the content of this thesis.

Signature: Hasan Tarar
Date: 08/01/2025

Abstract

This thesis investigates the detection, quantification, and localization of in-service damage in additively manufactured lattice structures using ultrasonic techniques. Lattice structures, characterized by their lightweight design and superior strength-to-weight ratio, have gained significant attention across aerospace, automotive, and biomedical industries. However, their intricate geometries and susceptibility to defects during additive manufacturing (AM) and operational use pose critical challenges to ensuring their structural integrity. The research aims to address these challenges by developing a robust methodology for structural health monitoring (SHM) in lattice structures, leveraging advanced ultrasonic testing and machine learning models.

The study focuses on strut-based lattice structures, which are particularly prone to damage such as cracking and breaking of struts, often initiated by inherent manufacturing anomalies like porosity, residual stresses, and delamination. Ultrasonic wave propagation within lattice geometries was analyzed to understand the interaction between high-frequency waves and structural discontinuities. Piezoelectric sensors, known for their precision and sensitivity, were deployed to generate and capture ultrasonic signals, enabling real-time damage detection. The methodology integrates numerical simulations and experimental setups to ensure comprehensive analysis and validation.

Key features were extracted from ultrasonic response signals using advanced signal processing techniques, including principal component analysis (PCA) and energy-based feature extraction. These features served as inputs to a machine learning neural network model, trained to classify the health states of the structures. The results demonstrated the ability of the proposed approach to accurately identify damage states, quantify damage severity, and localize damage zones within complex lattice structures. For damage detection, models achieved a high classification accuracy, distinguishing between healthy and damaged states with over 90% precision across 2D and 3D lattice configurations. The quantification study showed reliable predictions for the extent of damage, particularly for groups of damaged struts and damaged cells, with models achieving consistent accuracy in these classifications. The developed localization methodologies, using multiple sensors and spatial mapping of damage in different zones of the structure, proved highly effective, achieving damage zone localization accuracy of up to 85% for cases involving up to three damaged cells. Experimental validation using normalized datasets further affirmed the robustness of the methodology, with experimental predictions aligning closely with numerical simulations for 2D lattice structures.

The results of this research provide a detailed understanding of ultrasonic wave propagation in lattice structures and demonstrate the feasibility of using ultrasonic techniques for SHM in these complex geometries. The proposed methodology was

validated through experimental work involving 2D and 3D lattice structures, with findings highlighting the efficacy of the approach in real-world applications.

The novelty of this work lies in adapting ultrasonic SHM techniques to the complex geometries of lattice structures, bridging the gap between existing methods for traditional materials and the unique challenges posed by AM designs. The findings not only advance the theoretical understanding of ultrasonic wave interactions in lattice structures but also provide practical tools for ensuring their structural integrity. This research establishes a foundation for industry standards in the non-destructive evaluation of AM lattice structures, with implications for improved safety, maintenance practices, and operational efficiency.

Acknowledgement

First and foremost, I would like to express my heartfelt gratitude to my supervisors, Dr. Ian Maskery and Prof. Ian Ashcroft, for their invaluable guidance, encouragement, and support throughout this research journey. Your expertise and mentorship have been instrumental in shaping this work, and I am profoundly thankful for your patience and constructive feedback.

I also extend my sincere thanks to Prof. Dimitrios Chronopoulos, whose initial guidance and insights were pivotal in shaping the direction of this research. Your contributions during the formative stages of this journey have left a lasting impact, for which I remain truly grateful.

I am sincerely thankful to my colleagues and friends for their support throughout this journey—whether through sharing ideas, offering technical assistance, or simply providing encouragement.

Finally, I wish to acknowledge the University of Nottingham for providing the resources and a conducive environment to pursue this research, and the funding bodies and organizations whose contributions made this work possible.

This thesis is the culmination of the collective inspiration, guidance, and support I have received from all of you. Thank you.

Contents

List of Figures

List of Tables

Chapter 1

Introduction

1.1 Background

Damage detection in structures during service is a critical area that ensures the reliability and safety of a mechanical system. An early detection of cracks or flaws in aircraft components can prevent catastrophic failures, while in civil engineering, timely identification of structural damage can avert bridge collapses and other disasters. Structural Health Monitoring (SHM) is an *online* damage-detection and quantification strategy that has seen significant development in the past two decades [13, 14]. SHM systems employ active and passive techniques to measure system response to global or local excitation. The response is analysed using advanced signal-processing techniques to infer the health state of the structure. By far, the two methods that have been significantly used in SHM are vibrational and ultrasonic techniques. These techniques have been widely used to study the response of conventional materials *i.e.* metals and composites. Conventional structures here refer to monolithic metallic or fibre-reinforced components with continuous load paths, in contrast to architected cellular materials such as additively manufactured lattices.

Additive Manufacturing (AM) has seen significant development in the past decade. Global AM revenue grew from US\$4.1 billion in 2014 to US\$22 billion in 2024 [15], and scholarly output in the field increased six-fold over the same period [16]. Improvements in AM processes allow the design and manufacturing of complex structural parts not possible through conventional manufacturing methods. A lot of research is being directed at present to understand the mechanical behaviour of complex structures generated through additive manufacturing. Representative industrial successes include the Airbus "bionic" cabin partition, GE's LEAP fuel-nozzle core and trabecular titanium cranial implants, all of which contain AM lattices for weight saving or biological compatibility [17, 18, 19]. These real-world examples motivate the need for reliable in-service monitoring of lattice cores.

Lattice structures are an important class of additively manufactured structures. They are formed by a large number of interconnected nodes, struts or surfaces. Lattice structures have emerged as an important class of structure due to their desirable lightweight structures with superior mechanical properties. They are finding application in various engineering applications such as aerospace, automotive and civil infrastructures. Lattice structures are capable of giving superior strength-to-weight ratio due to their material efficiency and structural design able to withstand large structural loads. However, the intricate and lightweight geometry of lattice struc-

tures also makes them susceptible to cracks and damage during their service life thus reducing their structural strength and potentially compromising the structural integrity.Crack initiation mechanisms include (i) lack-of-fusion porosity and keyhole voids generated during powder-bed fusion, (ii) residual tensile stress accumulated during rapid thermal cycling, and (iii) cyclic bending of slender ($L/t > 15$) struts under service loads [20, 21]. These local defects are typically hidden within the lattice core, rendering external visual inspection ineffective. In particular, the strut type lattice structures which are formed by a large number of interconnected struts can see cracking and breaking of struts, accelerated by material anomalies inherent during additive manufacturing processes.

Non-destructive Evaluation (NDE) refers to scheduled, off-line inspection, whereas Structural Health Monitoring (SHM) is a continuous, in-situ process that autonomously evaluates a component during operation [22]. This thesis uses bulk-ultrasonic NDE data to train machine-learning classifiers that will ultimately operate in an SHM context, thereby linking both paradigms.

Damage detection in the lattice structures during service life is critical to ensure their desired mechanical performance, enhance their service life and to prevent any catastrophic failures. The intricate and concealed nature of lattice structures makes it even more important to develop novel methods for detecting damage in such structures not possible through traditional inspection methods such as visual inspection. There are various non-destructive evaluation (NDE) techniques which may be useful in detecting damage in lattice structures. In particular, ultrasonic testing can be useful in lattice structures as it uses high-frequency ultrasonic waves which can penetrate deep into structures.

Piezoelectric sensors, which convert electrical signals into mechanical vibrations and vice versa, are widely used in ultrasonic testing for their ability to generate and detect ultrasonic waves with high sensitivity and precision. They are particularly useful in setting an active sensing system which can provide real-time information about the health of the structure. The $10\,\text{mm}\,\varphi$, $2\,\text{mm}$-thick PZT-5H discs selected in this study resonate radially at $215\,\text{kHz}$, a frequency high enough to interact with 2–3 mm lattice struts yet low enough to avoid severe attenuation in Nylon-12. Each disc adds only $0.08\,\text{g}$, three orders of magnitude less mass loading than the smallest commercial accelerometers [12], making accelerometers impractical in this context.

Using an array of sensors, a system may be developed which can not only detect the damage in the lattice but also be able to quantify and localize the damage. A simple pitch–catch pair spaced $50\,\text{mm}$ apart—an arrangement common in guided-wave aircraft inspections [23]—is adopted here as the minimum array capable of time-of-flight localisation.

Physics-based amplitude or time-of-flight thresholds struggle when bulk waves traverse dozens of lattice nodes, producing high-dimensional, low-signal-to-noise data. Recent work has shown that convolutional neural networks and autoencoders can outperform classical algorithms for ultrasonic damage detection in composite plates and honeycombs [24, 25]. The present thesis extends those ideas to additively manufactured lattices.

1.2   Research Problem

There is no work in literature for the damage detection in additively manufactured lattice structures. Limited work is available for damage detection in some complex honeycomb and civil structures using vibrational techniques. However, to the best knowledge of the author, there is no dedicated research on additive manufactured lattice structures using ultrasonic techniques. So the research problem in this study is two-fold. First, to understand the behavior and interaction of ultrasonic waves with the lattice structure and then to develop and test a methodology for damage detection, quantification, and localization in these structures. This research, therefore, addresses two fundamental gaps:

1. Understanding the behavior and interaction of ultrasonic waves within lattice structures.

2. Developing and testing a novel methodology for damage detection, quantification, and localization in lattice structures.

The industrial examples cited above demonstrate why additively manufactured (AM) lattices are attractive, but they also highlight a fundamental limitation: once an AM lattice is built into a larger component, its internal struts are inaccessible to visual inspection or conventional NDE. A recent review of lattice-mechanical testing lists more than 300 papers on strength and stiffness, yet only three on in-service damage assessment, all of which rely on micro-CT and therefore require component removal from service [26]. Guided-wave SHM has been demonstrated for aluminium honeycomb sandwich panels and concrete bridges [27, 14], but the wave modes, boundary conditions and defect morphologies in open lattices differ markedly from those plate-like structures. To the authors' knowledge, no published study has integrated bulk-ultrasonic sensing with machine learning to detect, quantify and localise damage in AM lattices. Consequently, the research problem addressed in this thesis is two-fold

1. **Wave–lattice interaction.** Quantitatively model how high-frequency bulk longitudinal waves propagate through, and scatter from, the complex node–strut topology of a periodic lattice; identify measurable features that are sensitive to strut fracture or cell-level damage.

2. **SHM methodology.** Develop and validate a unified framework that (i) detects the presence, (ii) quantifies the severity, and (iii) localises the position of damage in AM lattices, using a minimal piezoelectric sensor array and data-driven classifiers that can ultimately operate on-board as part of an SHM system.

1.3   Aims and Objectives

The primary objective of this research is to develop a robust methodology for damage characterization in lattice structures using ultrasonic techniques. To achieve this primary objective, the specific research objectives are defined as below.

1. **Understanding Wave Propagation in Lattice Geometries:** To investigate the propagation and interaction of ultrasonic waves in lattice structures particularly the strut-based lattice structures, with a focus on how unique geometrical complexities and material properties influence wave behavior.

2. **Developing a methodology for damage detection and quantification:** To develop a methodology for damage detection and quantification in a representative lattice structure using piezoelectric sensors. This includes extracting useful information from response signals using signal processing techniques and using both numerical and experimental setups for developing and validating the methodology.

3. **Establishing a Damage Localization Methodology:** To develop a methodology for localizing the damage in a lattice structure using array of sensors. This included using numerical and experimental studies for validation of methodology

4. **Incorporating Machine Learning for Enhanced SHM:** Explore the application of ML algorithms to improve the accuracy and efficiency of damage characterization processes.

5. **Evaluating Scalability and Applicability:** Assess the scalability of the proposed methodologies to 3D lattice structures and their potential for real-world application.

1.4   Hypotheses

The research is guided by the following hypotheses:

1. Ultrasonic wave propagation in lattice structures is affected by the presence of discontinuances and damages.

2. The difference between response of healthy and damaged structures can provide a baseline for damage characterization.

3. Advanced signal processing techniques and machine learning algorithms, can be used for the detection and quantification of damage in lattice structures.

4. A systematic approach combining experimental data and numerical simulations can enhance the accuracy of damage quantification and localization in lattice structures.

To test these hypotheses, a combination of numerical simulations, experimental studies, and machine learning methods will be employed. Ultrasonic wave behavior in lattice structures will be analyzed through analytical modeling to understand the effects of discontinuities and material defects, which will be validated through numerical and experimental testing. Signal processing and machine learning techniques will be used to train and develop damage classification models.

1.5   Significance of the Study

The novelty of this research lies in its focus on the application of ultrasonic-based Structural Health Monitoring (SHM) techniques to additively manufactured lattice structures, a field that remains largely unexplored. While traditional SHM methodologies have been extensively applied to metals and composites, their adaptation to lattice structures introduces unique challenges due to the intricate and interconnected geometries. This study bridges this gap by developing a novel framework that integrates ultrasonic wave propagation analysis, signal processing, and machine learning (ML) algorithms to detect, quantify, and localize damage in these structures. The dual approach of combining numerical simulations with experimental validations further enhances the robustness and applicability of the proposed methodology. Following highlights the significances of this study in various areas of interest.

- **Theoretical Significance**: Enhancing the understanding of ultrasonic wave propagation in complex geometries and developing novel techniques for damage detection using Machine Learning.

- **Practical Significance**: Offering a reliable and non-invasive method for inspecting lattice structures, which can be applied in various applications to ensure structural integrity and safety.

- **Policy Implications**: Informing the development of guidelines and standards for the non-destructive evaluation of lattice structures, thereby improving maintenance practices and reducing the risk of structural failures.

1.6   Overview of the Thesis Structure

The structure of this thesis is organized as follows:

- **Chapter 2: Literature Review** - This chapter provides a comprehensive review of existing literature relevant to the study. It covers five main areas: (1) additive manufacturing processes and how they enable complex structures (highlighting differences between AM and conventional manufacturing), (2) the design, mechanical behavior, and typical defects of lattice structures, (3) current Structural Health Monitoring techniques with emphasis on vibration-based and ultrasonic methods, (4) prior work on damage detection in related structures (such as honeycombs or truss networks), and (5) applications of machine learning in SHM and damage detection. Through this review, the chapter identifies the knowledge gaps (particularly the lack of research on ultrasonic SHM for lattices) and justifies the approach of this thesis. It lays the groundwork by summarizing what is known and what remains to be solved, thereby contextualizing the subsequent methodology.

- **Chapter 3: Methodology** - In this chapter, the overall approach and design of the research are presented. It restates the aims and objectives for clarity and then describes the methodology adopted to achieve them. A high-level process flow is provided (with a schematic diagram) illustrating how the analytical,

numerical, and experimental components interconnect. By the end of Chapter 3, the reader should have a clear understanding of how the research will proceed and how validity and reliability are ensured (e.g., via repeat experiments or cross-validation of ML models).

- **Chapter 4: Numerical and Experimental Methods** - This chapter details the research design in terms of both the numerical simulations and the experimental setups used in the study. On the numerical side, it describes the finite element models of the lattice structures, including geometry, material properties, and how ultrasonic wave propagation is simulated (for example, using transient dynamic analysis or explicit time-stepping). Boundary conditions and defect modeling (how damage is introduced in the simulation) are explained. On the experimental side, the chapter describes the fabrication of physical lattice specimens (using additive manufacturing), the instrumentation with PZT sensors, and the experimental procedure for ultrasonic testing (including the excitation signals, sensor arrangement, and data acquisition parameters). Any custom equipment or software (such as a function generator or oscilloscope, and signal processing scripts) is also presented. By providing this detailed account, Chapter 4 ensures that the methodology can be reproduced and that the context for results (in later chapters) is well understood. Essentially, it translates the methodological plan of Chapter 3 into concrete implementations.

- **Chapter 5: Analytical estimation of ultrasonic transmission in Lattice structures** - This chapter addresses Objective 1 by focusing on the fundamental analysis of ultrasonic wave behavior in a lattice structure. It presents an analytical model for wave transmission and reflection in a simplified lattice element (often a unit cell or a repeating segment of the lattice). It then builds up to modeling a sequence of unit cells, predicting how waves attenuate or scatter as they travel through an intact lattice. The insights gained here directly support the hypotheses related to wave discontinuities and provide justification for using certain wave frequencies or sensor placements in the subsequent chapters.

- **Chapter 6: Damage detection and quantification** - In this chapter, the thesis demonstrates the development of the damage detection methodology (Objective 2) on a two-dimensional (planar) lattice structure. Chapter 6 combines numerical simulation results and experimental data to show how damage (of various sizes/severities) affects the ultrasonic response. Key features are extracted from the raw signals using signal processing techniques. These features are then used to distinguish between healthy and damaged states. The chapter introduces a classification model (e.g., a neural network or other machine learning classifier) trained on the features to automatically detect damage and possibly estimate the damage extent (number of broken struts, etc.).

- **Chapter 7: Damage Localization** - Building upon the damage quantification, Chapter 7 tackles Objective 3 by introducing and validating the damage localization methodology. Using the sensor array approach, this chapter shows how the position of damage within the lattice can be identified. It details the strategy for localization at various known locations in the lattice and record

the sensor responses to build a localization model. Then experiments are conducted where the lattice is damaged in specific cells or regions, and the sensor data is fed into the model to predict the damage location.

- **Chapter 8: 3D Lattice Structures** - Chapter 8 addresses Objective 5 by testing the developed methods on a three-dimensional lattice structure, thereby assessing scalability and broader applicability. A 3D lattice (with a volume of unit cells rather than a single layer) introduces additional complexity: waves can travel in all three dimensions, and there are more potential damage locations and patterns.

- **Chapter 9: Discussions, Future Work and Conclusions** - This chapter provides a holistic discussion of the research findings, connecting the results from Chapters 5 through 8 back to the hypotheses and objectives. It also presents challenges in the present work, the future research directions and conclusions.

Chapter 2

Literature Review

2.1 Introduction

This chapter explores the literature related to the scope of research in this study. It reviews the key developments in additive manufacturing (AM) for lattice structures, SHM techniques, and ML applications in damage detection. Each section is structured to provide a foundation for the methodologies explored in this thesis, addressing gaps in the current literature related to the unique challenges posed by AM-produced lattice geometries. The literature review is organized in the following areas.

- Overview of additive manufacturing

- Lattice structures

- Defects in lattice structures

- Structural health monitoring (SHM) and damage detection

- Statistical and Machine learning models for damage detection

- Identification of Research Gaps

2.2 Overview of additive manufacturing

Additive manufacturing (AM) is an advanced manufacturing method which uses material deposition techniques to build the structures layer by layer. It differs from conventional manufacturing in which material is removed when manufacturing, whereas in additive manufacturing material is added, hence the name additive manufacturing [28]. AM allows manufacturing of complex geometries and structures while reducing the material waste and thus has seen significant surge in its use [29]. During this work, various AM techniques were explored with specific application to lattice structures. Some of the major AM methods are discussed in the subsequent paras. Each of these AM techniques offers trade-offs between material compatibility, mechanical performance, resolution, build volume, and cost, and are selected based on the intended function of the final part.

2.2.1 Additive Manufacturing methods

There are various additive manufacturing methods depending on its materials, layering and machine technology used. A brief overview of few AM methods is given below [30, 31].

Material Extrusion

Material extrusion is one of the most accessible and widely used AM processes, especially in desktop 3D printers. A thermoplastic filament (e.g., PLA, ABS, PETG) is heated and extruded through a moving nozzle, depositing material layer by layer to form the object. The material solidifies upon cooling to form the final shape. While it is predominantly used for prototyping and low-strength applications, it has also been explored for biomedical scaffolds and tooling aids in aerospace and automotive sectors [32, 33]. A schematic of this method is shown in Figure 2.1.
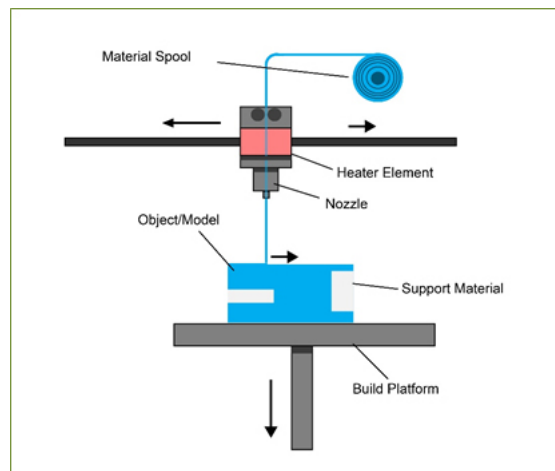
Figure 2.1: Schematic of Fuse deposition modeling (FDM) [1]

Powder Bed Fusion (PBF)

PBF techniques utilize a high-energy source (laser or electron beam) to selectively fuse regions of a powder bed. Common variants include Selective Laser Sintering (SLS), Direct Metal Laser Sintering (DMLS), Selective Laser Melting (SLM), and Electron Beam Melting (EBM). These methods are capable of producing complex, high-performance metal and polymer parts with good mechanical properties. PBF is used in aerospace (e.g., lightweight brackets, heat exchangers), medical (e.g., orthopedic implants), and tooling industries [34, 35]. A schematic of PBF is shown in Figure 2.2.

Direct Energy Deposition (DED)

DED involves melting material as it is deposited, typically through a nozzle with simultaneous energy input via a laser or electron beam. It is highly suitable for repair applications, large part fabrication, and gradient material deposition. DED enables precise control over material composition and is used in turbine blade repair, aerospace structural component enhancement, and functionally graded material fabrication [36, 37]. A schematic of DED is shown in Figure 2.3
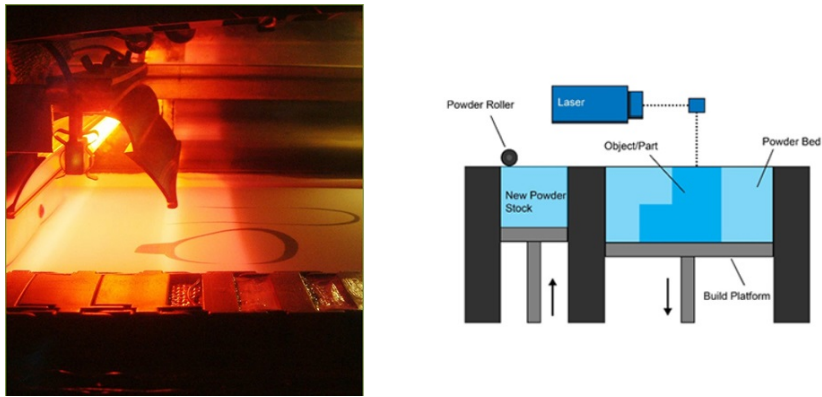
Figure 2.2: Schematic of Powder Bed Fusion (PBF) [2]
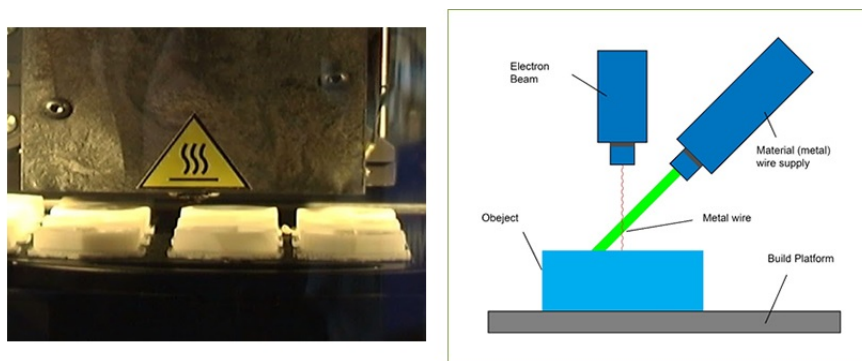
Figure 2.3: Schematic of Direct Energy Deposition (DED) [3]

VAT Photopolymerisation

This process uses a vat of liquid photopolymer resin cured layer-by-layer using a UV laser (SLA) or projector (DLP). It provides extremely high resolution and smooth surface finish. Applications include dental models, microfluidic devices, hearing aids, and jewelry casting molds [38, 39]. The schematic of process is shown in Figure 2.4.
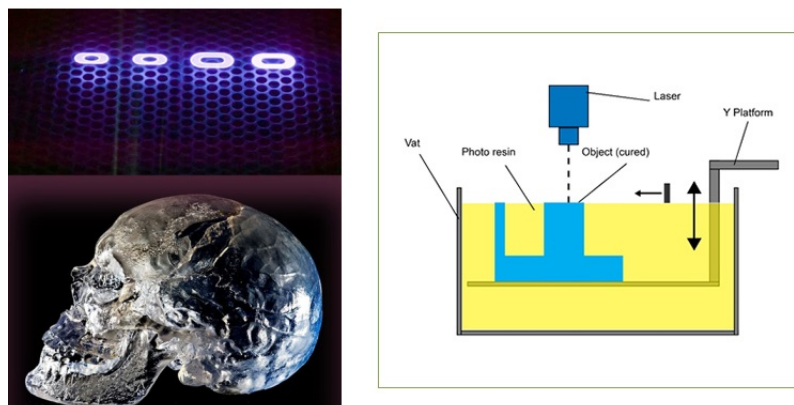
Figure 2.4: Schematic of VAT Photopolymerisation [4]

Material and Binder Jetting

Material Jetting involves the deposition of build material in droplet form, cured by UV light. It supports multi-material and color printing, making it ideal for prototypes, medical models, and anatomical simulations. Binder Jetting uses a liquid binder to selectively bond powder particles. It is commonly used in sand casting molds, ceramic parts, and low-cost metal component production [40, 41]. The process flows of both these techniques are represented in Figure 2.5.
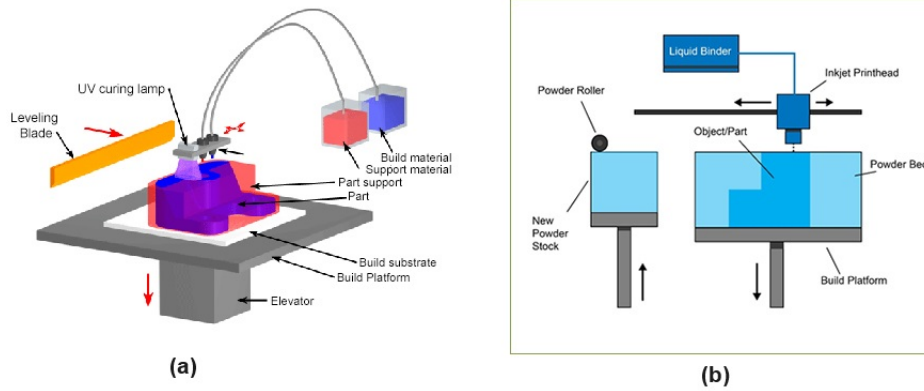
Figure 2.5: Schematic of (a) Material jetting (b) Binder jetting [5]

Sheet Lamination

Sheet Lamination includes Laminated Object Manufacturing (LOM) and Ultrasonic Additive Manufacturing (UAM). In LOM, adhesive-coated sheets (typically paper, polymer, or metal) are bonded and cut into shape using a laser or blade. UAM uses ultrasonic welding to bond metal foils. These methods are used in packaging prototypes, metal tooling inserts, and composite structures with embedded sensors [42, 43]. The process of sheet lamination is shown in Figure 2.6.
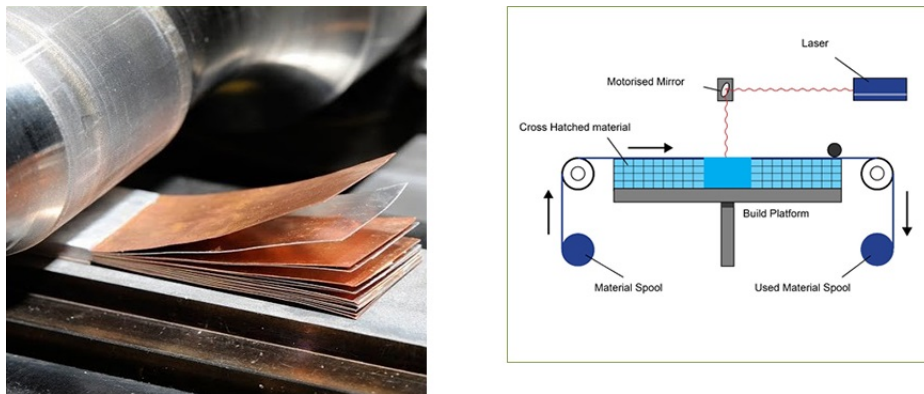
Figure 2.6: Schematic of Sheet Lamination process[6]

2.2.2 Defects Induced in Additive Manufacturing

Defects are a major concern in additive manufacturing (AM), primarily arising due to thermal gradients, layer-by-layer deposition, and variability in process parame-

ters. These defects compromise the structural integrity of parts, influence mechanical performance, and in some cases, lead to premature failure. A detailed discussion of key defect types, their origins, and reported effects in literature is provided below.

Porosity and Voids

Porosity is one of the most studied defects in AM, particularly in powder-based processes such as Selective Laser Melting (SLM). Greco et al. [44] investigated different porosity mechanisms, distinguishing between gas-induced and lack-of-fusion pores. Their study emphasized the importance of scan speed and hatch spacing in controlling pore distribution. While their simulations were validated experimentally, their analysis remained focused on static properties, without assessing fatigue performance. Leung and Tam [45] extended this by examining the fatigue behavior of Ti-6Al-4V parts with varying porosity levels. They demonstrated that pores near the surface had a disproportionately large impact on fatigue life due to crack nucleation. Their work, however, did not account for multi-axial loading, limiting its applicability in aerospace applications. Taheri et al. [46] experimentally demonstrated that irregular powder morphology and wide particle size distribution lead to heterogeneous melt pools and increased porosity, particularly in laser-based AM processes. Their work provides important insight into feedstock preparation but does not assess mechanical performance impacts. A depiction of porosity is shown in Figure 2.7.
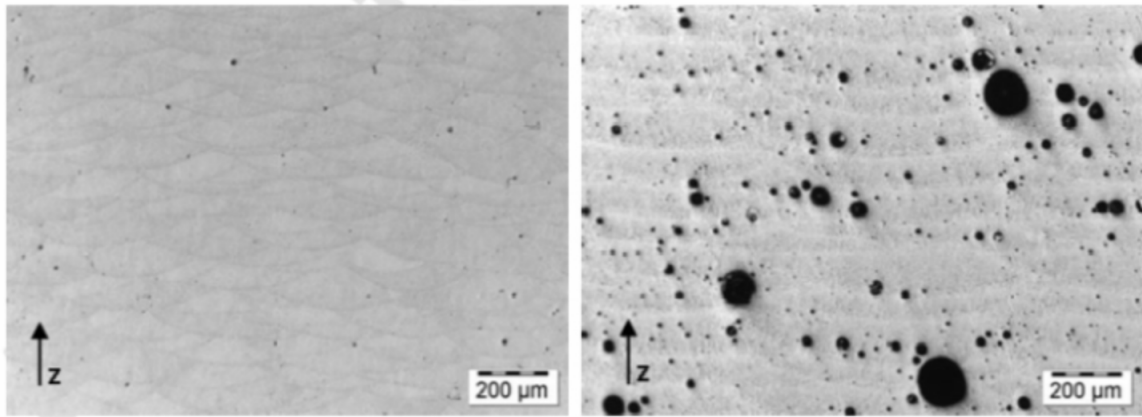
Figure 2.7: Microscopic porosity and voids [7]

Delamination and Cracking

Delamination is often observed in polymer-based AM processes and is attributed to weak interlayer bonding. King et al. [47] used high-speed imaging to capture melt pool dynamics and showed that insufficient overlap between melt pools was a primary cause of inter-layer separation. Their insights have helped in optimizing laser scan strategies, although their findings were limited to single-track builds. Mukherjee and DebRoy [48] provided a broader framework by linking delamination and cracking to thermomechanical stress accumulation. They proposed a thermal stress model that could predict crack-prone regions based on temperature gradients, although experimental validation was only partially addressed. Residual stress and

strains due to temperature differences also lead to cracking and delamination as depicted in Figure 2.9.
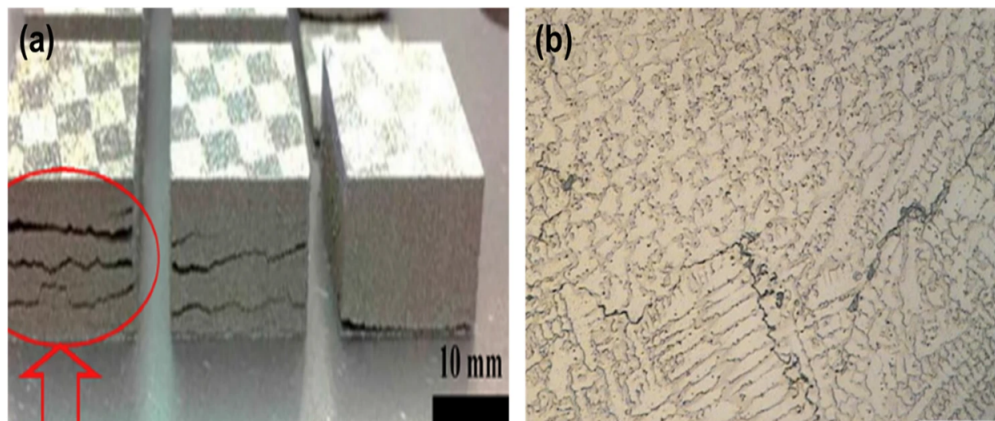
Figure 2.8: Delamination and cracking in additive manufacturing[8]

Residual Stresses

Residual stress is not a visible defect but can lead to warping, distortion, and ultimately crack propagation. Mercelis and Kruth [49] conducted one of the earliest experimental studies measuring residual stress in SLM using X-ray diffraction. They concluded that island scan strategies and post-build stress-relief treatments are effective in reducing internal stresses. Parry et al. [50] complemented this with a numerical approach, showing that scan pattern rotation between layers can reduce stress buildup. However, their model assumed constant thermal conductivity, which can vary during solidification, potentially affecting accuracy in real builds.
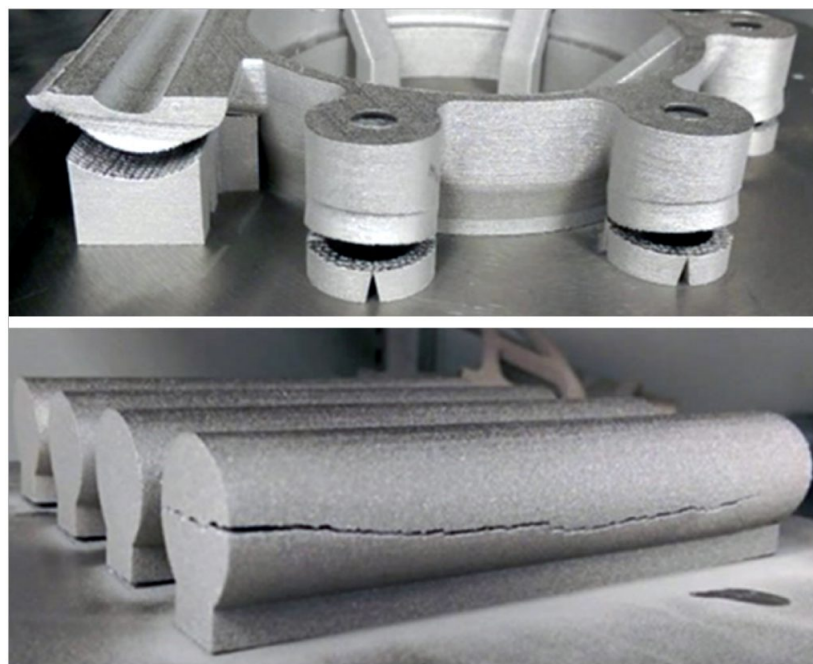
Figure 2.9: Residual stresses leading to cracks in the parts[9]

Surface Roughness

Surface roughness in AM is primarily a result of stair-step effects, unmelted powder, and poor melt pool stability. Strano et al. [51] analyzed roughness in SLM parts and correlated it to laser parameters and powder morphology. They showed that roughness levels could be significantly reduced by optimizing recoating parameters, although their study lacked mechanical performance validation. Song et al. [52] explored how rough surfaces affect fatigue strength, reporting that unmachined surfaces acted as crack initiation sites under cyclic loading. They highlighted the importance of post-processing but also acknowledged that mechanical polishing may not be feasible for intricate lattice structures.

Inclusions and Contamination

Inclusions are typically caused by powder contamination, oxidation, or environmental exposure during processing. DebRoy et al. [53] reviewed the role of feedstock quality and found that oxygen content and powder reuse cycles significantly influence inclusion formation. While their review was comprehensive, it mainly focused on metals, with limited applicability to polymers or composites. Yan et al. [54] investigated electron beam melting and reported frequent oxide inclusions at layer interfaces. Their study emphasized the need for chamber vacuum control and powder recycling protocols, but their findings were limited to a specific alloy system.

Overall, these studies highlight that defects in AM are multifaceted and strongly linked to process parameters, part geometry, and material system. Despite advances in process control and simulation, many challenges remain in predicting how defects evolve during printing and how they affect in-service performance—especially for complex geometries like lattice structures.

2.2.3   Effect of Defects on Structural Integrity

The presence of defects in additively manufactured (AM) components has a direct and often severe impact on their structural integrity. These effects are highly dependent on defect type, location, geometry, and material system. While some defects serve as stress concentrators and reduce fatigue life, others impair dimensional stability, load-bearing capacity, or cause catastrophic failure. Understanding these effects is essential for the design, certification, and long-term deployment of AM parts, particularly in safety-critical applications such as aerospace and biomedical implants.

Porosity and Fatigue Life

Porosity, especially near-surface pores, has been widely shown to degrade fatigue resistance. Leung and Tam [45] conducted fatigue tests on Ti-6Al-4V samples fabricated via SLM and reported that even small pores located near the surface acted as nucleation sites for crack growth. Their results were experimentally robust, though limited to uniaxial loading conditions. Sanaei and Fatemi [55] extended this understanding by developing a mechanistic model linking porosity parameters (size, distribution, aspect ratio) to fatigue crack initiation life. Their work is notable for its relevance to cellular structures, though the model remains semi-empirical and material-specific.

Cracks and Structural Collapse

Cracking due to thermal stress accumulation compromises global stiffness and introduces fracture paths under load. Mukherjee and DebRoy [48] linked such cracking in metal AM to non-uniform cooling rates and stress localization. While their simulations provided temperature-field predictions, mechanical property degradation was not quantified. In lattice structures, where localized stiffness plays a critical role, even small through-strut cracks can cause cascading failure. This highlights the importance of early crack detection and mitigation.

Residual Stress and Dimensional Instability

Residual stresses impact both geometric fidelity and in-service performance. Mercelis and Kruth [49] showed that high residual stress levels in laser-melted parts led to warping and delamination during build and post-processing. They recommended annealing protocols for stress relief, though effects on microstructure were not addressed. Parry et al. [50] further demonstrated that scan strategy optimization reduced residual stress gradients, indirectly improving dimensional stability. However, neither study assessed the combined effects of residual stress and defects under cyclic loading—common in aerospace components.

Surface Roughness and Crack Initiation

Rough surfaces act as stress raisers and promote early crack nucleation. Song et al. [52] correlated surface roughness parameters with fatigue crack growth rate, showing that higher roughness significantly reduces fatigue life in AM metals. Their study emphasized the importance of surface finishing, though such treatments are often infeasible in internal geometries typical of lattice structures. As a result, as-built surface conditions remain a limiting factor in the use of AM for lightweight truss-like components.

Inclusions and Fracture Toughness

Foreign inclusions, often resulting from powder reuse or oxidation, reduce ductility and fracture toughness. Brennan et al. [56] observed that inclusions act as crack initiation points, particularly in Ti alloys subjected to tensile and fatigue loads. Their results support stricter powder handling protocols but also indicate that even well-controlled processes are susceptible to internal flaws, especially in multi-build reuse scenarios.

Implications for Lattice Structures

Lattice structures, due to their slender struts and distributed load paths, are particularly sensitive to local defects. As shown in recent work by Sanaei and Fatemi [55], defects such as pore clusters or strut-scale residual stresses disproportionately affect stiffness, energy absorption, and fatigue resistance. Their study advocated for topology-aware quality control during manufacturing and post-processing. However, comprehensive experimental validation of such defect effects in real lattice geometries remains limited in literature.

In summary, defects in AM components influence a range of structural parameters including strength, stiffness, fatigue life, and dimensional accuracy. While general trends are understood, their behavior in architected geometries like lattices is still under investigation. Accurate modeling of defect interaction with complex geometries and the development of defect-tolerant design methodologies remain active research areas.

2.2.4 Motivation for Structural Health Monitoring in AM Structures

Despite advances in process optimization and post-processing, defects in additive manufacturing (AM) remain a persistent challenge. As established in the previous sections, defects such as porosity, microcracks, residual stresses, and inclusions can significantly degrade structural integrity, leading to early failure under mechanical or environmental loading. While mitigation strategies aim to reduce the occurrence of these flaws, they cannot guarantee defect-free builds—especially when dealing with complex geometries or large-scale components.

Moreover, AM parts often contain internal features or embedded channels that are difficult to inspect using conventional non-destructive evaluation (NDE) techniques. Post-build inspections may miss internal damage or fail to capture defect evolution during service, particularly under cyclic or fatigue loading where damage initiation and growth are not externally visible.

These limitations underscore the need for more proactive and integrated damage detection strategies. Structural Health Monitoring (SHM) offers a complementary approach to traditional inspection by enabling continuous, real-time assessment of component condition. SHM techniques, including ultrasonic sensing, vibration analysis, and acoustic emission, can detect changes in structural response indicative of internal damage. This capability is particularly valuable in AM, where variability in build quality and defect distribution can make conventional inspection insufficient.

Recent studies have highlighted the integration of SHM systems within AM components. For instance, de Baere et al. [57] proposed embedding SHM systems directly into AM structures, facilitating real-time monitoring without compromising structural integrity. Similarly, Khanafer et al. [58] reviewed various condition monitoring techniques in AM, emphasizing the role of SHM in ensuring product quality and reliability throughout the component's lifecycle.

Among the diverse design freedoms enabled by AM, lattice structures have emerged as a promising solution for achieving lightweight, high-performance components. However, the same architectural complexity that makes them attractive also renders them highly susceptible to manufacturing defects and difficult to inspect using conventional methods. The thin struts, internal voids, and intricate geometries of lattice structures make them particularly challenging in terms of defect mitigation and quality assurance. These challenges further strengthen the case for integrating SHM approaches tailored to such geometries. The next section provides an overview of lattice structures, their classification, and their relevance in advanced engineering applications.

2.3 Lattice Structures

Lattice structures represent a unique class of architected materials enabled by additive manufacturing (AM), offering tunable mechanical, thermal, and acoustic properties. Unlike stochastic cellular structures such as foams, which exhibit random internal geometry, lattice structures are defined by a periodic and controlled arrangement of struts or surfaces forming unit cells in three-dimensional space. Gibson and Ashby [59] define cellular materials as "an interconnected network of solid struts or plates which form the edges and faces of cells," a description that applies broadly to both foams and lattices.

The primary distinction lies in their geometry and manufacturability. While cellular foams are typically formed through stochastic processes such as gas injection into molten materials [60], lattice structures are designed with deterministic geometry, allowing precise tailoring of unit cell architecture and part-scale behavior. The rise of AM technologies has made it feasible to manufacture such complex lattice geometries, which were previously impractical or impossible using conventional methods.

Due to their superior strength-to-weight ratio and efficient use of material, lattice structures have found applications in aerospace, biomedical implants, and energy absorption systems. Natural analogues like honeycomb structures illustrate the strength of geometric optimization, and modern lattice topologies extend these principles to three dimensions. The following subsections provide a detailed overview of lattice types, design classifications, and applications in engineering systems, with emphasis on their relevance to defect sensitivity and structural reliability.

2.3.1 Type of lattice structures

Lattice structures are categorized based on their periodicity, structural elements, and spatial arrangement. These classifications are essential for selecting or designing the most appropriate topology for a specific mechanical or functional requirement.

Periodicity

Based on periodicity, lattice structures are classified as periodic and non-periodic or stochastic lattice structures. Periodic lattice structures have a regular and repeating pattern throughout the structure. On the other hand stochastic lattices have a random or non periodic arrangement of cells in the structure. The example of these lattice structures is given in Figure 2.10.

Structural elements

Based on structural elements, the lattice structures primarily fall into three categories (a) strut based lattice structures (b) planar or shell based lattice structures (c) Triply periodic minimal surface (TPMS) lattices. Strut based lattice structures are formed by various arrangements of interconnected rod like elements. Planar lattice structures are formed by thin plates or shells which are grown in a single direction. TPMS lattices are governed by mathematical equations that control the shape and size of structure. The three classes are shown in Figure 2.11.
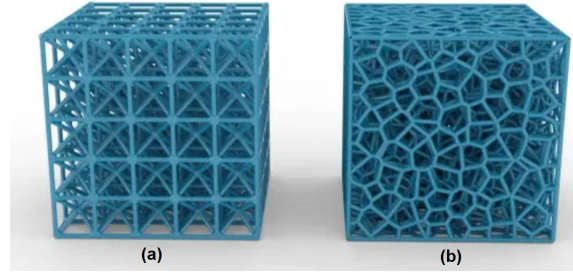
Figure 2.10: Periodic and non-periodic/stochastic lattice structure (a) periodic lattice (b) non periodic lattice [10]
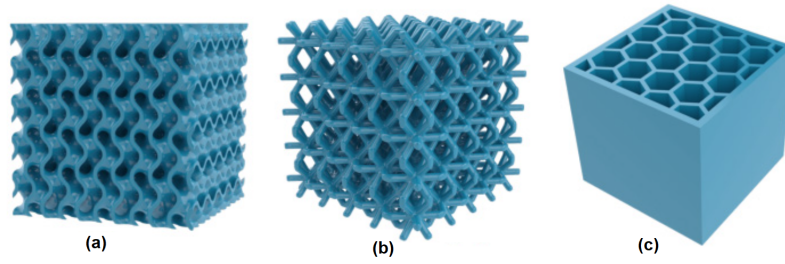
Figure 2.11: Classification of lattice structures (a) TPMS lattices (b) strut based lattice (c) planar lattice [10]

Lattice structure designs are also defined by their unit cell, which often falls into one of two categories: strut and surface based [11] as shown in Figure. 2.12. Strut-based unit cells consist of a network of often prismatic struts (i.e. constant cross section) connected at nodes, similar to truss structures. Surface-based unit cells also known as triply periodic minimal surfaces (TPMS) are mathematically defined as the surface connecting set of points for which a given function has a constant value, that is, an isosurface. Periodic arrangement of unit cells forms lattice structures which are designed to perform a desired function.
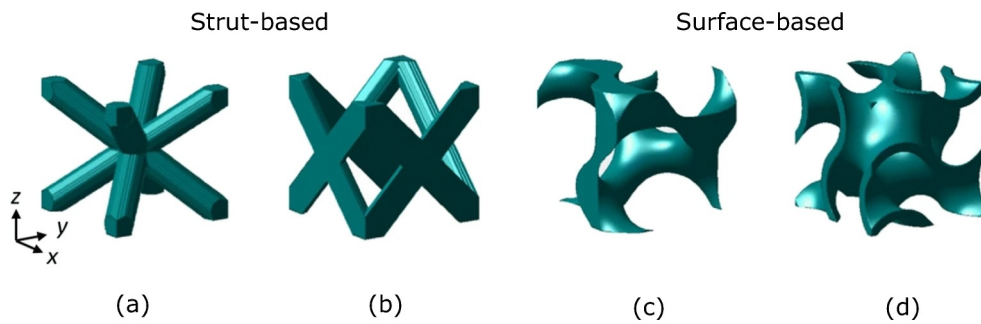
Figure 2.12: Types of unit cells: (a) body-centred cubic, (b) face-centred cubic, (c) gyroid (skeletal/network) and (d) double gyroid (sheet/matrix) [11]

Spatial arrangement

Lattices can either be volume-filling or surface-conforming. Volume-filling lattices occupy the entire domain and are typically used for internal lightweighting. Surface-conforming lattices follow the external geometry of the part, often used in impact

protection and thermal regulation.

Design Optimization of Lattice Structures

Design of lattice structures is increasingly aided by computational optimization techniques. Topology optimization is often employed to distribute material within a given design space for optimal stiffness or weight objectives [61]. Moreover, functionally graded lattices—where cell size, type, or orientation vary across the structure—allow tuning of performance under spatially varying loads. Finite element simulations are routinely used to assess and refine designs before fabrication. These strategies are critical to ensure that the manufactured lattice not only meets mechanical performance targets but is also robust to defects inherent to the AM process.

2.3.2 Applications of Lattice Structures

The design flexibility offered by additive manufacturing (AM) has enabled the integration of lattice structures into a wide range of engineering applications, particularly where weight efficiency, energy absorption, and tailored mechanical properties are critical. Their use has been widely reported in aerospace, biomedical, and automotive domains, where traditional manufacturing techniques often limit geometric complexity.

In aerospace, lattice architectures are increasingly used in load-bearing components such as brackets, stiffeners, and support frames. These structures benefit from optimized strength-to-weight ratios and can be topology-tailored to meet load paths while reducing inertial loads. Strano et al. [51] reported the implementation of lattice-filled brackets in aerospace components, highlighting significant weight reduction without compromising structural performance. Similarly, Leary et al. [62] investigated gyroid-type TPMS lattices as compact heat exchangers for aerospace cooling systems, demonstrating enhanced thermal performance due to increased surface area and controlled porosity.

Impact mitigation is another critical aerospace application. Li et al. [63] studied the energy absorption capabilities of BCC and Kelvin-type lattices and concluded that deformation under compressive loading could be tuned by adjusting cell geometry and wall thickness. These characteristics make lattices attractive for crash zones, protective housings, and landing gear structures.

Biomedical applications have similarly benefited from the controlled porosity and mechanical tunability of lattice structures. Sanaei and Fatemi [55] reviewed how lattice-based scaffolds offer porosity for tissue ingrowth, with mechanical properties tailored to mimic cortical or trabecular bone. Their work emphasized that strut thickness, unit cell type, and fabrication defects all influence biocompatibility and mechanical reliability.

However, the use of lattices in high-integrity systems, such as aircraft structures or biomedical implants, introduces challenges related to defect tolerance and inspection. Echeta et al. [64] emphasized that lattice structures, particularly those with thin features and high surface-area-to-volume ratios, are inherently sensitive to AM-induced defects. Their review stressed the importance of in-situ monitoring and robust design practices to ensure structural reliability. Brennan et al. [56] further highlighted how oxygen-related inclusions from powder reuse can compromise the integrity of lattice struts, particularly in Ti-6Al-4V components.

Taken together, these studies reflect the versatility and performance potential of lattice structures across sectors. Yet, they also reinforce the need for defect-aware design, robust process control, and integration of post-fabrication inspection or health monitoring strategies to ensure their successful deployment in mission-critical applications.

2.3.3 Strut-Type Lattice Structures

Strut-based lattice structures are the most commonly studied and applied category of architected materials in additive manufacturing. They are constructed from an array of interconnected struts forming repeating unit cells. The simplicity of their geometry, combined with predictable mechanical behavior, makes them highly suitable for numerical modeling, optimization, and experimental validation.

The mechanical response of strut lattices is largely governed by their relative density, which is the ratio of the lattice's bulk density to the density of the solid material. According to the scaling laws presented by Gibson and Ashby [59], the elastic modulus and yield strength of a strut-based lattice scale with the square or cube of its relative density, depending on whether the structure is bending- or stretching-dominated. Stretch-dominated lattices, such as the octet truss, exhibit higher stiffness and load-bearing capacity, while bending-dominated topologies like BCC or rhombic dodecahedron are more energy-absorbing and compliant under load.

Sanaei and Fatemi [55] highlighted that due to their periodic geometry, strut-based lattices enable localized tailoring of stiffness and strength. By varying strut thickness, length, and connectivity, engineers can adjust performance parameters such as energy absorption, load redistribution, and directional stiffness. This makes them particularly useful in applications requiring high performance-to-weight ratios.

In aerospace, strut-type lattices have been used in internal support structures for turbine blades, optimized brackets, and sandwich cores in panel stiffeners. These components benefit from the ability to reduce mass while maintaining mechanical integrity under complex loading. For instance, Maskery et al. [61] demonstrated that AlSi10Mg strut-based lattices produced via selective laser melting achieved stiffness values closely matching simulation predictions, confirming their viability for structural applications. Similarly, Deshpande et al. [65] characterized the crush response of a variety of periodic lattices and confirmed their suitability for aerospace energy absorbing systems.

Strut lattices are also employed in biomedical scaffolds, where open porosity is essential for tissue ingrowth and nutrient transport. Structures such as BCC or diamond lattices are often used in load-bearing orthopedic implants due to their favorable compressive properties and manufacturability using biocompatible alloys.

Overall, strut-type lattices offer a versatile design space for applications demanding lightweighting, energy absorption, or mechanical compliance. Their geometry can be tailored through unit cell selection and parameter tuning, while their behavior remains analytically tractable—making them an ideal candidate for both high-performance engineering systems and experimental prototyping.

Failure Mechanisms in Strut-Based Lattice Structures

The structural integrity of strut-based lattice architectures is often governed by the failure mechanisms of their slender elements. These struts are typically subjected to complex combinations of tensile, compressive, and bending loads depending on the applied boundary conditions and lattice topology. Due to their high slenderness ratios, struts are inherently prone to buckling, fracture, and plastic collapse, which may occur either in isolation or in combination, often leading to catastrophic progressive failure.

Gibson and Ashby [66] established that the fracture behavior of lattice structures is largely determined by whether the architecture is bending- or stretching-dominated. In bending-dominated structures, such as body-centered cubic (BCC) lattices, failure usually initiates from buckling or plastic yielding under compressive loading, whereas stretching-dominated structures, such as the octet-truss, tend to fail more abruptly via brittle fracture due to axial tensile stresses.

The susceptibility of lattice struts to fracture is further exacerbated by process-induced defects inherent in additive manufacturing (AM). Taheri et al. [46] reviewed the mechanisms by which internal porosity, lack of fusion, and surface roughness are introduced during powder-bed fusion, particularly in thin-walled features like struts. These imperfections act as stress concentrators and significantly reduce fatigue life and fracture resistance. Brennan et al. [56] emphasized the detrimental impact of such defects on fatigue crack initiation and propagation in metallic AM lattices, especially under cyclic or impact loading, which are common in aerospace and biomechanical environments.

Echeta et al. [64] provided further insight into the degradation of load-bearing capacity due to defect-sensitive collapse mechanisms in lattice structures. Their work revealed that even minor inconsistencies in strut geometry or surface morphology can trigger early fracture, particularly at nodal junctions. The authors recommended improved powder quality control and the implementation of in-situ monitoring strategies as essential steps toward improving strut reliability.

In addition to defect mitigation, structural optimization of the lattice geometry plays a key role in improving fracture resistance. By tailoring strut diameter, connectivity, and unit cell type, designers can delay the onset of local failure and prevent fracture propagation. This is particularly relevant for functionally graded lattices, where gradual variations in strut size or orientation help in redistributing stresses more evenly throughout the structure.

Ultimately, the fracture and breaking of struts determine not only the local failure but also the global mechanical response of the lattice. A comprehensive understanding of these mechanisms, informed by both experimental validation and computational modeling, is critical for deploying lattice-based structures in safety-critical applications.

Need for Structural Health Monitoring in AM Lattice Structures

Additively manufactured (AM) lattice structures, while offering significant advantages in terms of weight savings and tailored mechanical properties, are inherently susceptible to various defects and manufacturing inconsistencies. These include lack of fusion, residual porosity, surface roughness, geometric inaccuracy, and microstructural heterogeneity [46, 64, 56]. In lattice architectures, particularly those

employing slender struts, such flaws may not only compromise the mechanical performance but can also lead to premature fracture and progressive collapse under loading, as discussed in the previous sections.

Due to the distributed nature of damage in lattice materials and their geometric complexity, traditional non-destructive evaluation (NDE) techniques face limitations in detecting sub-surface defects or predicting failure. Furthermore, internal lattice regions are often inaccessible for post-manufacturing inspection, especially in functionally integrated components. This makes **in-situ sensing and monitoring during service or operation not only desirable but necessary**.

Structural Health Monitoring (SHM) systems offer a potential solution by enabling continuous or periodic assessment of structural integrity through embedded sensors, ultrasonic interrogation, or vibration-based methods. In the context of AM lattices, SHM is particularly relevant due to: - High sensitivity of mechanical response to micro-defects - Localized failure modes that may not exhibit external signs until final collapse - Load-bearing applications where failure has safety-critical implications

Several studies have begun to explore the adaptation of SHM techniques for AM lattices. For instance, ultrasonic wave-based SHM has been proposed to track changes in wave propagation due to micro-cracking or delamination in lattice cells. These methods rely on baseline comparison strategies and require accurate numerical models of wave behavior within periodic structures. Brennan et al. [56] emphasized that in highly porous and thin-strutted geometries, even subtle flaws can cause substantial local stress changes, further justifying the use of sensitive monitoring systems.

Moreover, the integration of SHM with digital twins, model-driven simulations of the lattice structure—has emerged as a promising concept for critical applications. In such systems, monitored data can be continuously compared against predictive models to assess damage progression, fatigue life, and failure probability. This is particularly attractive in aerospace and biomedical sectors, where AM lattices are already being employed in satellite components and load-bearing implants.

Thus, the development of effective SHM strategies tailored for AM lattice structures not only addresses current reliability concerns but also enables the design of intelligent, self-aware components capable of reporting their health state throughout their service life. This aligns with the broader shift toward condition-based maintenance and mission-critical material systems.

2.4 Structural Health Monitoring and Damage Detection

Additively manufactured (AM) components—particularly lattice structures—present new challenges for structural integrity assessment. Their complex internal geometries, thin features, and process-induced variability often make them unsuitable for traditional inspection techniques. As such, the demand for robust, integrated damage detection approaches has driven the advancement of both Non-Destructive Evaluation (NDE) and Structural Health Monitoring (SHM) methods.

NDE refers to techniques that allow inspection without causing damage to the part, and includes methods such as X-ray computed tomography (CT), ultrasonic

testing, eddy current testing, and thermography. These methods are typically applied at discrete time intervals and can be highly effective in detecting surface and subsurface flaws—particularly in planar or accessible regions. However, their applicability to internal regions of complex AM lattices is limited, especially when structures are enclosed or have high porosity. Moreover, NDE generally provides a snapshot in time rather than continuous monitoring.

In contrast, SHM refers to the continuous or periodic observation of structural state using embedded or surface-mounted sensors, with the aim of identifying changes that may indicate damage. SHM methods can be broadly categorized as either baseline-dependent or baseline-free. Baseline-dependent approaches compare sensor data to a known undamaged condition to identify changes, but establishing such a baseline can be difficult in AM components due to geometry-specific variability. Baseline-free methods, on the other hand, utilize statistical learning, pattern recognition, or unsupervised algorithms to detect anomalies without needing a pristine reference [67, 68].

Guided wave-based SHM has gained popularity due to its ability to propagate over long distances and interact sensitively with defects. These waves differ from surface waves in that they are confined within bounded media—such as thin plates or struts—and can be tailored for enhanced sensitivity to geometric discontinuities. This makes them particularly relevant for thin-walled AM structures where access is limited. Their widespread use is further supported by the availability of compact piezoelectric actuators, ease of signal processing, and high sensitivity to damage modes like cracking, delamination, or corrosion [69].

Ultimately, while NDE and SHM both contribute to the detection of manufacturing defects and in-service damage, SHM provides the added advantage of enabling proactive maintenance and real-time condition assessment. In the context of AM lattice structures, this distinction becomes critical, as defects can evolve under load and are often not detectable using surface-based techniques alone.

Among the various wave-based SHM techniques, surface waves and guided waves are frequently employed for damage detection. Surface waves, such as Rayleigh waves, propagate along the material surface and decay exponentially with depth. These are particularly effective for detecting shallow surface cracks or corrosion. Guided waves, in contrast, propagate within bounded media—such as plates, rods, or struts—and are influenced by both geometry and boundary conditions. Due to their ability to travel long distances and interact with both surface and internal discontinuities, guided waves are especially suited for monitoring complex geometries like those found in AM lattice structures [69].

Signal-based SHM systems typically operate by first acquiring dynamic response data through sensors such as piezoelectric actuators, strain gauges, or accelerometers. This raw data undergoes signal processing to extract informative features—such as frequency content, time-domain statistics, or modal shifts—that are sensitive to the presence of damage. These features are then fed into classification or regression algorithms to determine damage existence, severity, or location.

As Farrar and Worden [67] noted, feature extraction alone is insufficient for comprehensive SHM. A complete system must also include a decision-making framework capable of interpreting feature changes to identify not only if damage has occurred, but also what its implications might be. This is where the concept of **prognosis** becomes critical.

Prognosis refers to the prediction of future structural behavior based on current and historical monitoring data. Unlike detection and localization, which focus on identifying the presence and location of damage, prognosis aims to estimate remaining useful life (RUL) or time to failure. This capability is essential for transitioning from reactive to predictive maintenance, particularly in aerospace applications where operational safety and lifecycle optimization are paramount [70].

In vibration-based SHM, excitation sources play a critical role in generating dynamic responses sensitive to structural changes. These sources can include instrumented impact hammers, modal shakers, piezoelectric actuators, or embedded resonant devices. The choice of excitation depends on the frequency range, type of wave to be excited (e.g., bending modes, longitudinal waves), and the geometry of the structure. For AM lattice structures, localized excitation via surface-bonded piezoelectric elements is often preferred due to their scalability and compatibility with small features.

Following excitation and signal acquisition, the detection of damage does not stop at feature extraction. Rather, the extracted features—such as changes in natural frequencies, damping ratios, wavelet coefficients, or time-domain statistics—must be interpreted using a decision-making model. These models are typically data-driven and include supervised machine learning algorithms (e.g., support vector machines, neural networks), probabilistic classifiers (e.g., Gaussian mixture models), or threshold-based anomaly detection methods [67].

The use of features offers several advantages. They reduce dimensionality, enhance robustness to noise, and often provide physically meaningful indicators of damage progression. However, in some advanced applications, raw time-series or frequency-domain data can also be used directly as input to deep learning models such as convolutional neural networks (CNNs) or recurrent neural networks (RNNs), which automatically learn abstract representations of damage-related patterns. While this approach may eliminate the need for manual feature engineering, it requires large, well-labeled datasets and high computational cost—often impractical in real-world SHM deployments, especially for bespoke AM components.

Feature-based damage classification in SHM often employs supervised learning algorithms that learn decision boundaries from labeled examples. Among these, support vector machines (SVMs) are popular due to their ability to perform well in high-dimensional feature spaces with limited training data. Artificial neural networks (ANNs) have also been widely used, especially for capturing nonlinear damage patterns, though they require more extensive training data and are sensitive to overfitting. Probabilistic methods like Gaussian mixture models (GMMs) allow for uncertainty modeling, which can be useful in noisy or variable environments.

Principal Component Analysis (PCA) is a commonly used dimensionality reduction technique in SHM. It transforms high-dimensional feature sets into a reduced set of uncorrelated variables (principal components) that capture the directions of maximum variance in the data [70]. However, PCA assumes linear relationships between features and may not adequately capture nonlinear or localized damage patterns. It also relies on global variance, which may ignore subtle but critical features. These limitations motivate the use of nonlinear extensions such as Kernel PCA, t-SNE, or autoencoders, especially in systems with complex damage modes such as AM lattices.

For example, Worden and Manson [70] applied PCA to vibration-based damage

localization and demonstrated the utility of dimensionality reduction in detecting structural change. However, they also noted PCA's inability to resolve features in the presence of nonlinear damage evolution. More recent studies have proposed hybrid approaches that combine PCA with clustering or supervised classification for improved sensitivity and decision accuracy.

2.4.1 Overview of SHM and NDE Principles

Structural Health Monitoring (SHM) and Non-Destructive Evaluation (NDE) are two interrelated fields aimed at assessing the integrity and operational readiness of engineering structures without causing damage. While NDE is typically applied as an offline inspection technique during scheduled maintenance cycles, SHM extends this concept into real-time or periodic monitoring through embedded sensors or intelligent systems [67]. In both domains, the ultimate goal is to detect, locate, classify, and—when possible—predict the evolution of damage before catastrophic failure occurs.

Farrar and Worden [67] provided one of the foundational frameworks in this field, classifying SHM into five hierarchical levels: (1) damage detection, (2) localization, (3) classification, (4) severity assessment, and (5) remaining life estimation. Their structure is still widely adopted, but as Mousavi et al. [71] noted, practical implementation beyond detection is often limited due to data scarcity and inadequate feature robustness in complex systems.

Tibaduiza et al. [72] emphasized the integration of signal processing with classification algorithms to achieve Level 2 and 3 functionality. Their work utilized Principal Component Analysis (PCA) and Self-Organizing Maps (SOMs) to distinguish between various damage conditions. However, their study focused on metallic plates under laboratory conditions, limiting its generalizability to more intricate geometries like lattice structures.

Yang and Li [73] introduced a Bayesian decision framework for vibration-based SHM using wavelet packet features. While their method demonstrated high sensitivity in detecting damage in composite beams, it relied on assumptions of Gaussian-distributed features and prior knowledge of undamaged conditions. Such requirements are problematic in AM components, where the "healthy" state is often poorly defined due to embedded porosity and microstructural inconsistency.

The difference between SHM and NDE becomes more evident when considering the sensing infrastructure and intended application. Traditional NDE techniques, such as X-ray CT, ultrasonic pulse-echo, and eddy current inspection, offer high-resolution images or pointwise measurements but are limited to discrete inspections. In contrast, SHM leverages continuous monitoring through techniques such as piezoelectric sensing, guided wave interrogation, and modal analysis [74]. Cheraghi et al. used piezoelectric actuators and wavelet transforms to detect corrosion-induced degradation in pipelines, highlighting how real-time SHM can preempt the need for invasive NDE procedures.

Moreover, Dron et al. [75] and Pittner and Kamarthi [76] explored signal-based indicators such as kurtosis and wavelet energy for early damage detection. Their methods, while effective for conventional components, are constrained by the assumption of uniform geometry and repeatable signal conditions—assumptions rarely satisfied in lattice-based AM structures. These studies often omit how defect-

induced scattering or internal attenuation in porous lattices might obscure signal patterns or invalidate feature thresholds.

To summarize, SHM offers a broader, more proactive paradigm than traditional NDE, but its implementation is highly dependent on signal interpretation quality, environmental noise resilience, and system-specific tuning. The transition from feature extraction to reliable decision-making remains a challenge, especially for irregular geometries and novel materials. As such, the integration of SHM with advanced data processing methods and adaptive learning systems has become a key area of research—particularly for emerging domains like AM lattice structures, where embedded defects and inaccessible regions complicate conventional approaches.

2.3.2 Classification of damage state

There are five major levels in damage detection and prognosis. These levels are based on the answer to the following five questions [77]. Each damage detection study will vary depending upon which of these five question need to be answered.

- Level 1 - Damage detection - Is the damage present in the structure?

- Level 2 - Damage Analysis - What is the type of the damage?

- Level 3 - Damage quantification - What is the severity of the damage?

- Level 4 - Damage localization - What is the location of the damage?

- Level 5 - Damage prognosis - What is the useful life remaining?

2.3.3 Steps in damage detection

The damage detection explored and used here is based on the techniques of structural health monitoring which is used for on-line and active health monitoring. The steps involved in implementing a damage detection strategy are now discussed [78, 79].

Excitation source and response measurement

The first step in any damage detection strategy is to use a source to excite the structure. Exciting the structure is necessary to measure its response. Both undamaged and damaged structures will have different response to these excitations. Commonly used excitation sources in literature are vibration and ultrasonic methods. Vibration based SHM methods use low frequency (upto 20KHz) vibrations to measure global response of structure [80, 81]. In ultrasonic techniques, actuators (commonly piezoelectric) are used to send ultrasonic waves in the structure [82, 83].

Signal processing and feature extraction

Once the data has been acquired from the sensors, the next step is to process the data. This step includes data cleansing to filter noise and normalizing data to cater for any environmental variations [84]. In the next step, important information from the data is extracted, which effectively represents the state of structure. This process is called feature selection. The aim of feature selection is to reduce the dimensionality of the data and to use the features of the data that are most related

to the damage state of structure. The features chosen from the response signals which are sensitive to damage are also called damage features. The selection of the appropriate damage features from the signal is the most important step of any damage detection strategy. The most simple method of extracting useful information from signal is by using basic signal statistics such as mean and variance [79]. Other statistical features such as third and fourth centered moments known as skewness and kurtosis are also used as features. Kurtosis in particular is popularly used in condition monitoring [85, 75]. In the time domain, some of the features used for signal analysis are Normalized Root Mean Square Error between baseline signal and response signal [86, 87], correlation coefficients [88, 89, 90] and loss in temporal coherence [91, 88]. Features are also extracted by converting the time domain signal to frequency domain using Fast Fourier Transform (FFT) [92]. In time-frequency domain, some advanced signal processing techniques such as Short Time Fourier Transform (STFT) [93, 94], Empirical Mode Decomposition (EMD) and Hilbert-Huang Transform (HHT) [95, 96, 71] and features using Wavelet Transforms [76, 74, 73, 97].

Empirical Mode Decomposition (EMD)   EMD is a signal decomposition technique that adaptively breaks down non-linear and non-stationary signals into a set of intrinsic mode functions (IMFs). These IMFs isolate frequency components corresponding to local oscillatory modes in the signal. EMD has been used in SHM to extract features linked to structural damage with high temporal precision.

Hilbert–Huang Transform (HHT)   HHT combines EMD with the Hilbert Transform to compute instantaneous frequency and energy content of the signal. It enables localized time-frequency analysis, making it effective for detecting transient changes caused by damage. This technique is especially useful when conventional Fourier methods fail to capture non-stationary signal behavior.

Wavelet Transform   The Wavelet Transform provides a multi-resolution representation of the signal, capturing both time and frequency information simultaneously. It is particularly suited for detecting localized anomalies such as cracks or delaminations. Different wavelet bases allow tuning the transform to the nature of the damage and structural response.

Principal Component Analysis (PCA)   Principal Component Analysis (PCA) is a widely used unsupervised dimensionality reduction and feature extraction technique. It transforms the original data vector $\mathbf{x} = (x_1, x_2, \ldots, x_p)^T$ into a new vector $\mathbf{z} = (z_1, z_2, \ldots, z_p)^T$, where each z_i is a linear combination of the original variables and represents a principal component. The first principal component z_1 captures the direction of maximum variance in the data, with subsequent components z_2, z_3, etc., capturing the next highest variance orthogonally. This process effectively compresses the data while retaining the most informative structure, thereby simplifying downstream analysis such as clustering or classification.

In the context of SHM, PCA is employed to detect damage by identifying changes in the statistical structure of the monitored signals. Sharma [98] provides a foundational overview of PCA applications in multivariate systems, establishing the

theoretical basis for its use in engineering diagnostics. Tibaduiza et al. [72] applied PCA to reduce high-dimensional vibration signal data and combined it with self-organizing maps to classify damage states in composite structures. Their approach demonstrated high sensitivity in detecting subtle changes in signal behavior under varying damage conditions. Similarly, Yu et al. [99] conducted a parametric study on PCA's performance under different operational scenarios and sensor configurations, emphasizing its robustness and versatility across SHM systems.

While PCA is computationally efficient and interpretable, it has limitations. It assumes linear relationships between features and may not perform well if damage-related features lie in a non-linear subspace. Nonetheless, due to its simplicity and ability to reveal hidden structures, PCA continues to be a core preprocessing step in many SHM frameworks.

There are different studies which use the features of the signal such as amplitude and energy of the signal. [100, 101] have used time domain energy of the signal as the damage feature for damage detection. [102] used the magnitude changes in signal to measure the damage state of the structure. Energy of scatter signal was used as damage feature for damage detection in bridge structures by [103].

2.4 Damage classification models

Damage classification models play a pivotal role in structural health monitoring (SHM) and non-destructive evaluation (NDE), where the core objective is to detect, characterize, and predict damage in engineered structures before it leads to catastrophic failure [78, 104]. In many industrial sectors, including aerospace, automotive, civil infrastructure, and increasingly in additive manufacturing (AM) applications, these models help ensure safety, reduce downtime, and optimize maintenance schedules [105, 77].

The growing complexity of modern materials and designs—ranging from advanced composites to additively manufactured lattices—presents unique challenges for robust damage classification [106, 107]. Consequently, researchers have developed a variety of data-driven methods to interpret sensor signals (e.g., vibration, ultrasonic, acoustic emission) and map them to damage states [108, 109]. Generally, these methods fall into two overarching categories: **statistical classification models** and **machine learning classification models**. Within the machine learning category, neural networks have become particularly prominent due to their ability to handle complex, high-dimensional data [110].

This chapter focuses on the landscape of damage classification models, detailing the main approaches, their theoretical underpinnings, and examples of their use in SHM. Special attention is paid to neural networks in the context of machine learning classification models.

2.4.1 Statistical Classification Models

Overview

Statistical classification methods are typically grounded in probability theory, where the observable features of a structure (for example, amplitude of vibration modes or ultrasonic signal patterns) are modeled as random variables with underlying sta-

tistical distributions [111, 112]. The classification task then involves assigning new observations to a damage state based on likelihoods or posterior probabilities.

In practice, these methods assume that the feature space of damaged and undamaged states can be differentiated by analyzing probability distributions. They often work well in scenarios where the feature distributions are reasonably well-behaved (for example, unimodal Gaussian or mixtures of Gaussians) and where the physical system does not exhibit extreme nonlinearity [113].

Gaussian Mixture Models (GMM)

One popular approach is the **Gaussian Mixture Model (GMM)**. Here, each damage class is represented by a combination of Gaussian components. During classification, the model computes the probability that a given observation (feature vector) was generated by one of these Gaussians. The class with the highest posterior probability is assigned to the new observation [111].

For example, in a vibration-based SHM scenario, one might extract features such as natural frequencies or mode shapes and fit separate GMMs for "healthy" vs. "cracked" states [78]. If a newly measured feature lies closer to the "cracked" distribution in a probabilistic sense, the GMM signals the presence of damage.

Regression Models and Bayesian Inference

Regression models, such as linear or logistic regression, are also used for damage classification tasks [113]. In logistic regression, the probability of damage is modeled via a logistic function of a linear combination of features. This approach can be straightforward, often yielding interpretable parameter estimates indicating which features most strongly predict damage.

Bayesian inference extends these ideas by incorporating priors on model parameters, thus allowing uncertainty quantification and dynamic updating of damage probabilities as new sensor data becomes available [112]. Bayesian methods are particularly attractive when data is limited or noisy, since priors can mitigate overfitting and guide classification decisions.

2.4.2 Machine Learning Classification Models

2.4.3 Overview

While statistical methods are powerful, many contemporary SHM applications generate high-dimensional, multimodal data that can be difficult to model with purely statistical approaches [108, 84]. Machine learning (ML) methods, by contrast, often excel at learning complex decision boundaries in feature space, even when the underlying physics is only partially understood [110].

Classic ML classifiers include:

- **Decision Trees**: Build a hierarchical tree by splitting on features. Easy to interpret but prone to overfitting.

- **Random Forests**: An ensemble of decision trees, improving robustness and generalization.

- **k-Nearest Neighbors (k-NN)**: Relies on distance metrics; simplest if dimensionality is not too large.

- **Support Vector Machines (SVMs)**: Maximizes the margin between classes; can use kernels for nonlinear separation [114].

2.4.4 Neural Networks for Damage Detection

Among ML approaches, **neural networks**—especially deep neural networks—have gained significant traction in SHM due to their ability to capture highly nonlinear relationships and discover hidden features from raw sensor data [115, 116]. Neural networks come in various architectures, each well-suited to different data types and tasks:

Artificial Neural Networks (ANNs)

Artificial Neural Networks (ANNs) are computational models inspired by the brain, composed of layers of interconnected neurons (weights) that learn mapping functions from inputs to outputs. In **classification neural networks**, the final layer typically outputs class probabilities (for example, healthy, minor damage, major damage). Training is supervised, relying on labeled datasets of structural responses [117].

In damage detection tasks, a classification ANN might receive time-series signals or spectral features as input, passing them through multiple layers of transformations until it produces a probability vector over different damage categories. Because these networks can capture complex, nonlinear relationships, they are increasingly used in scenarios where simpler classification methods struggle to scale.

Multilayer Perceptrons (MLPs)

MLPs are the simplest feedforward neural networks, comprising multiple fully connected layers. In a typical SHM application, carefully engineered features (for example, wavelet coefficients from ultrasonic signals) feed into an MLP, which learns a mapping from these features to discrete damage classes (e.g., healthy, minor crack, major crack) [117].

Convolutional Neural Networks (CNNs)

CNNs employ convolutional filters to automatically learn spatial (or spatiotemporal) patterns from data arranged as images or 2D/3D arrays. This is particularly useful when ultrasonic scans, thermographic images, or time-frequency spectrograms are used for damage detection [118]. For instance, if a 2D representation of a guided wave signal indicates a crack, CNN filters can discover these crack-related patterns without extensive manual feature engineering.

Autoencoders

Autoencoders are specialized networks that learn to reconstruct the input through a bottleneck layer of reduced dimensionality. By training on "healthy" data only, an autoencoder will show high reconstruction error when faced with out-of-distribution

data that represents damage [119]. This approach can be effective when obtaining labeled damage data is challenging.

Applications of Neural Networks in SHM Neural Networks (NNs), particularly Artificial Neural Networks (ANNs) and their deep learning counterparts, have found extensive applications in structural health monitoring due to their capacity to model complex, non-linear relationships in high-dimensional sensor data. These models can learn from historical signals and automatically extract damage-sensitive features without requiring manual feature engineering. For instance, Tarassenko et al. [120] utilized ANNs for novelty detection to identify abnormalities in monitored structural states, demonstrating the potential of neural models in detecting subtle deviations from healthy baselines. In more advanced implementations, Convolutional Neural Networks (CNNs) have been employed for processing time-frequency spectrograms of ultrasonic or vibration signals. Modarres et al. [121] showed that CNNs can classify damage types from visual patterns in SHM datasets with high accuracy, making them suitable for image-like signal representations such as C-scans or STFT plots.

Autoencoders have also emerged as a popular architecture, particularly for anomaly detection in situations where damaged-state data is scarce. By training autoencoders solely on data from undamaged structures, the model learns to reconstruct healthy signal patterns. Pathirage et al. [?] illustrated that the reconstruction error can be used as a damage index, where higher error correlates with greater deviation from the undamaged state. These neural architectures are particularly useful for SHM of complex systems like composite structures, aircraft wings, or lattice topologies, where traditional linear models may struggle.

Despite their advantages, neural networks pose several limitations in SHM applications. One major challenge is the requirement for large volumes of labeled training data, which is often difficult to obtain, especially for damaged states in safety-critical aerospace and civil structures. Jia and Li [?] emphasized the issue of data scarcity and the need for data augmentation, simulation-based training, or transfer learning to overcome this bottleneck. Additionally, overfitting is a common concern in neural networks, particularly when training on small datasets. Techniques such as L2 regularization, dropout, and cross-validation are typically required to improve model generalization [122].

Interpretability remains another critical limitation, as deep networks often act as "black boxes," making it difficult to understand the rationale behind specific damage predictions. This is a serious drawback in fields where traceability and explanation of model decisions are necessary for certification and safety assurance. Furthermore, the computational cost associated with training and deploying deep neural networks can be significant, particularly for real-time or embedded SHM applications. While the advancement of hardware accelerators such as GPUs and TPUs has mitigated this to some extent, energy and processing constraints are still important considerations for onboard SHM systems.

2.4.5 Challenges of Machine learning models

Neural networks offer the benefit of feature learning—the capacity to discover relevant representations directly from raw signals. However, several key considerations

apply:

- **Data Scarcity**: Reliable damage classification often requires large labeled datasets. In many real-world SHM applications, damage events are rare or costly to replicate [123].

- **Overfitting and Generalization**: Complex networks can overfit smaller datasets. Methods such as data augmentation, cross-validation, and weight regularization help address this challenge.

- **Interpretability**: Deep neural networks are often considered "black boxes," posing challenges for safety-critical components.

- **Computational Resources**: Training large networks demands significant computational power, though modern GPUs have made this more accessible.

Despite these challenges, neural networks have shown promise for real-time damage detection, enabling the classification of subtle or intricate patterns that might be overlooked by purely statistical approaches [109, 110]. As sensor technology advances and generates richer datasets, deep neural networks are poised to play an increasingly central role in future SHM systems.

To summarize, the damage classification models are fundamental to ensuring the reliability of modern engineering structures, particularly in safety-critical industries. Statistical classification methods, such as Gaussian Mixture Models, regression, and Bayesian inference, excel when feature distributions are well-understood. Machine learning approaches, including neural networks, thrive in more complex or higher-dimensional scenarios, as they can discover intricate data patterns.

Neural networks range from MLPs for feature-based classification to CNNs for image-like data, LSTMs for time-series analysis, and autoencoders for anomaly detection. While each architecture has unique strengths and weaknesses, collectively they provide a robust set of tools for identifying and classifying damage. Ongoing research focuses on making these methods more data-efficient, interpretable, and generalizable—necessary steps for widespread adoption across fields like additively manufactured structures, where damage states can be highly variable.

2.6 Research Gaps

A critical review of the literature presented in this chapter reveals several limitations in the current approaches to structural health monitoring (SHM) and damage classification, particularly in the context of additively manufactured (AM) lattice structures. While a variety of sensing techniques, signal processing methods, and classification models have been proposed, most of these approaches are designed for traditional monolithic structures and do not adequately address the complexities introduced by AM geometries.

Firstly, existing SHM techniques—such as those based on vibration signals, wavelet transforms, and piezoelectric sensing—have largely been developed and validated for metallic plates, beams, and composite laminates [74, 72, 73]. These methods assume geometric uniformity and rely on consistent boundary conditions, which do not hold for lattice structures with distributed struts and internal voids.

The wave-based techniques demonstrated by Cheraghi et al. [74] and the Bayesian classification approaches by Yang and Li [73] are effective for continuous geometries but have not been extended to discontinuous and porous domains typical of AM designs.

Secondly, many of the damage detection frameworks are heavily baseline-dependent. They require either a known undamaged state for comparison or rely on handcrafted features that are sensitive to geometric and material inconsistencies [71, 76]. In AM components, where process-induced defects such as porosity and incomplete fusion are inherent, obtaining an accurate and representative baseline is impractical. Baseline-free or unsupervised approaches remain underexplored.

Third, the classification models reviewed—such as those in Jameel et al. [124] and Tarassenko [109]—are generally trained and validated on clean, well-structured datasets. These models often assume feature separability and class consistency, conditions that are rarely satisfied in AM lattice components due to their high intra-class variability and limited dataset availability. The use of traditional classifiers such as SVM, k-NN, and even neural networks in these contexts may lead to poor generalization without appropriate regularization, augmentation, or domain adaptation techniques.

Another key limitation in the literature is the overreliance on global features such as natural frequencies, spectral energy, or modal shifts [72, 75]. These features, while useful in detecting severe damage or stiffness loss, are not sensitive to small, localized defects like strut cracking or node detachment in AM lattices. Localized indicators and high-resolution sensing strategies are needed to detect early-stage damage in such complex geometries.

Moreover, guided wave-based techniques, though promising in flat or shell-like structures, face significant challenges when applied to AM lattices. The geometric complexity leads to scattering, wave mode conversion, and attenuation, reducing diagnostic resolution [74]. There is little evidence in the literature of successful calibration or deployment of such methods within strut-dominated architectures.

Finally, there is a distinct gap in integrating structural modelling with SHM. While many studies focus on signal processing and pattern recognition, they do not leverage the mechanical behavior predicted by numerical models of AM lattices. A combined approach—where structural simulation informs signal interpretation or aids in feature design—has the potential to improve both sensitivity and interpretability but remains largely absent from current research.

These gaps highlight the need for damage detection and classification frameworks that are specifically tailored to AM lattice structures. Such systems must incorporate geometry-aware sensing strategies, robust feature extraction under stochastic conditions, and machine learning models capable of generalizing from limited, noisy datasets. Addressing these challenges is essential for enabling reliable SHM in the next generation of AM aerospace and structural components.

Linking Research Gaps to Thesis Objectives

1. Lack of SHM Studies on Additively Manufactured Lattice Structures Although SHM using ultrasonic techniques is well-established for conventional metallic and composite structures [125, 126, 127], the literature lacks dedicated research focused on additively manufactured (AM) lattice structures. Their

complex geometries, especially in strut-based designs, pose unique challenges for wave propagation and damage detection. This research directly addresses this gap by investigating the behavior and interaction of ultrasonic waves within such lattice configurations, as pursued under **Objective 1**, which aims to understand wave propagation in AM lattice geometries.

2. Absence of Integrated Experimental and Numerical Methodologies
Most SHM studies rely either on simulations or limited physical testing, often lacking rigorous experimental-numerical validation—especially for structures with micro-defects like porosity, delamination, or strut fracture. This research fills this methodological gap by developing and validating a complete SHM framework using both experimental setups and numerical simulations, informed by ultrasonic response and sensor data. This work aligns with **Objective 2**, which focuses on developing and validating a methodology for damage detection and quantification in lattice structures using piezoelectric sensors and signal processing techniques.

3. No Effective Damage Localization Approaches for Lattice Structures
Damage localization remains a challenge in AM lattices due to the inherent signal scattering and geometrical irregularities within 3D cellular architectures. Traditional localization techniques used for plates or beams are not directly transferrable. In response, this study develops a robust localization strategy using a sensor array-based approach tailored to the complexity of lattice geometries, integrating both simulation and experimental validation. This addresses **Objective 3**, which focuses on establishing a methodology for localizing damage in lattice structures.

4. Limited Use of Machine Learning in Ultrasonic-Based Lattice SHM
Machine learning (ML) models have demonstrated utility in SHM of composites and metallic structures, yet their application to ultrasonic data from AM lattice structures remains limited. The current study bridges this gap by integrating ML algorithms for classification and quantification of damage using extracted ultrasonic features. This directly supports **Objective 4**, which explores the application of ML to improve the accuracy and efficiency of damage characterization. The evaluation of these methods on 3D lattice configurations further advances **Objective 5**, which focuses on assessing scalability and real-world applicability.

5. No Analytical Models for Ultrasonic Transmission in Lattice Structures A theoretical gap exists in modeling ultrasonic wave transmission through lattice geometries. Conventional wave propagation models assume continuous media and fail to account for the scattering and attenuation effects inherent to lattice configurations. This thesis develops an analytical formulation for ultrasonic wave transmission specific to lattice geometries, presented in **Chapter 5**, thereby strengthening the theoretical foundation for wave-based SHM in support of **Objective 1**.

2.5 Conclusion

A detailed literature review was undertaken in the areas of additive manufacturing and lattice structures. It was identified that various inherent defects in lattice structures may act as stress concentrators and lead to cracks or fractures of lattice struts. With growing applications of lattice structures in various industries i.e. aerospace, automotive, medicine, etc. it may become essential to have methodologies for damage characterization of such structures. Due to non-destructive nature of ultrasonic testing and ease of setting up ultrasonic systems, it can be used for testing lattice structures. Fundamentals of structural health monitoring, damage detection, and various signal processing techniques were discussed in the literature review. Statistical and machine learning damage classification models were also covered in the review. Based on these findings and an exhaustive literature review on SHM and damage detection, the research methodology was designed.

Chapter 3

Methodology

3.1 Introduction

This chapter presents the overall methodology adopted to achieve the research aims outlined in Chapter 1. Rather than reiterating the objectives, this section focuses on structuring the sequence of activities that led to the development, validation, and extension of damage detection techniques in lattice structures using ultrasonic testing and machine learning.

The novelty of this methodology lies in integrating analytical modelling, numerical simulations, experimental testing, and data-driven techniques in a cohesive pipeline tailored for complex lattice geometries. Particular emphasis is placed on how ultrasonic wave propagation is influenced by structural damage and how this phenomenon can be harnessed for diagnostic purposes.

The chapter is structured to follow a logical sequence of investigations: beginning with analytical evaluation of ultrasonic transmission through idealized lattice unit cells, followed by numerical modelling and classification of damage states using machine learning. Experimental validation complements these efforts. Subsequently, the study advances toward damage localization and scalability through application to 3D lattice structures. The methodologies described here form the backbone of the research contributions made in later chapters.

3.2 Research Design

The methodology used to achieve the objectives of this study are now presented. A flow chart of the methodology is given in Figure. 3.1. At the onset of this study, an analytical evaluation of a lattice structure is carried out to estimate ultrasonic transmissions in a lattice structure. This analytical work will also be used to demonstrate the effect of damage on ultrasonic transmission in a lattice structure. In the next part, a detailed study is undertaken for damage detection and quantification in a lattice structure. This study is conducted using a 2D lattice structure. Numerical simulations are used to develop a methodology that is validated by experimental work. Machine learning is used for classification of damage in the structure. Subsequently, a detailed damage localization study is carried out using both numerical simulations and experimental investigations. Finally, a 3D lattice structure is analyzed for damage characterization. The salient parts of the methodology are now discussed as follows.
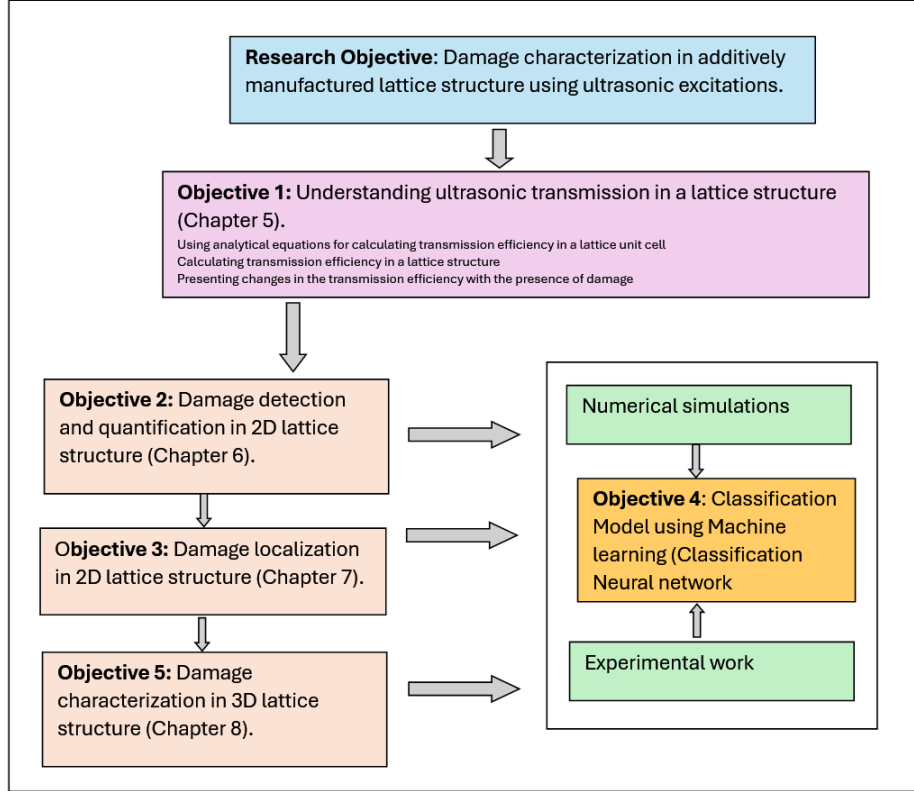
Figure 3.1: Flowchart of methodology

3.2.1 Analytical study

The aim of analytical study is to provide a proof of concept and understanding of ultrasonic transmission in the lattice structure. The analytical study involves using formulations to calculate the ultrasonic transmission coefficients in a lattice unit cell which is referenced and presented in Chapter 5. The lattice unit cell will form the building block of the structure studied for damage characterization. The steps involved in the analytical study are as follows.

- Using equations to calculate the ultrasonic transmission and reflection coefficients in a lattice unit cell.

- Calculate the transmission efficiency of the ultrasonic wave in the lattice unit cell.

- Evaluating the transmission efficiency in lattice structure using the results of the lattice cell.

- Showing the effects on transmission efficiency in the presence of damage.

- Provide an efficient method to estimate the transmission efficiency in different lattice structures.

- Present analytical formulations for different configurations of lattice unit cells.

The analytical study provides an understanding of ultrasonic transmission in strut type lattice structures and offers an insight on the effect on transmission with the presence of damage.

3.2.2 Damage detection and quantification

The analytical study provides an understanding of changes in ultrasonic transmission in the presence of damage. To characterize damage in the structure, a detailed numerical and experimental study is conducted. The methodology for damage detection and quantification is as follows.

- A nine cell 2D lattice structure is designed based on the unit cell solved in the analytical work.

- The damage considered for the study is breaking of struts. Up to ten damaged struts are considered for this study with an aim to quantify the severity of damage in the structure.

- A numerical model is designed and simulated in Abaqus with a large sample size to collect the response for both undamaged and damaged structures.

- Raw data from numerical simulations is processed to acquire features of data sensitive to damage.

- A classification neural network is trained to classify the state of damage in the structure.

- Experiments are conducted to validate the methodology.
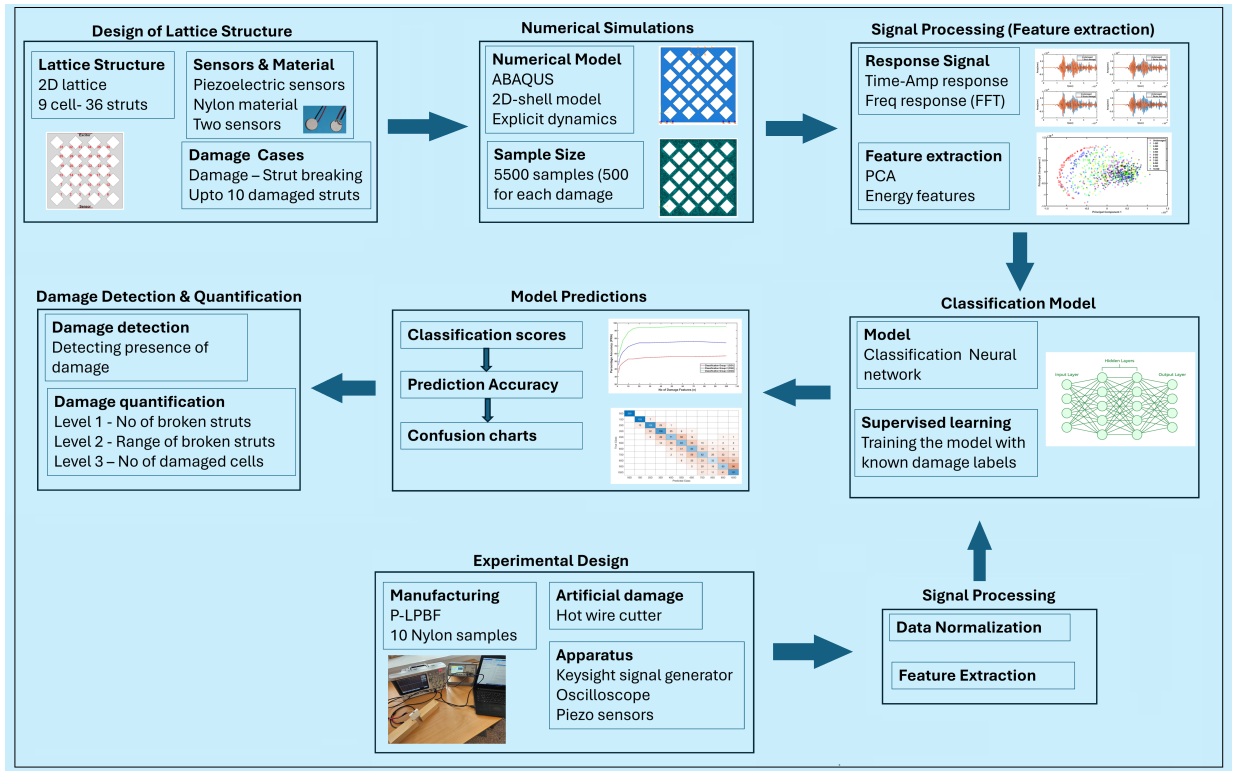
Figure 3.2: Process flow of damage detection and quantification

3.2.3 Damage Localization

Damage localization study involves estimating the location of damage in the structure. Localizing the damage in a complex lattice structure is challenging. The methodology for damage localization is described below.

- The 2D lattice structure is considered for damage localization study.

- Localization of up to three damaged struts is undertaken in this study.

- Due to the complexity of problem, localization study is first done on a smaller four cell lattice structure.

- Numerical simulations are used to test various localization problems.

- A strategy of zoning structure is used for effective damage localization.

- Neural network model is used for classification of data.

- Experiments are conducted to validate the methodology.
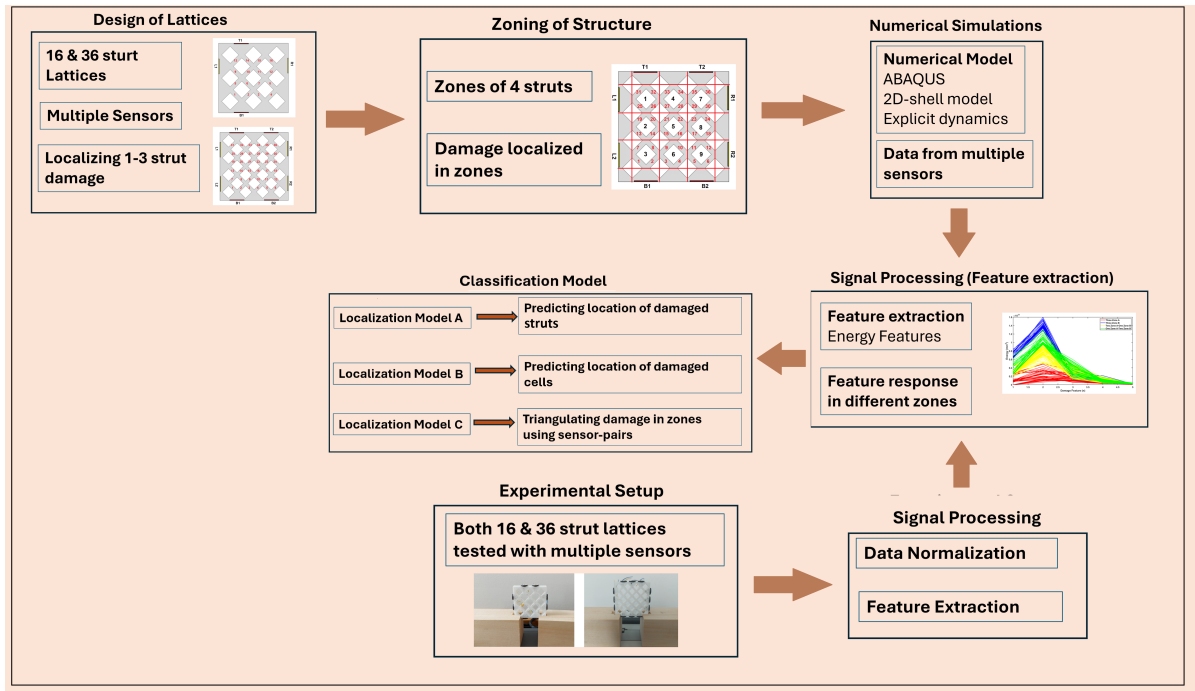
Figure 3.3: Process flow of damage localization

3.2.4 3D Lattice structure

After developing and validating a methodology for damage detection, quantification, and localization on a 2D lattice structure, it is applied to a 3D lattice structure. Analyzing a 3D lattice structure will be useful to extend the application of daamge detection methodologies to real life structures being used in various applications. 3D lattice structures could be formed with various configurations of unit cells some

common being body-centered cubic (BCC), face-centered cubic (FCC), and tetrahedral designs, each with unique mechanical properties. For this particular study, a BCC lattice cell is used to form a 8-cell lattice structure. Each cell is formed with eight struts making a total of sixty four struts in the structure. Both numerical simulations and experimental testing of the 3D lattice structure is done to validate the methodologies developed for 2D lattice structure.

3.3 Conclusion

This chapter outlines the basic methodology adopted to achieve the research aims of damage characterization in a lattice structure. A detailed methodology for damage detection, quantification and localization is developed using numerical simulations and a neural network was used as damage classification model. The numerical study is followed by validation through experimental work. The methodologies are first developed on a 2D lattice structure and are then applied to a 3D lattice structure. The details of materials, sensors and methods used for numerical and experimental work as well as structure of classification model are given in the next chapter.

Chapter 4

Numerical and Experimental Methods

4.1 Introduction

This chapter presents the detailed numerical and experimental methods employed to characterize damage in lattice structures using ultrasonic-guided waves and machine learning. These methods form the foundation of the study, supporting the development, training, and validation of the proposed structural health monitoring (SHM) framework introduced earlier.

The primary aim of this chapter is to describe the tools, techniques, and configurations that make the results in subsequent chapters replicable and scientifically rigorous. Both simulation-based and experimental approaches are outlined in an integrated fashion to establish a validated methodology for damage detection and quantification.

A numerical modelling strategy is developed to simulate ultrasonic wave propagation through additively manufactured lattice structures under various damage scenarios. Experimental methods are used in parallel to validate these simulations through real-world measurements. To support generalizability and robustness of the classification model, signal processing and feature extraction techniques are introduced, culminating in the development of a supervised learning algorithm for multi-class damage identification.

The chapter is organized as follows. Section 4.2 gives the details of the lattice structure, sensors, and materials chosen and used for this work. Section 4.3 outlines the setups used for numerical simulations, experimental work, and data collection for damage detection and quantification. In section 4.5 the details of different signal processing techniques that are explored in this work are given along with feature extraction techniques. Details of the classification model are given in section 4.6. Finally, the experimental analysis methods are discussed in section 4.7.

4.2 Structure, Sensors and Materials

In this section, details of the lattice structure designed for this study are given. Properties of lattice structure, piezoelectric sensors, and materials used for this research are also provided in this section.

Lattice structure design

Lattice structure is built from the multiplication of its unit cell which acts as its building block. A four strut lattice unit cell was designed for this study. Four mutually perpedicular struts were designed with each stur having a length of 7mm and width of 2.5mm. The choice of four strut unit cell was driven by the use of a beam crossing for analytical study as presented in Chapter 5. The beam crossing forms a four strut unit cell. Using this unit cell, a nine-cell lattice structure was formed with 36 struts to study damage detection and quantification. The choice of number of unit cells was arbitrary and was selected optimally to reduce computational and manufacturing costs while giving a well populated structure for damage characterization. The damage considered for this study is the breaking of the struts in lattice structure. Strut type lattice structures are formed with large number of struts with strut thickness only a small percentage of overall size of structure. The significance of this form of damage in lattice structures is extensively discussed in Chapter 2. The struts could crack or break due to manufacturing defects and operational loads. Since there are large number of struts in the structure, progressive damage could lead structural degradation and failure [128]. Therefore, damage quantification can provide a useful tool to determine the amount of damage present in the structure and whether it can be kept in service. The unit cell of structure which was used to form the structure along with the lattice structure is shown in Figure 4.1. A 1.5mm crack was modeled in the structure to simulate the breaking of a strut.The size of the crack was chosen due to the limitation of the hot wire cutter which was used to impart artificial damage in manufactured samples. The minimum damage resulting from hot wire cutter was close to 1.5 mm. Damage is also indicated in Figure 4.1.
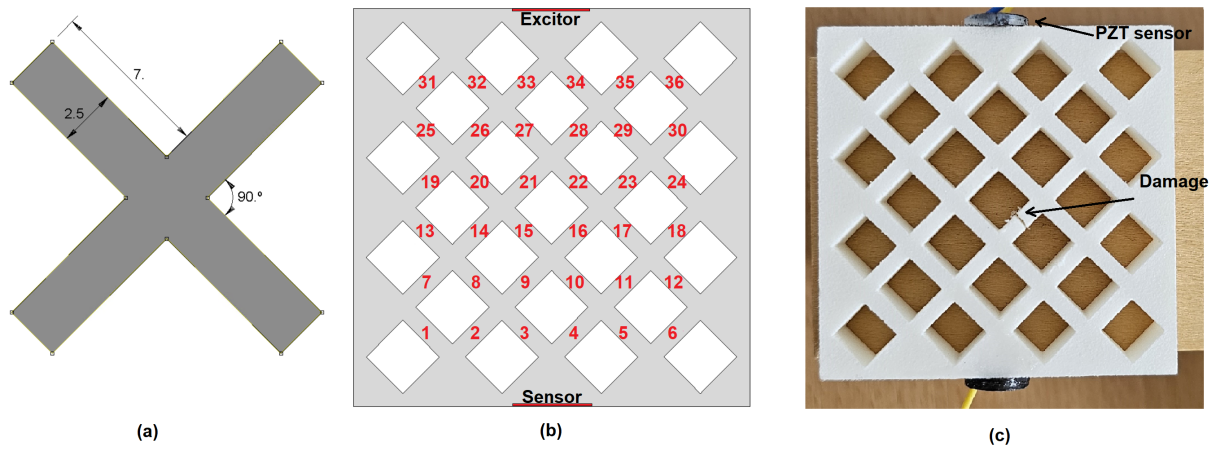
Figure 4.1: Lattice structure chosen for the present study (a) unit cell of chosen lattice structure (all units are mm), (b) 36 strut lattice structure (50x50mm) designed for numerical study (c) Lattice manufactured for experimental work, artificial damage induced on one strut is shown

Sensor selection and configuration

Piezoelectric (PZT) sensors were used to excite ultrasonic waves inside the structure, and the response signal was measured at the opposite end of the structure. The piezoelectric sensor used for this work is Steminc Piezo ceramic disc SMD10T2R111WL

with sensor material SM111 [12]. The sensor and its material properties are given in Figure 4.2. The sensors were 10 mm in diameter and 2 mm in thickness, with a resonant frequency of 215 kHz in radial mode and 1 MHz in thickness mode. Both these modes are excited when an electric excitation is applied to the sensors. Since, bulk response of waves is being measured, both the wave modes add to the frequency excitation and amplitude and were modeled in a similar fashion in numerical modeling as well.

Electromechanical coupling coefficient		K_p	0.58
		K_t	0.45
		K_{31}	0.34
Piezoelectric constant	$\times 10^{-12}$ m/v	d_{33}	320
		d_{31}	-140
	$\times 10^{-3}$ Vm/N	g_{33}	25
		g_{31}	-11
Mechanical Quality Factor	-----	Q_m	1800
Dielectric Constant	@1KHz	$_\varepsilon T_{33/\varepsilon 0}$	1400
Density	g/cm^3	r	7.9

Figure 4.2: Piezoelectric sensor with its material properties [12]

Material properties

The lattice structure was fabricated using Nylon-12, a widely used polymer in additive manufacturing due to its favorable mechanical properties, low cost, and excellent ultrasonic transmission characteristics [129]. Its ductility also allows controlled introduction of artificial damage without causing brittle failure. Nylon-12 was selected specifically to accommodate both the structural requirements of the lattice and the practical needs of ultrasonic testing.

To characterize the mechanical properties of the material, uniaxial tensile tests were conducted on standard dog-bone specimens fabricated from the same batch of Nylon-12 used for the lattice samples. The tests were carried out using an Instron 5969 universal testing machine in accordance with ASTM D638 [130]. Five specimens were tested to establish repeatability. The average elastic modulus was found to be 1620 ± 50 MPa, and the material density was measured as 949 ± 7 kg/m^3. These values were used in both numerical simulations and for evaluating experimental uncertainty. The standard deviation reported reflects the variation observed across the five specimens. The results of one of the samples are shown in Figure 4.3
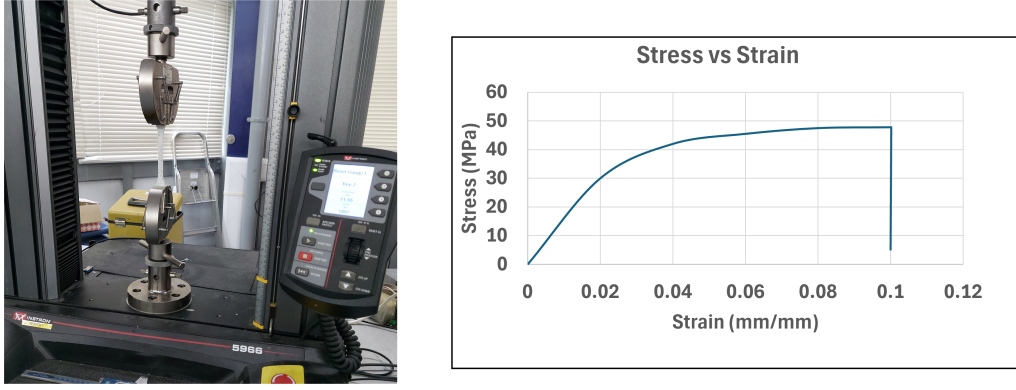
Figure 4.3: Tensile testing of Nylon Samples

4.3 Numerical Methods

Numerical simulations form an important part of this work. The methodologies for damage characterization are first developed using data from detailed numerical simulations. This section provides details for numerical modeling. The details are provided for 2D lattice structure and similar methods were used for 3D simulations as well.

4.3.1 Model Setup and Excitation

The lattice structure was modeled numerically in `ABAQUS/Explicit` to simulate ultrasonic wave propagation and structural response under damage scenarios. An explicit dynamic solver was selected due to its superior performance in solving short-duration, high-frequency wave problems without the need for complex convergence controls. This approach is widely recommended in time-domain simulation of guided waves in SHM applications due to its computational efficiency and accuracy for transient loading problems [131, 132].

The geometry modeled was identical to the experimental lattice, a 3×3 array of unit cells with a total of 36 struts as shown in Figure 4.1. A planar shell model was created using 2D geometry extruded into shell elements with a thickness of 10 mm, consistent with the fabricated specimen. Material properties of Nylon-12 were assigned to the model based on tensile test results discussed above.

A piezoelectric actuator was simulated by applying a prescribed displacement at one end of the structure, representing the effect of an attached PZT sensor. The excitation was applied as an *in-plane displacement* in the radial as well as thickness direction, corresponding to the 215 kHz resonance of the selected sensor (SMD10T2R111WL). Fixed boundary conditions are used at the bottom end of the sample. The boundary conditions are also consistent with the conditions used in the experimental set-up. Loading and boundary conditions are shown in Figure 4.4.

The waveform applied was a **3-cycle Hanning windowed sinusoid** centered at 215 kHz as shown in Figure 4.4. This signal shape is commonly used in SHM to achieve a balance between frequency localization and time compactness, minimizing reflections and spectral leakage [133]. The choice of 3 cycles ensures sufficient energy while maintaining temporal resolution, which is critical in distinguishing wave

packets reflected from damaged regions.

Displacement amplitude was scaled to approximate the actuation effect of a 10V PZT sensor, though exact electro-mechanical coupling was not modeled. Instead, the excitation was imposed kinematically using displacement boundary conditions, which is a validated simplification in SHM simulation literature [132]. The amplitude is calculated by using Equation 4.1 for a voltage of 10V that is used for sensors in the experimental setup.

$$\Delta L_{long} = d_{33}V \tag{4.1}$$

$$V = -\frac{4g_{33}t}{\pi D^2}F \tag{4.2}$$
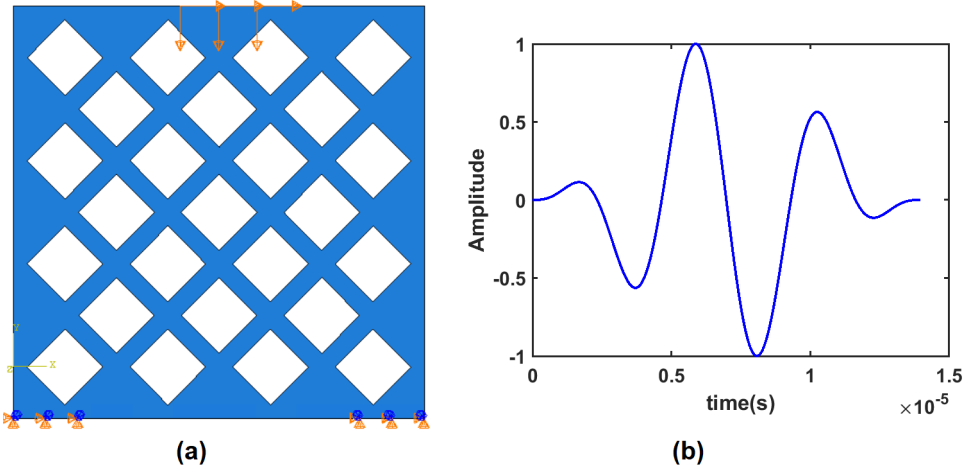
Figure 4.4: (a) Boundary and forcing conditions (b) 3-cycle excitation wave with central frequency of 215 kHz

Meshing and Solver Settings

The numerical model of the lattice structure was discretized using 8-node linear brick elements with reduced integration (C3D8R) in `ABAQUS/Explicit`. This element type offers a good balance between computational efficiency and accuracy for wave propagation simulations. Reduced integration minimizes volumetric locking and allows proper wave transmission, provided the mesh is sufficiently refined. To resolve ultrasonic wave propagation accurately, the mesh density was guided by the wavelength of the 215 kHz excitation signal. The wavelength λ was calculated using the relation $\lambda = v/f$, where $v = \sqrt{E/\rho}$. With an elastic modulus of 1620 MPa and a density of 949 kg/m^3 for Nylon-12, the longitudinal wave speed is approximately 1308 m/s, yielding a wavelength of approximately 6 mm.

A mesh size of 0.25 mm was selected, corresponding to 24 elements per wavelength. This satisfies the widely accepted guideline of using at least 20 elements per wavelength in ultrasonic simulations to avoid numerical dispersion and artificial attenuation [132]. Mesh convergence was confirmed by observing that further reduction in mesh size did not significantly alter the response amplitude at the receiver node as shown in Fig. 4.5. The simulation was run for a total time of 0.0004 seconds. ABAQUS automatically computed a stable time increment of approximately

6.66×10^{-8} seconds, based on the Courant condition and material properties. This resulted in approximately 6000 time steps, which provided sufficient resolution to capture wave propagation and reflections.

Ultrasonic actuation was applied as a prescribed in-plane displacement at the actuator location. The signal followed a 3-cycle Hanning-windowed sinusoid centered at 215 kHz. The response is recorded as time-amplitude response signal at the sensor location. The resultant displacement magnitude at the sensor surface was extracted at all time steps.
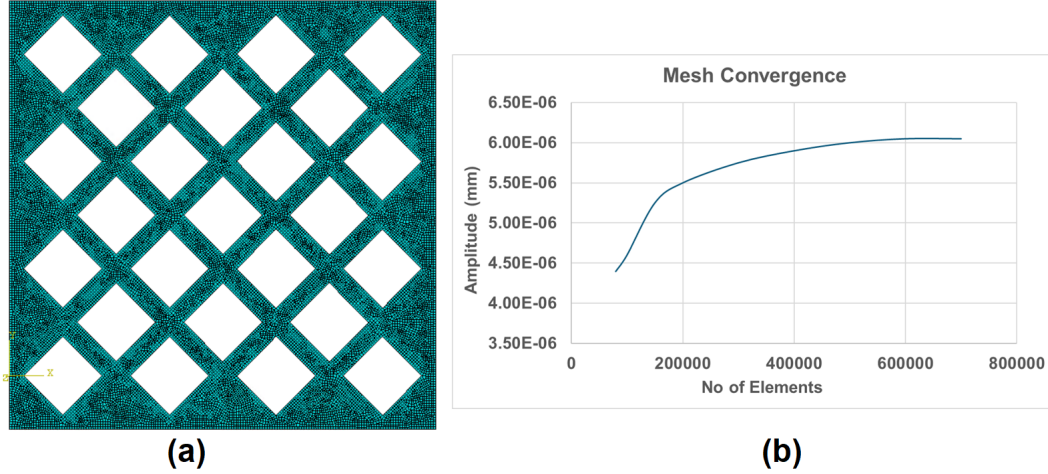
Figure 4.5: (a) Representative mesh with element size of 0.25mm (b) Mesh convergence

Modeling uncertainties

To improve the robustness and generalization of the machine learning-based damage classification framework, uncertainty was introduced into the numerical simulations to reflect realistic variability found in experimental conditions. This modeling accounts for minor deviations in both material properties and sensor placement, which are common in practical structural health monitoring (SHM) implementations. To make the simulations match closely with the real structures, two type of uncertainties are also included in the numerical model (a) variation in material properties (b) variation in sensor locations. Variation in material properties is evident from experimental measurements of tensile testing as given in section 4.2 with mean and standard deviation known. Piezoelectric sensors are installed to the structure using adhesive. The process of installing the sensors is prone to errors and can result in mispositioning of sensors from its central locations. Normal distribution of these uncertainties are included in the damage classification. Uncertainties were randomly assigned from the normal distribution to the samples in the numerical study. The uncertainty in sensor location is modeled with the normal distribution of $\mathcal{N}(0, 2^2)$ as shown in Fig. 4.6. The maximum value of 2mm for error in sensor location is large enough to cater for human error in installing sensors. The uncertainties were randomly assigned to the samples in numerical simulations
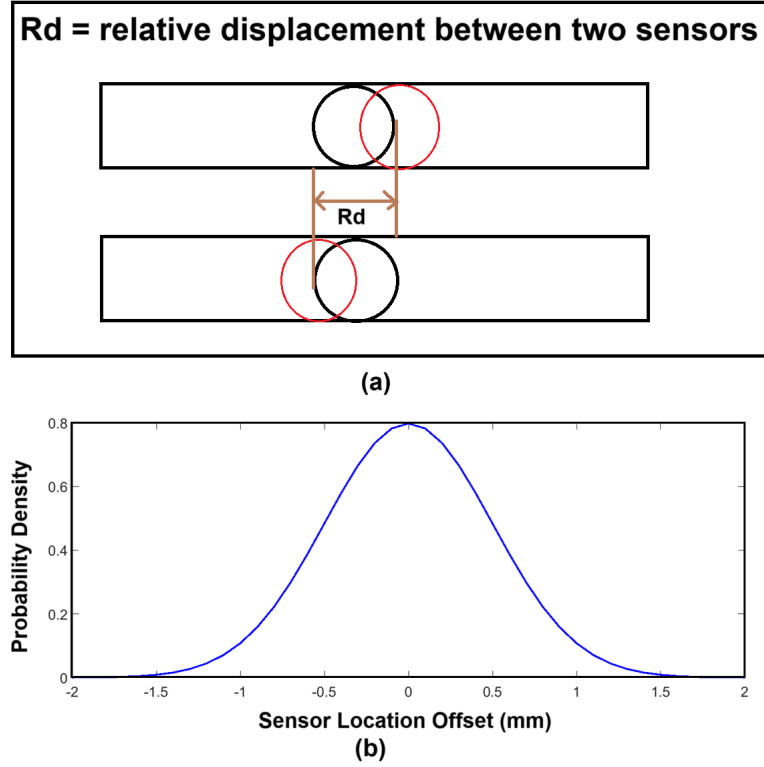
Figure 4.6: (a) Uncertainty in sensor location modeled in numerical simulations (b) Uncertainty modeled as a Gaussian distribution

4.4 Experimental testing Setup

The overall experimental setup is shown in Figure 4. A Keysight 33512B arbitrary waveform generator was used to generate a steady-state sinusoidal waveform at a specific frequency, and a DSOX2014A oscilloscope was used to digitize the signals using a sampling frequency of 9.6 MHz, with an average of 32 measurements to increase the signal-to-noise ratio. A total of 10 samples of lattice structures were manufactured using the Polymer-laser powder bed fusion (P-LPBF) method in a controlled laboratory setup. Sensors were installed on the structure using cyanoacrylate glue to give a strong adhesive bond. Artificial damage was induced to the structure using hot wire cutter.

4.5 Signal Processing and extracting Damage Features

Signal processing is a major step in any damage detection study. Once the raw data is collected, the challenging step is interpreting the data and processing it to extract useful information. The useful information in the context of damage detection are features in the data which are sensitive to the damage. Identifying these features of data is critical in developing a robust model.

A representative response signal for undamaged and a two-strut damaged structure is shown in the Fig. 4.8. The response signal comprises thousands of data points which is not feasible for the damage classification algorithm. The aim of
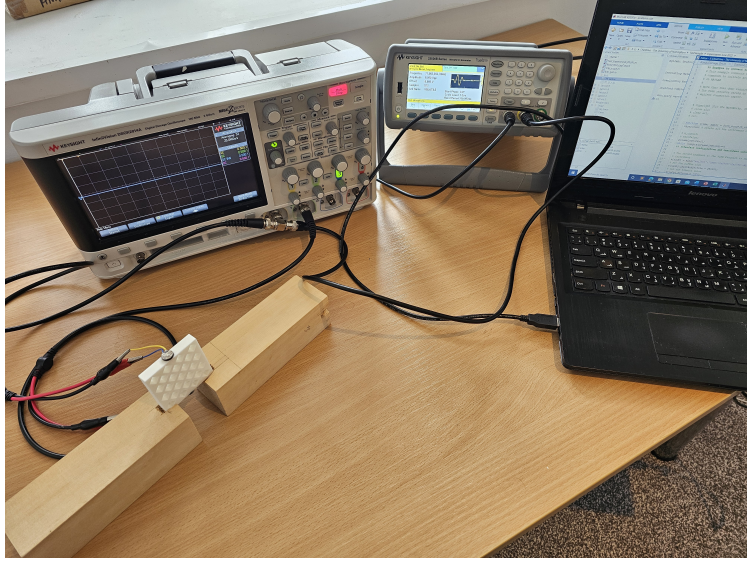
Figure 4.7: Experimental Setup

feature extraction is to reduce the size of the data while retaining all the useful information of the signal. There are two techniques that are used in this study to reduce the dimensionality of the data and to extract features.

4.5.1 Feature extraction using Principal Component Analysis

Principal Component Analysis (PCA) was employed as a dimensionality reduction technique and feature extraction tool for ultrasonic signal data. Each pre-processed time-domain waveform was treated as a high-dimensional vector, with each time sample representing a single variable. PCA projects this data onto a lower-dimensional space, capturing the directions of maximum variance.

The principal components with maximum variability were extracted for each signal and used as input features for the classifier. These components summarize key variations in signal shape and amplitude, which are known to be sensitive to the presence and severity of damage.

PCA provides several benefits in the context of structural health monitoring (SHM). First, it reduces feature dimensionality, thereby minimizing redundancy and the risk of overfitting in machine learning models. Second, it captures the dominant waveform characteristics in a compact form, enabling effective comparison across different damage states. Lastly, as an unsupervised method, PCA does not require predefined labels or assumptions about the signal, making it adaptable to a wide range of structural configurations.

The use of PCA in SHM is well-supported in literature. Raghavan and Cesnik [134] applied PCA to ultrasonic signals for damage detection in composite structures. Farrar and Worden [67] emphasized PCA's utility in condition monitoring and anomaly detection. Sohn et al. [135] demonstrated the application of PCA in statistical pattern recognition-based SHM frameworks.

4.5.2   Feature extraction using energy of signal

The second method for feature extraction is using the energy of the signal as a feature. It is seen in our study that the energy of the signal is sensitive to the presence and severity of damage. Variations in the energy of the signal are seen in different time domains of the signal depending on the damage present in the structure. As the wave travels through the structure, its interaction with the damage varies depending on the location and severity of the damage. Important information, therefore, is contained in the time history of the signal. The signal is divided into multiple time regions of equal width, and the energies of the signal are calculated individually for each region. The calculated energies from different regions of the signal form the damage features as govened by Equation 4.3.

$$\textbf{Damage Features} = \textbf{Energies of signal in different regions of signal}(\textbf{E1, E2, E3...En})$$
$$(4.3)$$
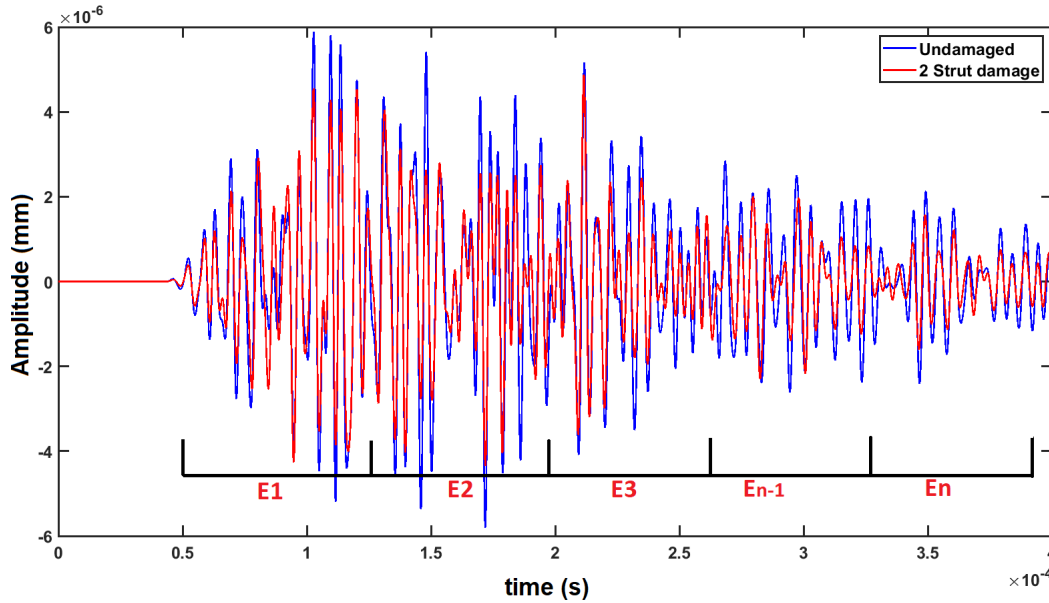
Figure 4.8: Response signal for damaged and undamaged structure. blue line is for undamaged structure, red is for 2-strut damaged structure. Energies E1-En are extracted from n time regions of signal of equal width

4.6   Classification Model

A classification neural network is used to train and classify the data. The method of supervised learning is used for this study. Data from the numerical samples are assigned known damage classes which is then used to train the neural network. The parameter space used was based on the features extracted from samples of one to ten strut damages. The trained network is then validated with 20% of the data to measure the prediction accuracy of the model. Categorical cross entropy is used as loss function which is suitable for multi class categorization. The model was trained using a fixed stopping criterion based on the training loss. Specifically, training was

terminated once the training loss fell below a predefined threshold value of 0.02. This threshold was chosen based on empirical observations where further reductions in loss did not lead to meaningful improvements in classification accuracy.

A maximum cap of 300 epochs was also set to avoid unnecessarily long training times in case the loss threshold was not reached. In practice, convergence was typically achieved within 120–180 epochs. No validation set was used during training; the model's performance was later evaluated on a separate test set after training completion. The prediction accuracy is calculated as a percentage of correct predictions of classes. Validation of the classification model is done using the experimental data. The complete scheme of classification is shown in Figure 4.9.
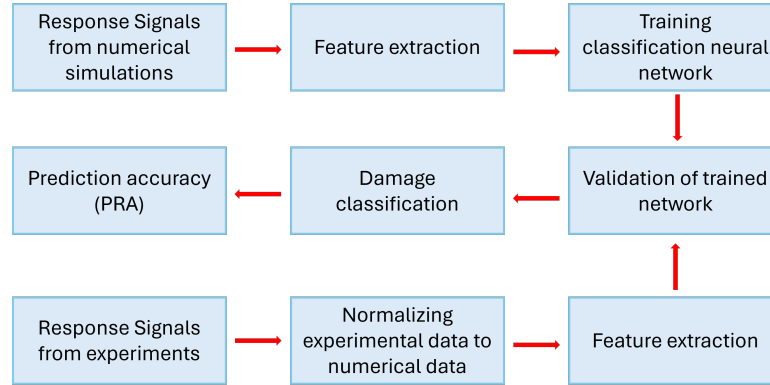
Figure 4.9: Classification scheme used for damage quantification

4.6.1 Structure of Neural network

The structure of neural network is shown in Figure 4.10. Various components of the neural network are elaborated in subsequent paragraphs.

Input features

The input features are the features extracted from the response signals using PCA and energy features. These features are assigned the class labels based on their actual damage state. This form the training data for the classification model.

Input Layer

The input layer is the first layer of the neural network model which links the input neurons with the features of the training data. The number of neurons in input layer correspond to the size of feature matrix. In this study, different feature sizes will be studied, so the input layer size will be variable.

Hidden Layers

Two fully connected hidden layers are used for classification model in this study. The activation between the layers is achieved through Rectified linear unit (ReLU) function. Activation function is a mathematical operator which is applied to each neuron for smooth and consistent transfer of information between layers. It also adds nonlinearity to the model to train and model complex data. ReLU performs a
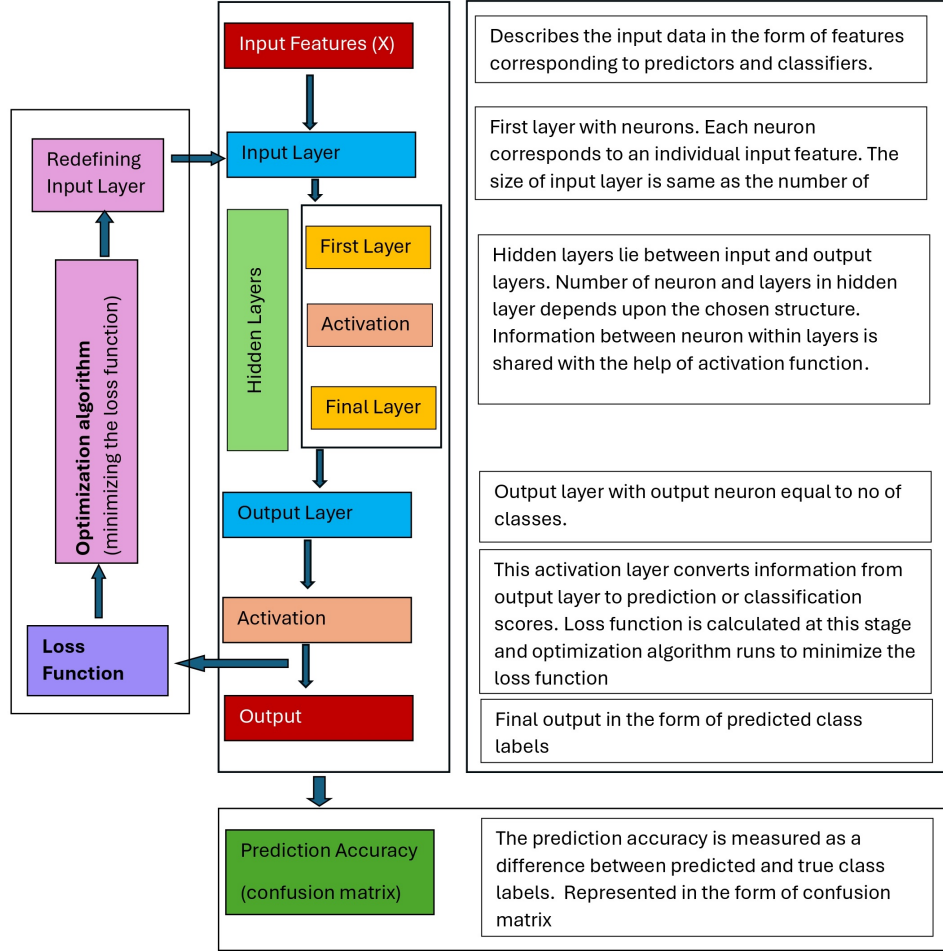
Figure 4.10: Structure of the classification neural network

threshold operation on each element of the input, where any value less than zero is set to zero, that is,

$$f(x) = \begin{cases} x, & \text{if } x \geq 0 \\ 0, & \text{if } x < 0 \end{cases} \tag{4.4}$$

The number of neurons in hidden layers was chosen based on the optimized feature size resulting in maximum prediction accuracy. The optimization of parameters of neural network is discussed in detail in Chapter 6.

Output Layer

The output layer has the final predictions of the neural network. The number of neurons in output layer are equal to the number of classes in the model. An activation function is applied to the output layer to transform the raw information from neurons (logits) into the actual classifications. Softmax activation function is used at this stage which outputs the probabilities or classification scores for various classes. Softmax function is given as:

$$\text{Softmax}(z_i) = \frac{e^{z_i}}{\sum_{j=1}^{K} e^{z_j}} \text{ for } i = 1, \ldots, K, \text{ where } K \text{ is the number of classes.} \tag{4.5}$$

Loss Function

The loss function calculates the classification loss which is a measure of predictive inaccuracy of classification model. The aim of the optimization algorithm used in classification model is to minimize the loss function thus achieving the best prediction accuracy. The loss function used for this study is categorical cross-entropy loss function which is suitable for multi- class classification.

$$\text{Categorical Cross-Entropy} = -\sum_{c=1}^{C} y_{\text{true},c} \log(y_{\text{pred},c}) \tag{4.6}$$

L2 Regularization

To improve the generalization capability of the machine learning model used in this study, L2 regularization was incorporated into the loss function. L2 regularization reduces the risk of over-fitting by penalizing large weights in the model, thus encouraging simpler models that generalize better to unseen data. The regularized loss function is defined as:

$$\text{Loss}_{\text{total}} = \text{Loss}_{\text{original}} + \lambda \sum_{i} w_i^2 \tag{4.7}$$

where:

- $\text{Loss}_{\text{original}}$: The original loss function which in our case is Categorical Cross-Entropy Loss.

- λ: The regularization parameter, a hyperparameter controlling the trade-off between minimizing the original loss and penalizing large weights.

- w_i: The weights of the model.

During training, λ was treated as a hyperparameter and optimized using cross-validation. This ensured a balance between fitting the training data and controlling model complexity. The regularization parameter was varied in the range $\lambda \in [0.001, 0.1]$, and the optimal value was selected based on validation performance.

Optimization Algorithm

The optimization algorithm used in this study is the limited-memory Broyden-Fletcher-Goldfarb-Shanno quasi-Newton algorithm (LBFGS) algorithm, a quasi-Newton method for minimizing the cross-entropy loss during training. Unlike first-order optimizers such as Stochastic Gradient Descent (SGD), L-BFGS uses curvature information by approximating the inverse of the Hessian matrix based on a limited history of previous gradients and parameter updates. This allows the algorithm to converge quickly in smooth loss landscapes without computing the full second-order derivatives, making it computationally efficient for medium-scale problems [136]. L-BFGS was chosen in this study because it is particularly effective when using full-batch updates, which were feasible given the moderate size of the dataset. Compared to SGD and its adaptive variants like Adam, L-BFGS typically requires fewer iterations to converge but has a higher per-iteration computational cost. Preliminary experiments showed that L-BFGS consistently achieved lower final training

loss and more stable convergence than SGD with momentum or Adam. While Adam adapts learning rates per parameter and is widely used for deep learning applications, it sometimes led to fluctuations near convergence in this study [137]. SGD, though simple and scalable, required careful tuning of the learning rate and more epochs to reach acceptable loss values. Therefore, L-BFGS was selected as the preferred optimizer due to its faster and smoother convergence in this controlled, simulation-driven setup. A detailed overview of these optimization algorithms and their trade-offs is provided in Ruder's comparative study [138].

Output

Once optimization is achieved, the final classification scores are calculated which is given as the output of the model. These classification scores give the probability distribution of a feature belonging to a particular class.

4.6.2 Measuring performance of the classification model

The performance of classification is represented and measured by three methods in this study.

1. Classification scores

2. Confusion matrix

3. Prediction accuracy

Classification scores

The classification scores are the posterior probabilities of data belonging to particular class labels. There are no hard classification outputs from the neural network; instead it gives a probability distribution over most probable class labels.

Prediction accuracy

The performance of the model is measured as the prediction accuracy. Predicted class labels are assigned to the classes with the highest classification score.

$$\text{Accuracy} = \frac{\text{Number of correct predictions}}{\text{Total number of predictions}} \tag{4.8}$$

Confusion matrix

Confusion matrix is a physical representation of predicted vs true class labels. It gives both a measure of the performance of the model as well as the spread of particular class labels to the neighboring class labels.

4.6.3 Summary of neural network

Various features of the classification neural network used for this study are given in Table 4.1. Size of the input, output and hidden layers were optimized to maximize the prediction accuracies.

Table 4.1: Properties of Classification Neural Network

Property	Value
Input Layer	Variable depending on number of damage features
Hidden Layers	2 hidden layers with optimized size (ref Ch 6)
Activation Functions	ReLU for hidden layers, softmax for output layer
Output Layer	Variable depending on output classifiers
Loss Function	Categorical cross-entropy
Optimization Algorithm	LBFGS
Training Data	11,000 labeled samples
Evaluation Metrics	Multi-class confusion matrix, Prediction accuracy
Regularization	L2 regularization with optimized λ
Model Evaluation	Validation dataset with 20% of training data

4.7 Classification of experimental data

Experimental data is critical for validating the neural network classification model developed using numerical simulations. However, the limited availability of experimental data made it impractical to train a standalone classification model for the experimental data. Instead, the experimental data is tested on the numerical classification model after normalizing the experimental data. The prediction accuracy of the model with experimental data is then measured. This approach evaluates the model's generalization capability in real-world scenarios.

Normalizing the experimental data to scale it to the numerical simulated data is a critical step. To address differences in scale and distribution between numerical and experimental data,a robust scaling technique was used as given below. First, the experimental data is normalized and scaled to the numerical data. Data normalization is based on Equation 4.9.

$$x' = \frac{x - \min(x)}{\max(x) - \min(x)} \tag{4.9}$$

where x is the original value and x' is the normalized value. To rescale to a range between an arbitrary set of values $[a, b]$, the formula used is as follows:

$$x' = a + \frac{(x - \min(x))(b - a)}{\max(x) - \min(x)} \tag{4.10}$$

The normalized experimental data is fitted to the classification model trained with numerical data, and prediction accuracy is calculated.

4.8 Summary and Conclusion

In this chapter, the details of materials and methods for damage characterization were given. The material properties, lattice structure, and sensors were discussed. The methodology for numerical simulations and experimental setup was presented in detail. Subsequently, the signal processing methods used for this study were discussed. Toward the end, the parameters of the neural network classification model used for this work were presented and discussed. The methodologies outlined

in this chapter provide a systematic approach for integrating numerical simulations and experimental data in the structural health monitoring of lattice structures. The proposed framework addresses the challenges associated with limited experimental data, noise, and feature discrepancies through signal preprocessing and machine learning techniques. Having established the complete methodology of the study, the results will be presented in the subsequent chapters.

Chapter 5

Ultrasonic Wave Propagation in Lattice Structure

5.1 Introduction

Before developing a methodology for damage characterization in a lattice structure, it is important to understand, explore and investigate the interaction and behaviour of an ultrasonic wave within a lattice structure. This is achieved by solving analytical formulations for a structure which can act as a building block of a lattice structure also called the unit cell. Ultrasonic propagation is solved for the unit cell to calculate the reflection and transmission coefficients and efficiencies in the lattice unit cell. The results from the unit cell are then multiplied to a bigger structure formed by an arrangement of unit cell to calculate the transmissions in that structure. Following are the core areas which have been explored in this Chapter:

- **Beam Crossing Analysis:** First, the interaction of ultrasonic waves at a beam crossing, which serves as a basic unit cell of a lattice structure is studied. Analytical formulations are used to calculate reflection and transmission coefficients with is unit cell formed by a beam crossing.

- **Wave Behavior in Larger Structures:** Next, the behavior of waves is extended from a single unit cell to a multi-cell lattice structure. This helps to understand wave transmission and attenuation within a complete lattice structure.

- **Impact of Damage:** The effect of defects is explored by analyzing how they alter wave transmission and reflection within the structure. This step is crucial for identifying and locating damage.

- **Advanced Configurations:** Finally, the basic beam crossing model is expanded to include angular and 3D configurations, which can enable the analysis of a variety of lattice geometries.

This chapter sets the stage for the rest of the thesis by building a foundational understanding of ultrasonic wave propagation in lattice structures. The methods and results presented here form the basis for developing advanced techniques for damage characterization in later chapters. The chapter is arranged as follows: Section 5.2 gives the analytical formulations in a beam crossing which is similar to the lattice

unit cell used in this work. Section 5.3 covers the multiplication of the unit cell to calculate transmissions in a four cell lattice structure and effects with the presence of damage. In section 5.4, a summary of analytical results for different unit cell are presented. The final discussions and conclusion from the chapter are given in section 5.5.

5.2   Ultrasonic transmission in a beam crossing

In this section, an analytical approach is explored to calculate transmission efficiency of ultrasonic waves in a lattice unit cell. When an ultrasonic wave traveling through a medium encounters a boundary, a part of wave is reflected back whereas a part of wave is transmitted. Reflection and transmission coefficients for a beam crossing will be calculated for cross section shown in Figure 5.1. These calculations are based on the formulations given in [139]. Although the original formulation cited in [139] was developed in the context of audio-frequency acoustic wave propagation, the underlying physics i.e. linear elasticity and wave equation solutions, remain valid at higher frequencies, including the ultrasonic range.

Because the linear elastic wave equation is derived from Newton's laws and Hooke's law, it is inherently scale and frequency independent and consequently, the same formulations developed for audible sound remain valid at ultrasonic frequencies provided the medium behaves as a linear, homogeneous (or suitably modeled anisotropic) continuum and the wave amplitudes stay within the small-strain limit. In elastic solids, the Navier–Cauchy equations yield frequency-independent longitudinal and shear wave speeds, so raising the frequency from kilohertz to megahertz merely shortens the wavelength without changing the governing mathematics. Classic acoustics and elasticity texts explicitly state that ultrasonic waves are physically identical to lower-frequency sound waves under these assumptions, and decades of practice in nondestructive testing and medical ultrasound confirm that linear audio-frequency theory accurately predicts ultrasonic propagation when attenuation or dispersion, if present, is incorporated through frequency-dependent material parameters [140, 141, 142].

When a longitudinal ultrasonic wave is incident at a corner, a part of wave is converted to bending wave and vice versa [139]. So, other than reflection and transmission of waves, mode conversion of waves also takes place across boundaries. The equations given below assume that both longitudinal and bending waves are incident from the segment 1 of the structure. The incident velocity is v_{1_+} (subscript showing the direction and segment) and the amplitudes of longitudinal and bending waves are A_L and A_B, respectively. The velocity relations in different segments of the structure are given in Equations (5.1).

$$
\begin{aligned}
v_{B1}(x) &= v_{1_+}(A_B e^{-jk_{B1}x} + r_B e^{jk_{B1}x} + r_j e^{k_{B1}x}), \\
v_{L1}(x) &= v_{1_+}(A_L e^{-jk_{L1}x} + r_L e^{jk_{L1}x}), \\
v_{B2}(y) &= v_{1_+}(t_{2B} e^{-jk_{B2}y} + t_{2Bj} e^{-k_{B2}y}), v_{L2}(y) = v_{1_+} t_{2L} e^{-jk_{L2}y} \\
v_{B3}(x) &= v_{1_+}(t_{3B} e^{-jk_{B3}x} + t_{3Bj} e^{-k_{B3}x}), v_{L3}(x) = v_{1_+} t_{3L} e^{-jk_{L3}x} \\
v_{B4}(y) &= v_{1_+}(t_{4B} e^{-jk_{B4}y} + t_{4Bj} e^{-k_{B4}y}), v_{L4}(y) = v_{1_+} t_{4L} e^{-jk_{L4}y}
\end{aligned}
\tag{5.1}
$$

Here, $\{r_B, t_{2B}, t_{3B}, t_{4B}\}$ are reflection and transmission coefficients associated with
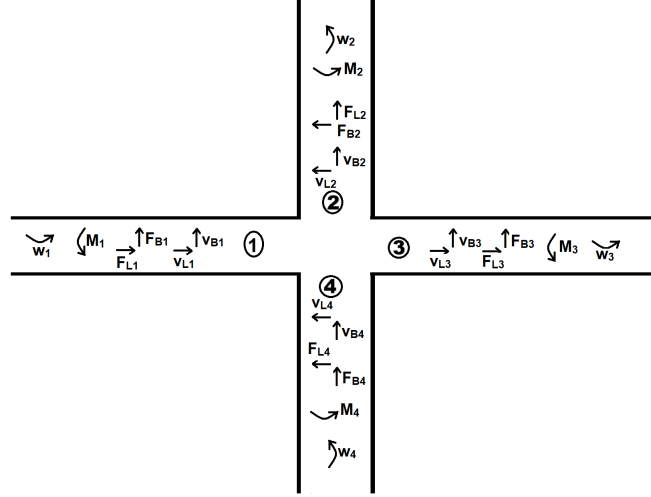
Figure 5.1: Transmission of ultrasonic wave at a rigid beam crossing. Incident wave enters from segment 1 and a part of it is transmitted to other three segments. A part of wave is also reflected back. velocity, force and moment components in each segment represent longitudinal and bending waves.

bending waves, $\{r_L, t_{2L}, t_{3L}, t_{4L}\}$ are reflection and transmission coefficients associated with longitudinal waves, and $\{r_j, t_{2Bj}, t_{3Bj}, t_{4Bj}\}$ are nearfield coefficients associated with bending waves. There are a total of 12 unknown reflection and transmission coefficients. To find out the 12 unknown coefficients , we make use of boundary condition equations. The are a total of 12 boundary conditions at the intersection of 4 segments and are as given in Equations (5.2). The boundary conditions applied to the lattice segments are as follows. First, **displacement continuity** is enforced at all junctions, meaning that the displacements at the connecting ends of adjacent segments must be equal to ensure geometric compatibility. Second, **force and moment equilibrium** is maintained by ensuring that the internal forces (or stress resultants) and moments at each interface are balanced, in accordance with Newton's third law. Finally, compatibility of velocity transmission is ensured at boundaries.

$$
\begin{aligned}
&M_1 = M_2 + M_3 + M_4, \\
&w_1 = w_2 \ , \ \ w_1 = w_3 \ , \ \ w_1 = w_4, \\
&F_{L1} = -F_{B2} + F_{L3} - F_{B4} \ , \ \ F_{B1} = -F_{L2} + F_{B3} - F_{L4}, \\
&v_{L1} = -v_{B2} \ , \ \ v_{L1} = v_{L3} \ , \ \ v_{L1} = -v_{B4} \\
&v_{B1} = v_{L2} \ , \ \ v_{B1} = v_{B3} \ , \ \ v_{B1} = -v_{L4}
\end{aligned}
\tag{5.2}
$$

M, w, and F are defined as a function velocities and are given by Equations (5.3)

$$M_1 = -\frac{B_1}{j\omega}\frac{\partial^2 v_{B1}}{\partial x^2} \quad , \quad M_2 = -\frac{B_2}{j\omega}\frac{\partial^2 v_{B2}}{\partial y^2} \quad ,$$

$$M_3 = -\frac{B_3}{j\omega}\frac{\partial^2 v_{B3}}{\partial x^2} \quad , \quad M_4 = -\frac{B_4}{j\omega}\frac{\partial^2 v_{B4}}{\partial y^2}$$

$$w_1 = \frac{\partial v_{B1}}{\partial x} \quad , \quad w_2 = \frac{\partial v_{B2}}{\partial y} \quad , \quad w_3 = \frac{\partial v_{B3}}{\partial x} \quad , \quad w_4 = \frac{\partial v_{B4}}{\partial y}$$

$$F_{B1} = \frac{B_1}{j\omega}\frac{\partial^3 v_{B1}}{\partial x^3} \quad , \quad F_{B2} = \frac{B_2}{j\omega}\frac{\partial^3 v_{B2}}{\partial y^3} \quad , \tag{5.3}$$

$$F_{B3} = \frac{B_3}{j\omega}\frac{\partial^3 v_{B3}}{\partial x^3} \quad , \quad F_{B4} = \frac{B_4}{j\omega}\frac{\partial^3 v_{B4}}{\partial y^3} \quad ,$$

$$F_{L1} = -\frac{E_1 S_1}{\omega}\frac{\partial v_{L1}}{\partial x} \quad , \quad F_{L2} = -\frac{E_2 S_2}{\omega}\frac{\partial v_{L2}}{\partial y} \quad ,$$

$$F_{L3} = -\frac{E_3 S_3}{\omega}\frac{\partial v_{L3}}{\partial x} \quad , \quad F_{L4} = -\frac{E_4 S_4}{\omega}\frac{\partial v_{L4}}{\partial y} \quad ,$$

E_n is the modulus of elasticity for each section respectively. S_n is the surface area of n_{th} segment. Considering c_{Ln} and c_{Bn} as speed of longitudinal and bending waves respectively in n_{th} segment, relations for k_n, k_{Ln} and B_n are given as:

$$c_{Ln} = \sqrt{\frac{E_n}{\rho_n}} \quad , \quad c_{Bn} = \sqrt{1.8 h_n f c_{Ln}}$$

$$k_{Ln} = \frac{\omega}{c_{Ln}} \quad , \quad k_n = \frac{\omega}{c_{Bn}} \tag{5.4}$$

$$B_n = \frac{c_B^4 m'}{\omega^2}$$

where $m' = S_n \rho_n$ and h_n is thickness of n_{th} segment. By solving the governing equations (5.1) using 12 boundary conditions in Equation (5.2), the 12 unknown reflection and transmission coefficients can be calculated. Considering all segments with uniform thickness h and defining a parameter $P = \sqrt{1.8hf/c_{Ln}}$, the 12 unknown coefficients for $A_L = 1$ and $A_B = 0$ are given by Equations (5.5).

$$r_B = \frac{0.5 + 0.5j}{(2 - 2j) + 3P} \qquad r_{Bj} = \frac{0.5 + 0.5j}{(2 - 2j) + 3P} \qquad r_L = -\frac{3P}{(2 - 2j) + 3P}$$

$$t_{2B} = -\frac{1.5 - 0.5j}{(2 - 2j) + 3P} \qquad t_{2Bj} = -\frac{0.5 + 0.5j}{(2 - 2j) + 3P} \qquad t_{2L} = 0$$

$$\tag{5.5}$$

$$t_{3B} = \frac{1.5 - 0.5j}{(2 - 2j) + 3P} \qquad t_{2Bj} = -\frac{0.5 + 0.5j}{(2 - 2j) + 3P} \qquad t_{3L} = \frac{2 - 2j}{(2 - 2j) + 3P}$$

$$t_{4B} = -\frac{1.5 - 0.5j}{(2 - 2j) + 3P} \qquad t_{4Bj} = -\frac{0.5 + 0.5j}{(2 - 2j) + 3P} \qquad t_{4L} = 0$$

However, more useful than coefficients are reflection and transmission efficiencies which are dimensionless and provide a direct interpretation of magnitude of reflected

and transmitted waves. The power propagated by the flexural and longitudinal wave is given as:

$$W_{Bn} = 2m'_n c_{Bn} v^2_{Bn} \ , \ W_{Ln} = m'_n c_{Ln} v^2_{Ln} \tag{5.6}$$

The reflection and transmission efficiencies then are given as follows. For an incident longitudinal wave ($A_L = 1, A_B = 0$) the efficiencies are given by Equations (5.7). In the notation of efficiencies (ρ, τ), the first subscript indicates the incident wave and the second subscript indicates reflected or transmitted wave and the number indicates the segment. τ_{LL2} thus means that the incident wave is longitudinal and the efficiency is related to the transmitted longitudinal wave in segment 2.

$$
\begin{aligned}
\rho_{LL1} &= \frac{W_{L1}}{W_{1+}} = \frac{m'_1 c_{L1} v^2_{L1}}{m'_1 c_{L1} v^2_{1+}} = |r_L|^2 \\[2mm]
\rho_{LB1} &= \frac{W_{B1}}{W_{1+}} = \frac{2m'_1 c_{B1} v^2_{B1}}{m'_1 c_{L1} v^2_{1+}} = \frac{2c_{B1}}{c_{L1}}|r|^2 \\[2mm]
\tau_{LL2} &= \frac{W_{L2}}{W_{1+}} = \frac{m'_2 c_{L2}}{m'_1 c_{L1}}|t_{2L}|^2 \ , \ \tau_{LB2} = \frac{W_{B2}}{W_{1+}} = \frac{2m'_2 c_{B2}}{m'_1 c_{L1}}|t_2|^2 \\[2mm]
\tau_{LL3} &= \frac{W_{L3}}{W_{1+}} = \frac{m'_3 c_{L3}}{m'_1 c_{L1}}|t_{3L}|^2 \ , \ \tau_{LB3} = \frac{W_{B3}}{W_{1+}} = \frac{2m'_3 c_{B3}}{m'_1 c_{L1}}|t_3|^2 \\[2mm]
\tau_{LL4} &= \frac{W_{L4}}{W_{1+}} = \frac{m'_4 c_{L4}}{m'_1 c_{L1}}|t_{4L}|^2 \ , \ \tau_{LB4} = \frac{W_{B4}}{W_{1+}} = \frac{2m'_4 c_{B4}}{m'_1 c_{L1}}|t_4|^2
\end{aligned}
\tag{5.7}
$$

In a similar fashion, the equations for reflection and transmission efficiencies for an incident bending wave ($A_L = 0, A_B = 1$) can be set up. For a beam crossing with all segments having uniform thickness h, the reflection and transmission efficiencies as a function of frequency, thickness, and longitudinal wave speed ($P = \sqrt{1.8hf/c_{Ln}}$) are plotted in the Figure 5.2. This figure can be used to calculate the reflection and transmission coefficients for a given thickness, excitation frequency and wave speed governed by the material properties. It is important to note that sum of all efficiencies equals to one. The reflection and transmission efficiencies of an incident longitudinal and bending wave in Nylon-12 ($\rho = 949kg/m^3$ $E = 1620MPa$ at an excitation frequency of 215KHz are shown in Figure 5.3. For an incident longitudinal wave, only bending wave is transmitted to the perpendicular legs of beam crossing and transmission efficiency of longitudinal waves in these legs is zero. 46 percent of wave amplitude is transferred in the horizontal leg of beam crossing and 15 percent of wave amplitude is reflected back. These calculations will now be extended to a multiplication of unit cells forming a lattice structure. The joining of lattice cells can give rise to various configurations of lattice structures; however, only one structure is tested for this particular cell formed by the presented beam crossing. In the later sections, formulations for different other unit cells will also be discussed including 3D beam crossing and cells having angular struts. These findings can be particularly useful for the solution of ultrasonic transmissions in strut-based lattice structures.
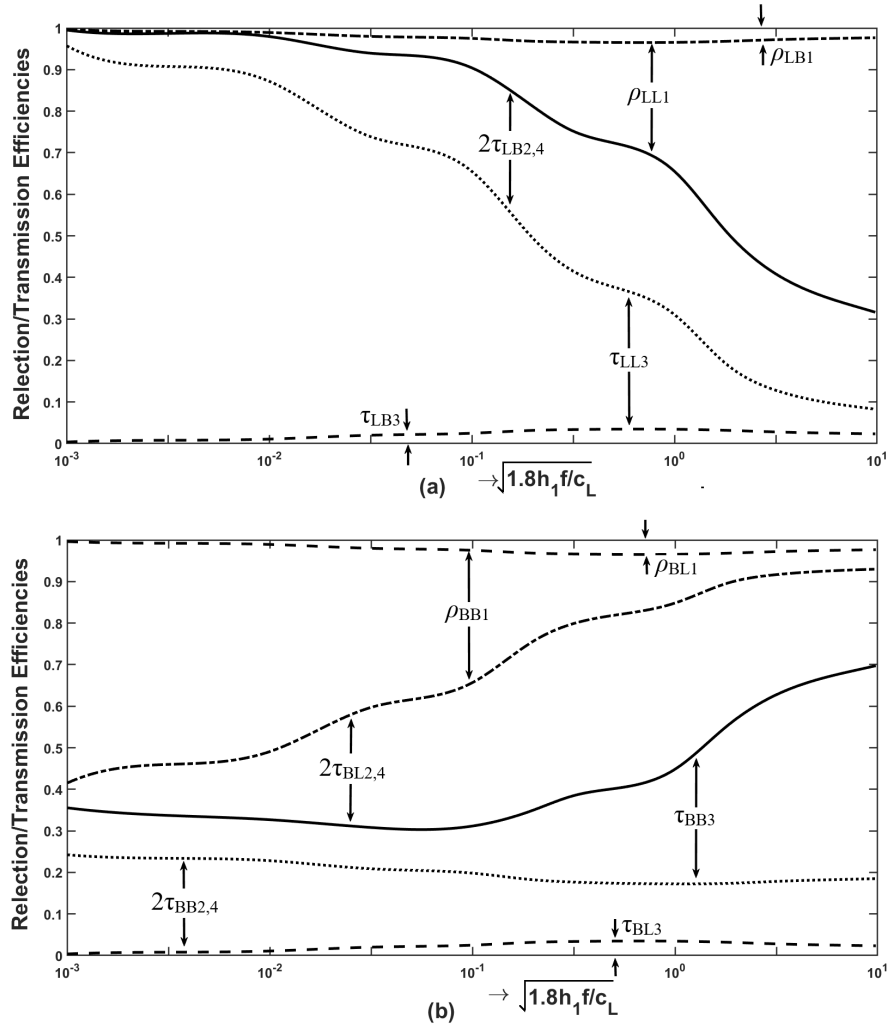
Figure 5.2: Reflection and Transmission efficiencies for a beam crossing as a function of $P = \sqrt{1.8hf/c_{Ln}}$ represented as difference of curves on graphs. (a) Incident Longitudinal wave $(A_L = 1, A_B = 0)$ (b) Incident Bending wave $(A_L = 0, A_B = 1)$
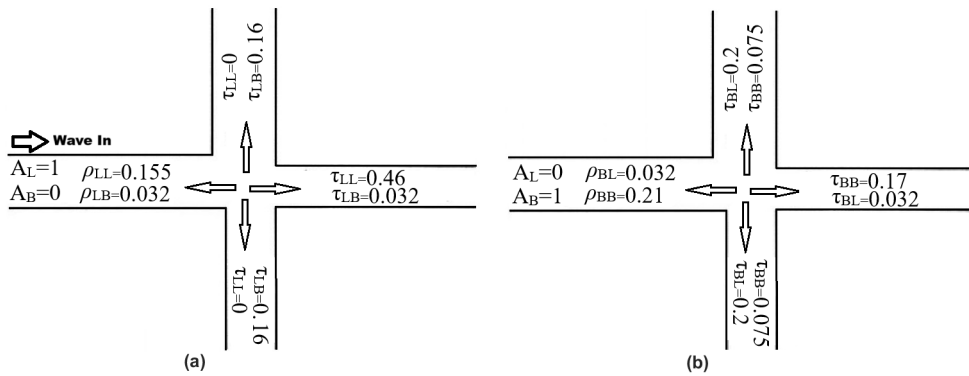
Figure 5.3: Transmission efficiencies of an incident longitudinal and bending wave in Lattice unit cell of Nylon-12 at incident frequency of 215 kHz and beam thickness of 10mm (a) Incident longitudinal wave (b) Incident bending wave

5.3 Ultrasonic transmission in a lattice structure

The above sections provides the analytical equations for calculating ultrasonic transmissions in a lattice unit cell. Calculations for the unit cell are now extended to calculate transmission within a structure formed with the unit cell. A four cell lattice structure is shown in Figure 5.4. Transmission of an incident longitudinal wave with unit amplitude was calculated through this structure. There are total seven beam crossings in the structure marked as p1 to p7. At each crossing, part of amplitude will be transmitted and reflected in different directions. Wave reflection from the damage and other boundaries of the structure is calculated using Equation (5.8). Z_1 and Z_2 are the wave impedance of the two mediums at boundary. At the damage location, which is being considered as the breaking of struts, air is taken as impedance medium at the damage boundary. The amplitude of reflected wave at these boundaries is taken into account for wave transmission calculations.

$$\rho = |r|^2 \ , \quad \tau = 1 - \rho$$

$$r = \frac{Z_1 - Z_2}{Z_1 + Z_2} \tag{5.8}$$

$$Z_1 = \rho_1 c_{L1} S_1 \ , \quad Z_2 = \rho_2 c_{L2} S_2$$
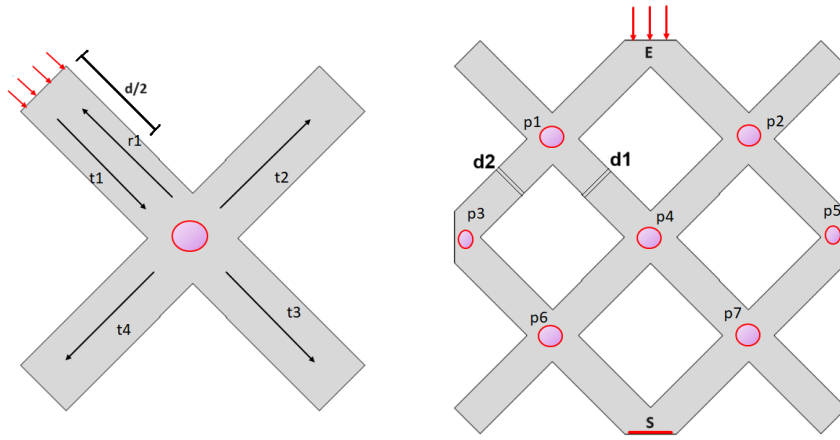
Figure 5.4: Unit cell of a lattice structure and a four cell lattice structure formed from the unit cell. Two damage locations are marked in the structure as d2 and d1 corresponding to Strut 9 and 10 respectively. A longitudinal wave enters at point E and transmissions are calculated at point S.

The transmission efficiency in the structures was calculated as follows:

- A incident longitudinal wave with unit amplitude enters the structure from location E.

- The wave speeds of both longitudinal and bending waves were calculated using Equation (5.4). Using the material properties of Nylon, thickness of 10mm and frequency of 215KHz, the speed of longitudinal wave is 1306 m/sec and speed

of bending wave is 2248 m/s almost twice the speed of longitudinal wave. For simplicity, the speed of bending wave is assumed twice the speed of longitudinal wave.

- As the amplitude travels through the structure, its position and transmission are calculated at each time interval. One time interval t is the time taken by wave to travel the distance d/2, which is one half the length of strut.

- The new location of wave is estimated after each time interval. Since the speed of bending wave is twice the speed of longitudinal wave, at any given time interval, wave will have two possible locations (a) center of strut (b) at the beam crossing

- When wave reaches beam crossing, its transmission and reflection amplitudes are calculated using results given in Figure 5.3.

- When the wave encounters a boundary or damage, its behaviour is calculated using Equation (5.8).

- The final amplitude of the wave at location S is calculated.

- Calculations at the location S for 35 time intervals are shown in Figure 5.5. It also includes the wave response for damages d2 and d1 corresponding to breaking of Strut-9 and 10 in the structure.

Figure 5.5 shows the transmission amplitude for 35 intervals at location S in the structure. At each interval, the transmitted amplitude is calculated at multiple locations in the structure, and the total amplitude at location S for each interval is plotted in the figure. Results for two damaged struts, Strut-9 (d2) and Strut-10 (d1) are also shown in the figure. Changes in the transmitted amplitude are seen with the presence of damage. Strut-9 (d2) lies in the direct path of longitudinal wave amplitude and hence higher wave attenuation is seen for the damage d2. This finding confirms the hypothesis that damage alters the wave transmission in lattice structure. This finding will also form the basis for damage characterization in the lattice structure where changes in the energy of response signal will act as key indicator of damage. The maximum amplitudes recorded for the structure are compared with the numerical and experimental results. These comparisons are shown in Table 5.1 for a four-cell and a nine-cell lattice structure. These cells are extensively explored in in proceeding chapters using both numerical and experimental studies (Chapter 6 and 7). The results of these cells calculated numerically and experimentally are given along with analytical calculations in Table 5.1 which shows a close agreement in these results. Hence, the analytic formulations provided here can also provide a quick mean of estimating the transmission efficiency in a multi-cell lattice structure.

Table 5.1: Transmission efficiency through a lattice structure excited by a longitudinal wave of unit amplitude. Numerical and experimental results are taken from the study on same structures in Chapter 6 and 7.

Lattice Structure	Analytical	Numerical	Experimental
4 Cell	0.082	0.080	0.078
9 Cell	0.022	0.020	0.018
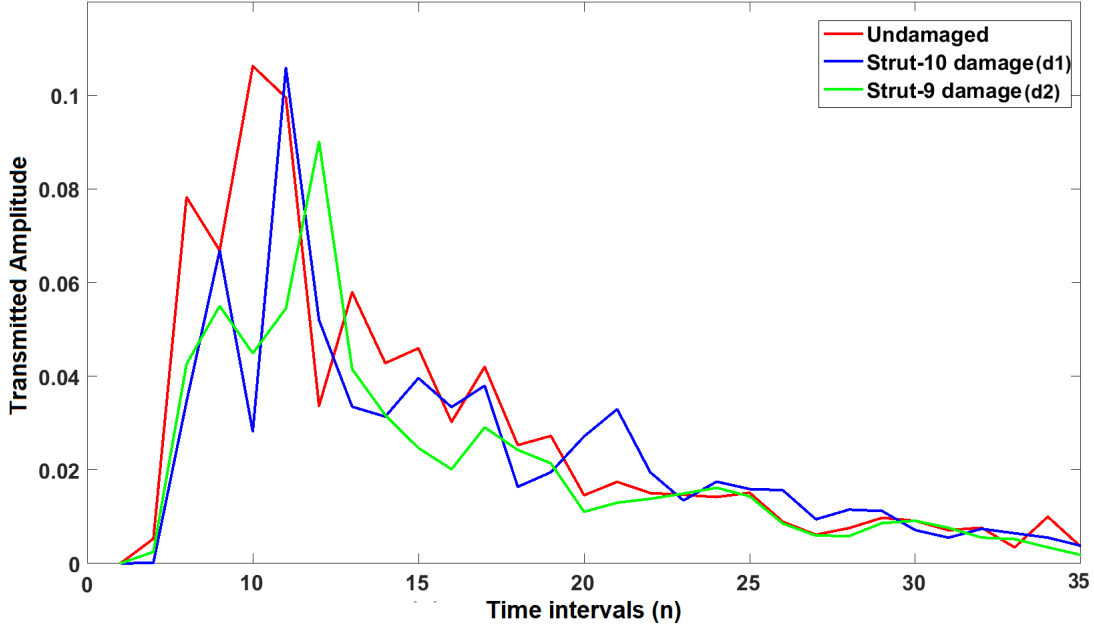
Figure 5.5: Analytical estimation of transmitted energy in lattice structure shown in Fig. 5.4. Calculations are shown for 35 time intervals, effects of two damaged struts are also shown.

5.4 Formulations for an angular and a 3D cell

To generalize the ultrasonic wave propagation analysis beyond simple beam crossings, this section introduces formulations for angular and three-dimensional (3D) lattice unit cells. These configurations represent more complex and practical geometries commonly encountered in real-world lattice structures. By expanding the scope of the analysis, the behavior of ultrasonic waves in diverse lattice arrangements can be systematically evaluated. A 3D and an angular beam crossing as shown in Figure 5.6. The changes in the equations as compared to simple beam crossing explored in the previous sections are presented along with results for a representative cell. The formulations will enable analytical modeling of a variety of lattice structures.

5.4.1 Angular beam crossing

An angular beam crossing includes one or more struts oriented at an angle θ relative to the others. This configuration reflects the design-specific orientations often seen
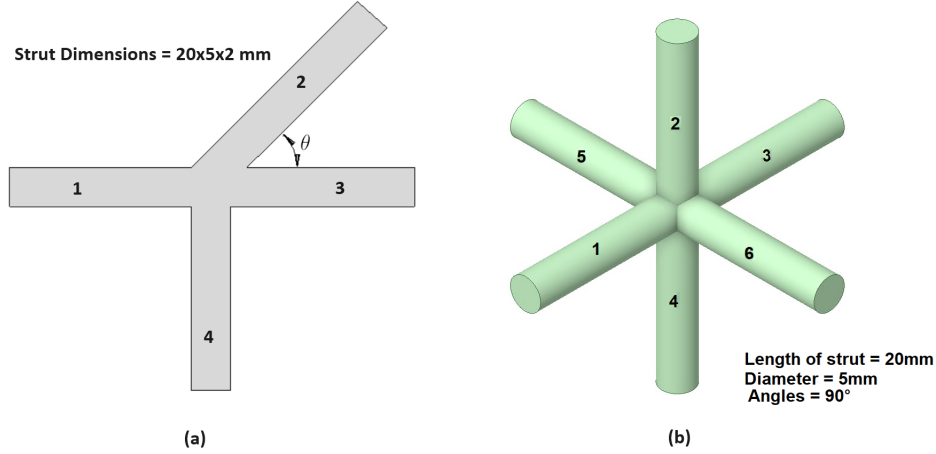
Figure 5.6: Representation of Angular and 3D Unit cells (a) Angular Cell (b) 3D Cell

in advanced lattice designs. Analytical modeling of such crossings involves resolving wave components along multiple axes to capture the effects of angular orientations on transmission and reflection. The angular beam crossing is shown in Figure 5.6(a). One strut of beam is at an angle of θ. The updated velocity equations for the structure are given by Equations (5.9). Strut 2 which is at an angle θ will have two x and y components now. The resultant transmission in strut 2 is calculated from the component transmissions in x and y directions. The results for an incident longitudinal wave ($A_L = 1$) for the cross section are given in Table 5.2. The key aspects involved in the analysis of an angular beam are follow:

- **Decomposing Wave Components:** For the strut oriented at an angle θ, the incident wave is resolved into its x- and y-components. The transmitted wave's amplitude in the angular strut is derived by combining the contributions of these components.

- **Modified Velocity Equations:** The standard velocity equations are updated to incorporate angular dependencies, where the angular strut contributes distinct velocity terms for the horizontal and vertical components. These components are coupled through boundary conditions, ensuring consistency at the crossing point.

- **Reflection and Transmission Efficiencies:** The reflection and transmission efficiencies for longitudinal and bending waves are calculated, taking into account the angular orientation. For example, when a longitudinal wave is incident, the angular strut redistributes wave energy, leading to variations in transmission efficiency compared to a straight beam crossing.

The updated velocity equations for the angular beam crossing are as given below.

The only change is seen in equations of v_{B2}.

$$
\begin{aligned}
v_{B1}(x) &= v_{1_+}(A_B e^{-jk_{B1}x} + r_B e^{jk_{B1}x} + r_j e^{k_{B1}x}), \\
v_{L1}(x) &= v_{1_+}(A_L e^{-jk_{L1}x} + r_L e^{jk_{L1}x}), \\
v_{B2}(x) &= v_{1_+}(t_{2Bx} e^{-jk_{B2}} + t_{2Bjx} e^{-k_{B2}}), v_{L2}(x) = v_{1_+} t_{2Lx} e^{-jk_{L2}} \\
v_{B2}(y) &= v_{1_+}(t_{2By} e^{-jk_{B2}} + t_{2Bjy} e^{-k_{B2}y}), v_{L2}(y) = v_{1_+} t_{2Ly} e^{-jk_{L2}} \\
v_{B3}(x) &= v_{1_+}(t_{3B} e^{-jk_{B3}x} + t_{3Bj} e^{-k_{B3}x}), v_{L3}(x) = v_{1_+} t_{3L} e^{-jk_{L3}x} \\
v_{B4}(y) &= v_{1_+}(t_{4B} e^{-jk_{B4}y} + t_{4Bj} e^{-k_{B4}y}), v_{L4}(y) = v_{1_+} t_{4L} e^{-jk_{L4}y}
\end{aligned} \tag{5.9}
$$

For the strut oriented at an angle θ, the wave components are resolved into their x- and y-components as:

$$
\begin{aligned}
t_{2L_x} &= t_{2L} \cos\theta, & t_{2L_y} &= t_{2L} \sin\theta, \\
t_{2B_x} &= t_{2B} \cos\theta, & t_{2B_y} &= t_{2B} \sin\theta.
\end{aligned} \tag{5.10}
$$

Reflection and transmission efficiencies for the angular crossing incorporate these decomposed components.

Table 5.2: Transmission efficiencies of an incident longitudinal wave in Lattice unit cell of Nylon-12 at incident frequency of 215 kHz and beam thickness of 10mm

ρ_{LL1}	0.155	ρ_{LB1}	0.032
τ_{LL2}	0.13	τ_{LB2}	0.11
τ_{LL3}	0.33	τ_{LB3}	0.023
τ_{LL4}	0	τ_{LB4}	0.22

5.4.2   3D Beam Crossing

Three-dimensional beam crossings involve multiple struts oriented along the x, y, and z axes, creating a highly interconnected network. Such configurations are representative of 3D lattice structures used in real-world applications. The 3D beam crossing is shown in Figure 5.6(b). There are total of six struts in x, y and z directions. The updated velocity equations for the structure are given by Equations (5.11). The results for an incident longitudinal wave ($A_L = 1$) for the cross section are given in Table 5.3.

$$
\begin{aligned}
v_{B1}(x) &= v_{1_+}(A_B e^{-jk_{B1}x} + r_B e^{jk_{B1}x} + r_{jB} e^{k_{B1}x}), \\
v_{T1}(x) &= v_{1_+}(A_T e^{-jk_{T1}x} + r_T e^{jk_{T1}x} + r_{jT} e^{k_{T1}x}), \\
v_{L1}(x) &= v_{1_+}(A_L e^{-jk_{L1}x} + r_L e^{jk_{L1}x}), \\
v_{B2}(y) &= v_{1_+}(t_{2B} e^{-jk_{B2}y} + t_{2Bj} e^{-k_{B2}y}), \quad v_{L2}(y) = v_{1_+} t_{2L} e^{-jk_{L2}y} \\
v_{T2}(y) &= v_{1_+}(t_{2T} e^{-jk_{T2}y} + t_{2Tj} e^{-k_{T2}y}) \\
v_{B3}(x) &= v_{1_+}(t_{3B} e^{-jk_{B3}x} + t_{3Bj} e^{-k_{B3}x}), \quad v_{L3}(x) = v_{1_+} t_{3L} e^{-jk_{L3}x} \\
v_{T3}(x) &= v_{1_+}(t_{3T} e^{-jk_{T3}x} + t_{3Tj} e^{-k_{T3}x}) \\
v_{B4}(y) &= v_{1_+}(t_{4B} e^{-jk_{B4}y} + t_{4Bj} e^{-k_{B4}y}), \quad v_{L4}(y) = v_{1_+} t_{4L} e^{-jk_{L4}y} \\
v_{T4}(y) &= v_{1_+}(t_{4T} e^{-jk_{T4}y} + t_{4Tj} e^{-k_{T4}y}) \\
v_{B5}(z) &= v_{1_+}(t_{5B} e^{-jk_{B5}z} + t_{5Bj} e^{-k_{B5}z}), \quad v_{L5}(z) = v_{1_+} t_{5L} e^{-jk_{L5}z} \\
v_{T5}(z) &= v_{1_+}(t_{5T} e^{-jk_{T5}z} + t_{5Tj} e^{-k_{T5}z}) \\
v_{B6}(z) &= v_{1_+}(t_{6B} e^{-jk_{B6}z} + t_{6Bj} e^{-k_{B6}z}), \quad v_{L6}(z) = v_{1_+} t_{6L} e^{-jk_{L6}z} \\
v_{T6}(z) &= v_{1_+}(t_{6T} e^{-jk_{T6}z} + t_{6Tj} e^{-k_{T6}z})
\end{aligned}
\tag{5.11}
$$

Table 5.3: Transmission efficiencies of a 3D beam crossing for an incident longitudinal wave of unit magnitude in Lattice unit cell of Nylon-12 at incident frequency of 215 kHz and beam thickness of 10mm

ρ_{LL1}	0.155	ρ_{LB1}	0.032
τ_{LL2}	0	τ_{LB2}	0.0.08
τ_{LL3}	0.46	τ_{LB3}	0.032
τ_{LL4}	0	τ_{LB4}	0.08
τ_{LL5}	0	τ_{LB5}	0.08
τ_{LL6}	0	τ_{LB6}	0.08

5.5 Conclusions

In this chapter the formulations for calculating ultrasonic transmission in a cross beam were solved. The cross beam can act as a unit cell for a lattice structure. The ultrasonic transmissions calculated as a function of incident wave frequency are given in Figure 5.2. Based on the results of the unit cell, the transmission efficiencies of a four cell structure were calculated and the changes in the transmission efficiency with the presence of damage were also calculated. This analytical method can provide a quick and efficient method of calculating ultrasonic transmission a lattice structure. Changes to the transmissions with the presence of damage also provides an analytical validation for further damage characterization studies. The velocity equations for an angular and 3D unit cell are also given which are used to calculate the transmission efficiencies for a particular unit cell as given in Table 5.2 and 5.3 respectively. Different form of unit cell can be used for evaluation of different 2D and 3D lattice structures.

Chapter 6

Damage Detection and Quantification

6.1 Introduction

This chapter presents the findings of the damage detection and quantification study conducted on a 2D lattice structure, fabricated using the Polymer-Laser Powder Bed Fusion (P-LPBF) method of additive manufacturing (AM). AM enables the creation of highly complex and customized geometries, which are especially advantageous for lightweight, high-performance structures. The lattice structure used in this study consists of a nine-cell 2D configuration made from Nylon, a material chosen due to its cost-effectiveness in manufacturing and its favorable ultrasonic transmission properties. Nylon is a commonly used material in AM due to its affordability and ease of processing. Furthermore, its ability to transmit ultrasonic waves effectively makes it suitable for ultrasonic testing.

While Nylon was selected for this study, the methodology developed can be easily extended to other AM materials, which may have different properties or applications. AM allows for the use of a wide range of materials, including metals, polymers, and composites, and this damage detection framework is versatile enough to be applied to other materials commonly used in AM, such as titanium or aluminum alloys, which are frequently used in aerospace and automotive industries.

The intricate internal geometries inherent to AM structures, like the fine lattice struts, make them highly susceptible to various types of damage, including fracture or breaking under stress. These complex structures are prone to manufacturing defects, such as incomplete fusion or internal voids, which can compromise their performance. Additionally, stress concentrations within the geometry can lead to premature damage. Traditional damage detection methods, such as visual inspection, are not practical for such complex geometries, underscoring the need for non-invasive and reliable damage detection techniques like ultrasonic testing.

Alternative non-contact techniques such as infrared thermography, X-ray computed tomography (CT) and vibration-based modal analysis were reviewed but not considered for the present study. Thermography is well-suited to near-surface defects in thin composites, yet its spatial resolution (0.5–1 mm) and sensitivity decrease markedly for polymer lattices thicker than 5 mm [143]. X-ray CT provides excellent volumetric resolution but requires long scanning times and high capital cost, making it impractical for in-situ monitoring of large, additively-manufactured lattices

[144]. Vibration-based methods detect global stiffness changes, which are insensitive to single-strut failures in lightweight periodic structures and typically require substantial mass-normalization and boundary-condition control [**?**]. Ultrasonic guided waves, by contrast, offer (i) sub-millimetre defect sensitivity, (ii) rapid single-shot interrogation, and (iii) straightforward integration of low-cost piezoelectric discs. Hence, this work focuses on ultrasonic SHM while acknowledging that thermography, CT and modal analysis remain valuable complementary tools for other defect types or validation purposes.

In this study, ultrasonic wave propagation was utilized to detect and quantify damage within the lattice structure. Ultrasonic waves are sensitive to internal changes, such as strut fractures, and offer an effective way to assess the structural integrity of these complex geometries. The research explores a range of damage scenarios, from one to ten broken struts, to assess how ultrasonic signals can detect and classify varying levels of damage. Different feature extraction techniques were used to extract useful information from the response signal which were then used to train a classification model for damage characterization.

This chapter is organized as follows:

- Section 6.2 describe the details of the testing setups, numerical modeling, and feature extraction.

- Section 6.3 presents the results of damage quantification based on the numerical work.

- Section 6.4 discusses the damage detection results and their interpretation.

- Section 6.5 provides details of the experimental results, validating the damage detection framework.

6.2 Numerical model and feature extraction

This section presents the numerical model used for simulating damage in a 2D lattice structure, the damage cases considered, and the techniques employed for feature extraction. Ultrasonic wave propagation is analyzed, and response signals are processed using Principal Component Analysis (PCA) and energy-based methods to extract features for damage classification. These features form the basis for training a neural network to assess the health state of the structure.

6.2.1 Lattice structure for numerical simulations

The lattice structure for numerical simulations is shown again in Figure 6.1. The 2D lattice structure comprises nine unit cells with a total of 36 struts. Two sensors are simulated for the structure, one at the top marked as Excitor and one at the bottom marked as Sensor, however they were also used in opposite roles. A 1.5 mm crack is simulated as damage in the structure. A 2-strut damage is shown in Figure 6.1(c) marked as d1 and d2.
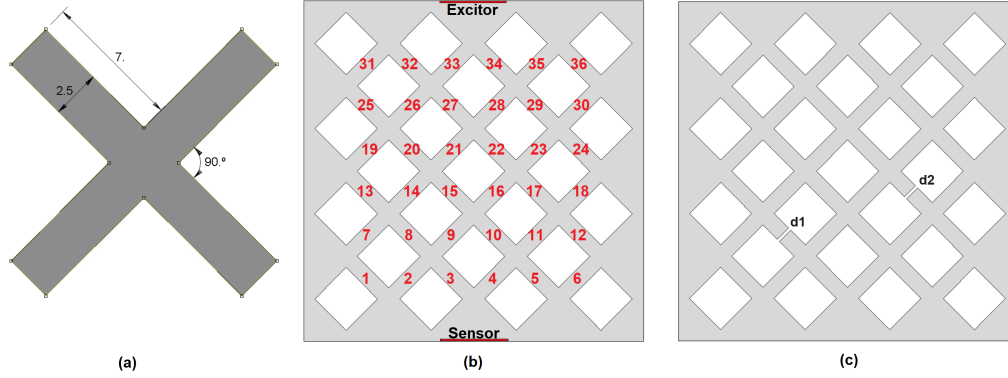
Figure 6.1: 2D lattice structure for numerical damage quantification (a) unit cell with mutually perpendicular struts(b) A 2D 36-strut lattice structure with two sensors (one at top and one at bottom) (c) lattice with simulated damage - two strut damage marked as d1 and d2

6.2.2   Damage cases and Sample size

One to ten strut damage is considered for the study. This forms a total of eleven damage cases i.e. one undamaged and 10 damaged cases for different number of strut damages. The nomenclature used to identify **strut damage** is **SD**. For clarity, 0-SD is designated as undamaged, 1-SD is for one strut damage and 10-SD is for ten strut damage. The number of possible damage locations increases exponentially as number of damaged struts increases with possible damage locations for ten strut damage close to twenty million. The factors that drive the sample size are (a) improving accuracy of the classification model (b) computational limitations (c) adequately covering the design space. Latin hypercube sampling (LHS) technique [145] is used for sample selection throughout the design space. LHS is a quasi-random sampling technique that ensures more distributed sampling. 36 parameters were assigned to LHS based on the locations of 36 struts, which were used to drive the design space. 500 samples are modeled for undamaged and for each damage case respectively. The sample size was chosen as 500 to keep a balance between computational and model efficiency. A total of 5500 samples are simulated in ABAQUS. For each sample, two responses are recorded: one with the transducer at the top and sensor at the bottom, and the other with the transducer at the bottom and sensor at the top. This leads to a total of 11000 unique data points with 1000 data points for each damage case. Material properties and error in sensor locations are randomly assigned to each sample from the normal distribution of these uncertainties as given is section 4.3.1.

6.2.3   Simulation of wave propagation

The simulation of wave propagation in the lattice structure is shown in Figure 6.2 for an undamaged and damaged structure (this simulation can be viewed when the document is open in Acrobat reader). The wave travels from the excitor and its response is captured at the other end of the structure. The total time of wave simulation is 0.001 sec but the frames have been slowed down to appreciate the wave response. The limits of magnitude are recalculated in each frame to better visualize as wave moves through the structure. The reflection of the wave from damage can

be seen in the initial frames.

Figure 6.2: ABAQUS simulation of wave propagation in an undamaged and damaged structure: The figure illustrates the propagation of ultrasonic waves from the excitation point, with the response captured at the opposite end of the structure. In the damaged structure, wave reflections from the damaged struts are visible, indicating the interaction of the wave with the damage. These reflections play a key role in damage detection.

6.2.4 Response signals

The raw response signals recorded at the opposite end of the structure are shown in Figure 6.3. The time domain response signal is recorded for a total time of 0.0004 sec. The amplitude of response is given in mm. The response signals are plotted for different damaged states against the undamaged response signals. Changes in response signals with the presence of damage can be seen for different damage cases.

6.2.5 Frequency response

The frequency response of the structure calculated using FFT is shown in Figure 6.4. The frequency response is centered around the excitation frequency of 215 kHz. While there is a change in the magnitude of the frequency response with damage, no phase shift is observed when damage is introduced.

6.2.6 Feature extraction

The response signal consists of more than 6000 data points. To reduce the dimensionality of the data and to extract useful features of data, two techniques were employed. The details of these techniques are already provided in 4.5 and extracted features are discussed below.

Features extraction using PCA

Principal component analysis(PCA) is used to extract features while significantly reducing the dimension of data. Principal components which defined the greatest variability in the data were identified. The number of principal components defining
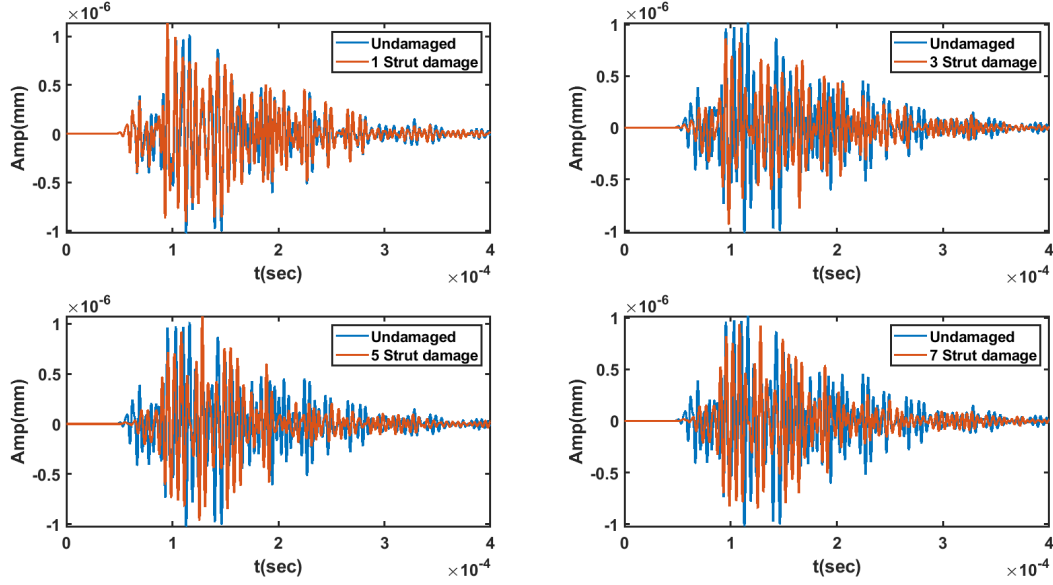
Figure 6.3: Raw time-domain response signals for four damage cases compared with the undamaged case: The plots show the amplitude of the response signal recorded at the opposite end of the structure for different damage states. As the number of damaged struts increases, the change in the signal amplitude becomes more pronounced, indicating the presence and severity of damage.
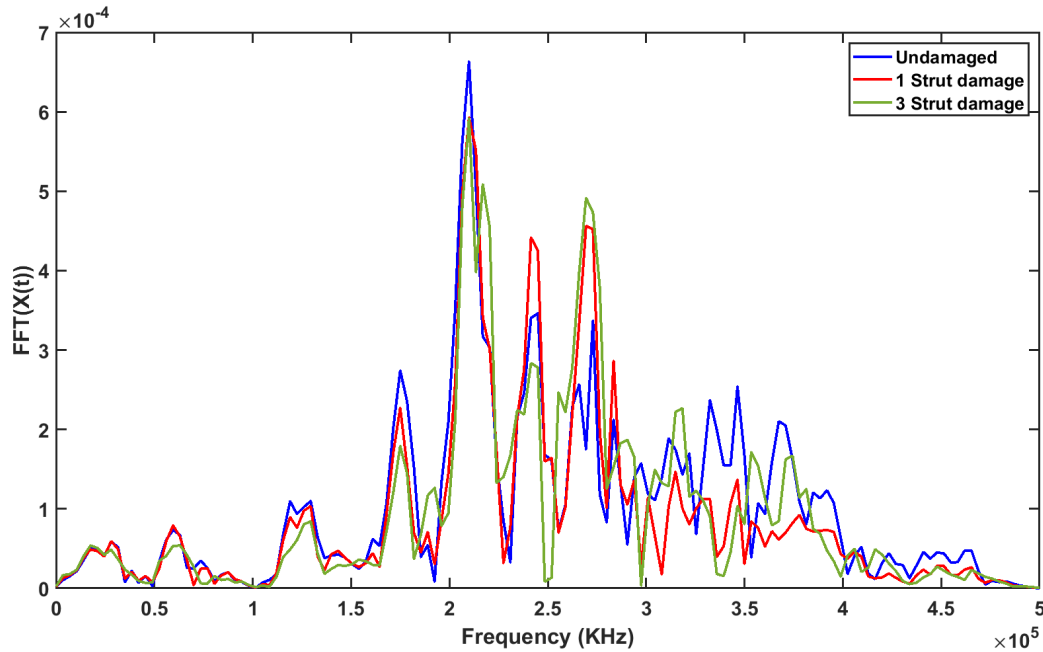
Figure 6.4: Frequency response (FFT) of the numerical model of the 2D lattice structure: The frequency response is centered around the excitation frequency of 215 KHz. Changes in the magnitude of response signal are observed

the percentage variability of data is shown in Table 6.1 below. It is seen that ninety percent of the data is defined by the first 29 principal components.

The plot of the first two principal components is shown in Figure. 6.5 which shows the variability of data and clustering for undamaged and damaged cases (SD-

Table 6.1: No of Principal components defining the percentage variability of data

No of Principal Components	Variability of data (%)
6	60
17	80
29	90
45	95
79	99

strut damage). There is better variability of data for lower damage cases whereas a lot of overlap is seen for higher damage cases.
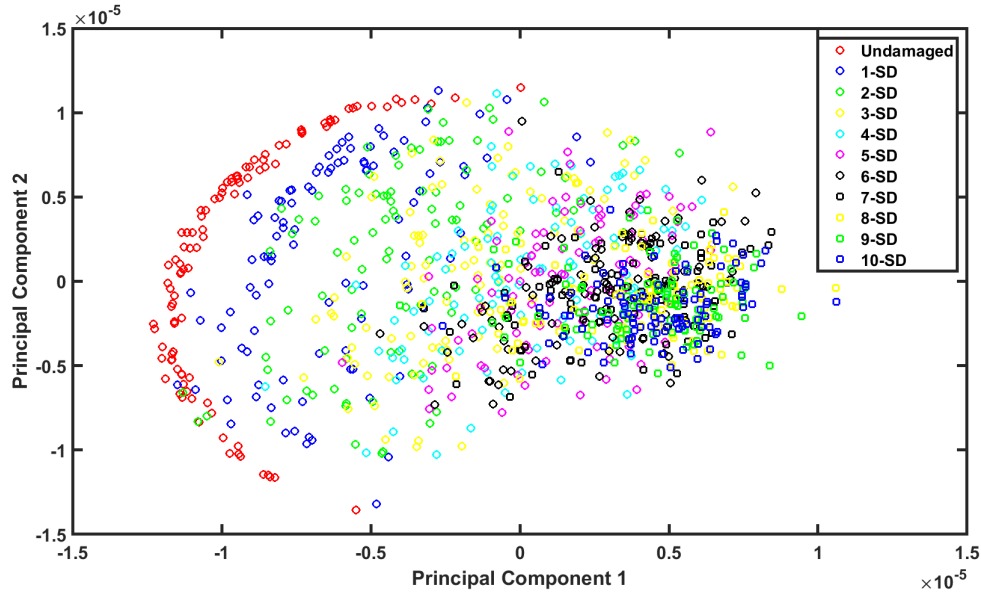
Figure 6.5: First two Principal Components of the numerical data. This plot shows the variability of the data for undamaged and damaged cases (SD-strut damage). The first two principal components account for a large portion of the variability in the data, with lower damage cases showing distinct separation, while higher damage cases exhibit more overlap

Energy Features (EFs)

The second method to extract features is to calculate the energy of the signal in different regions and using them as damage identification features. It was seen from the analytical study and the actual response signals (Figure 6.3) that the energy of the signal changes by the presence of damage. So, it is intuitive to use energy of signal as a damage sensitive feature. The plot of two energy features is shown in Figure. 6.6. A progressive change in the energies of signal is seen as the severity of damage increases. This shows that energy of signal is sensitive to the presence and severity of damage. The figures also shows that distinction between damage classes is good for lower damage cases. But for higher damage classes, the distinction starts to decrease. There is lot of overlap seen between the damage features in higher damage classes. This forms the basis of classification in damage quantification.
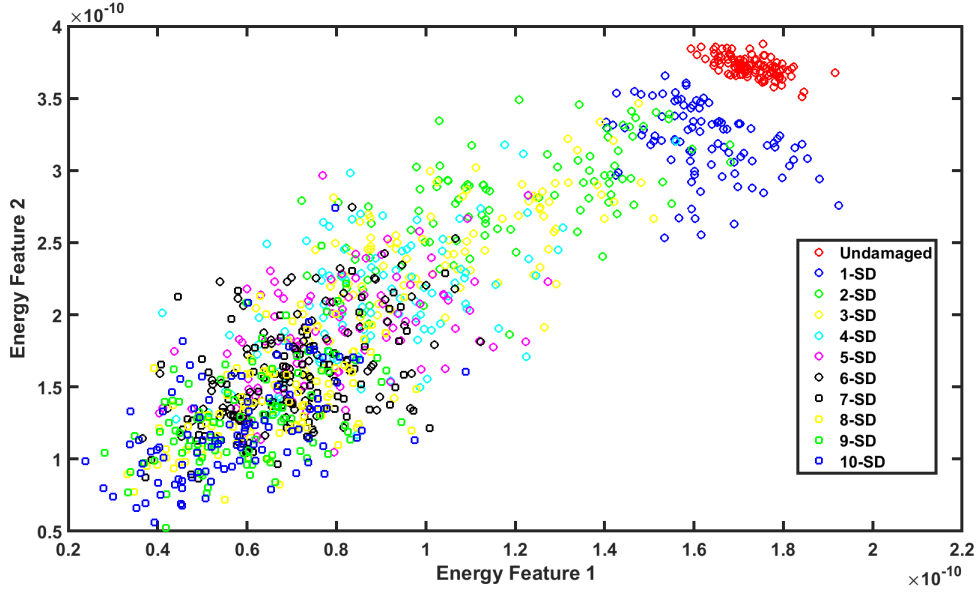
Figure 6.6: Energy feature plot for the numerical data for different damage states . The plot compares two energy features across different damage cases (SD-strut damage). As the number of damaged struts increases, the energy of the signal decreases progressively. However, the distinction between damage classes diminishes for higher damage cases, indicating a challenge in differentiating severe damage

6.2.7 Optimizing the classification model

The classification neural network is fitted to the data to determine the health state of the structure. One of the outputs of the classification model is the prediction accuracy of the model. Prediction accuracy is the percentage of correct predictions made by the classification model. Parameters of classification model were optimized to extract the best prediction accuracy. The optimized parameters of classification model are discussed below. Each parameter was optimized by fixing the other parameters of the model.

Optimizing the size feature vector

Size of feature vector is the number of features used to build the classification model. Prediction accuracy of the classification model was measured using different size of feature vectors. The increase in the size of the feature vector was seen to result in an improved accuracy of the classification model until an optimized value was reached. This is shown for both energy features and principal components in Figure 6.7. The optimized size of energy features is 50 and the number of principal components that provide the best prediction accuracy is 100 which describes more than 99% variability of data.

Optimizing the structure of Neural network

The parameters of the classification neural network were optimized to yield the best prediction accuracy. The number of hidden layers and the size of the hidden layers play an important role in the performance of the classification model. The parameters and their optimized values are given in Table 6.2. Parameter optimization
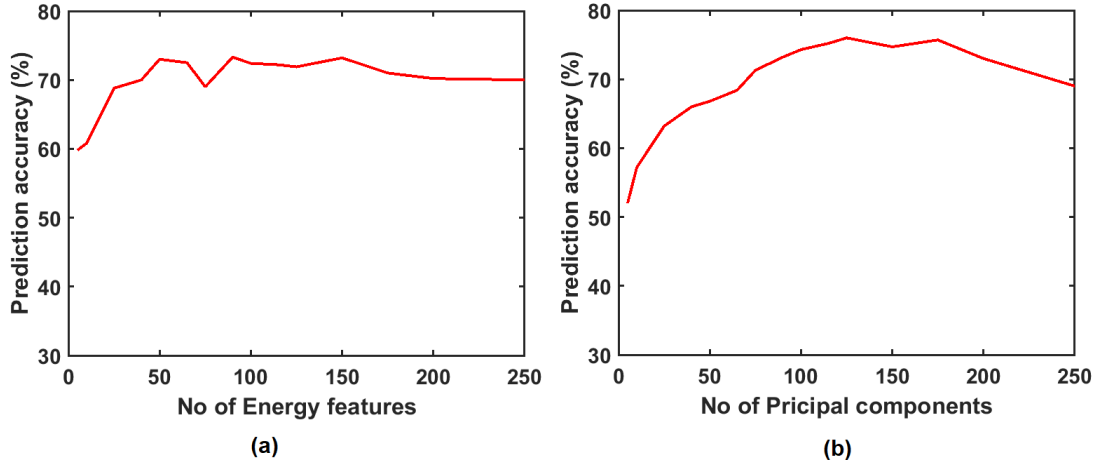
Figure 6.7: Optimizing Feature Vector Size: The graphs illustrate the impact of feature vector size on prediction accuracy for (a) energy features and (b) principal components. Accuracy improves with increasing vector size, stabilizing at optimal values of 50 for energy features and 100 for principal components. This demonstrates the importance of balancing feature size to enhance model performance without overfitting

results are depicted in Figure 6.8. Maximum two hidden layers were sufficient to produce optimized results and any increase in number of hidden layer did not offer any improvement in the performance of the model. Similarly, the optimized size of neurons in each layer also corresponds to the optimized feature vector size.

Table 6.2: Optimized parameters of neural network

Parameter	Optimized value
No of hidden layers	2
Size of first hidden layer	100 for PCA 50 for Energy features
Size of 2nd hidden layer	05 (half the size of output vector)

L2 Regularization Optimization

The regularization parameter λ was treated as a hyperparameter and optimized using a grid search in the range $[0.001, 0.1]$. This process was carried out through 5-fold cross-validation, where the dataset was split into training and validation subsets to assess generalization performance. For each value of λ, the neural network was trained, and the average validation accuracy across the folds was computed to ensure robust evaluation. The model's performance peaked at an optimal λ value of approximately 0.02, balancing the trade-off between overfitting and underfitting. This approach ensured that the model maintained complexity appropriate for accurate predictions while avoiding overfitting to the training data.

Having discussed the optimization of the classification model, the results of the damage detection and quantification will now be presented.
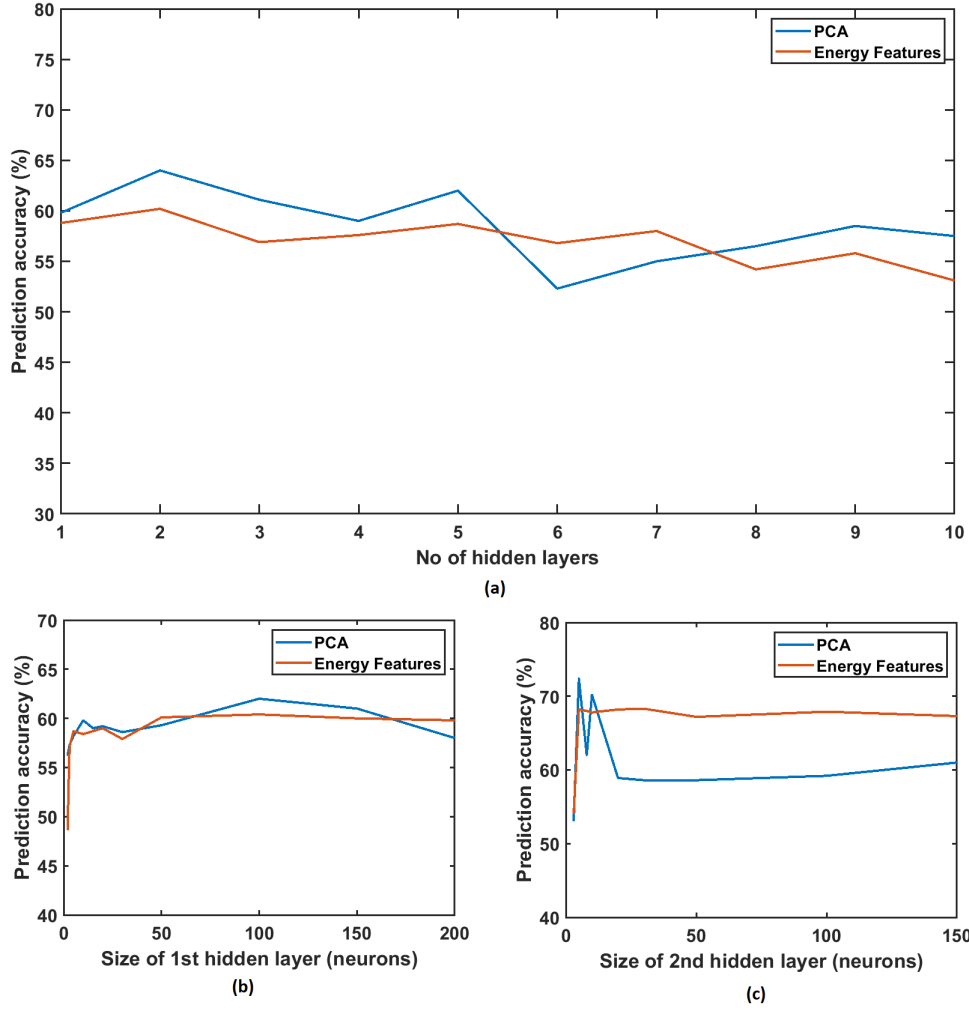
Figure 6.8: Optimizing Neural Network Parameters: The graphs depict the effect of varying (a) the number of hidden layers, (b) the size of the first hidden layer, and (c) the size of the second hidden layer on prediction accuracy

6.3 Numerical results for damage quantification

In this section, the numerical results of damage quantification are presented. The results of damage quantification are presented before damage detection as damage detection will be a subset of the damage quantification problem and will be treated as a binary classification problem. So, the results of damage detection will be a later stage. Damage quantification involves quantifying the severity of damage in the structure which in this case will be to determine the number of damaged struts in the structure. As previously discussed, a total of 11 damage states are being considered in this study, where one damage state is for undamaged and 10 damage states correspond to the number of damaged struts in the lattice varying from one to ten. Three different damage quantification levels were explored in this study. Each level is differentiated from the other on its treatment of damage cases and classification scheme. The three quantification models are enumerated below, followed by their details and results.

1. Level 1 quantification: Quantifying the exact number of damaged struts (from

> one to ten strut damage)

2. Level 2 quantification: Quantifying the damage into a group of broken struts (like a group of three to five damaged struts)

3. Level 3 quantification: Measuring the number of damaged cells in the structure

6.3.1   Level 1 quantification

For the level 1 quantification, the aim was to predict the total number of damaged struts in the structure. There are a total of 11 classifiers in this level, each corresponding to a number of damaged struts. One classifier is for undamaged and ten classifiers for one to ten strut damages. Features were extracted from 11,000 response signals of the simulated samples.

Training data

Eighty percent of the data was prepared as training data for the classification model. Eleven class labels were assigned to the corresponding damage state of the data. Class labels were named as 0SD (Strut Damage) for undamaged, 1SD for one strut damage, and so on, with the final class label 10SD for ten strut damage.

Results

The performance of the classification model is represented in three forms, i.e. classification scores, confusion matrix, and prediction accuracy. An example of the classification scores of four damage cases is shown in Figure 6.9. The green bars represent the actual number of damaged struts. The classification scores are distributed to the neighboring classifiers as well. Moreover, the classification scores are in the range of 0.3-0.4, indicating low confidence levels of measurement.

Prediction accuracy of the model is measured by assigning the predicted class to the damage case with highest classification score. The confusion matrices showing a comparison of the true and predicted classes using both Principal components (PCs) and Energy features (EFs) is shown in Figure 6.10. The confusion matrices shows good performance of the model for lower damage classes, with the classifiers being confused with the neighboring classifiers only. For higher class labels , the performance of the model is significantly reduced and a wide spread of classifier confusion is seen.

The prediction accuracy of the model was then measured, which shows how well the model is able to predict the true class labels. The prediction accuracy using eleven classifiers is given in Table 6.3 showing a prediction accuracy of 67% using PCs. It is important to mention here that prediction accuracy is not a good measure of the performance of the model in this case of eleven classifiers, as there is a lot of spread in the data and the classification scores are low for the predicted classes. It is better to view these results as a probability distribution of the data in multiple class labels giving a better understanding of the probable damage state of the structure. The probability distribution of the classified data along with the density estimate is shown in Figure 6.11. The density estimate shows a distribution of classification scores with neighboring classifiers. The probability distribution to the neighboring classes is high for the higher classes of damage.
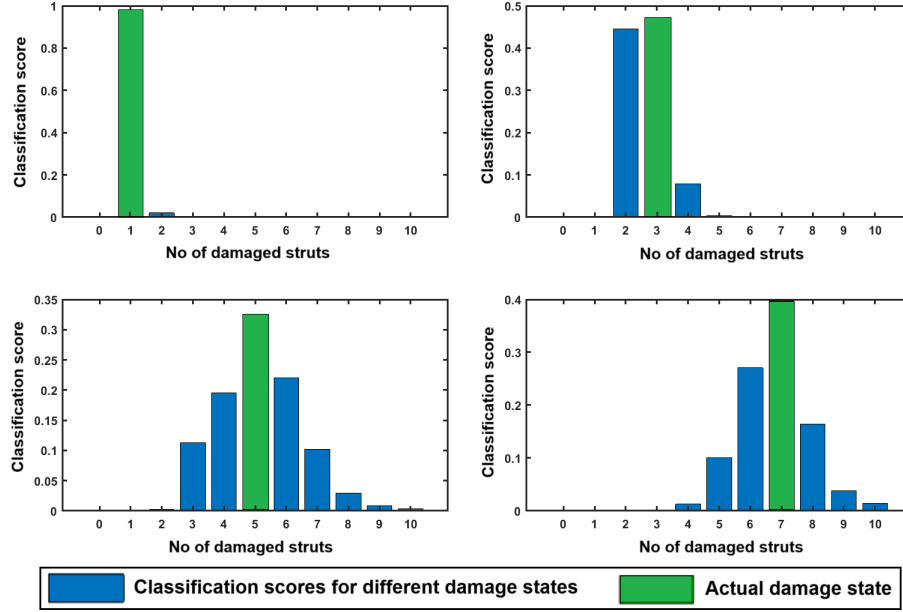
Figure 6.9: Classification scores for different strut damage levels. The green bars indicate the actual damage states, while the distributed scores across neighboring classifiers demonstrate the uncertainty in predictions. The spread reflects decrease in classifier accuracy, especially for higher damage states

Table 6.3: Prediction accuracy of classification model using 11 classifiers

	Using PCA	Using EFs
Prediction Accuracy (%)	67%	63%
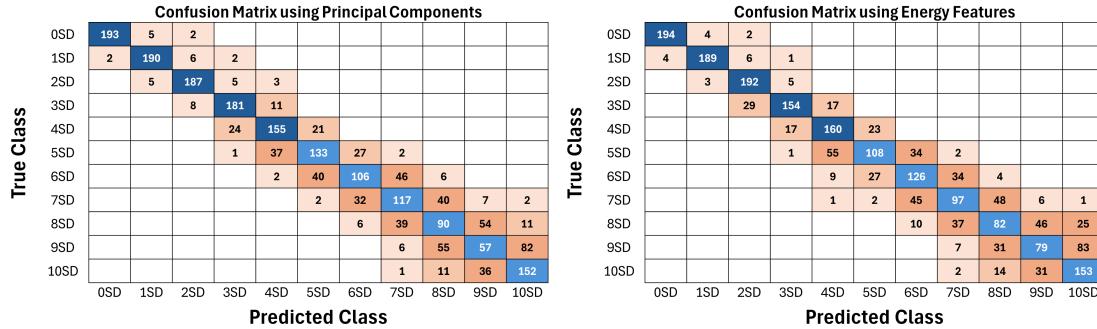
Figure 6.10: Confusion matrix showing classification results for 11 classifiers using principal components and energy features. The matrix highlights good performance for lower damage levels, but significant confusion among neighboring classes, particularly for higher damage states

6.3.2 Level 2 quantification

In the level 2 quantification, the number of classifiers were reduced by combining different damage states of the structure. The model with eleven classifiers did not provide a good classification of the data, especially for higher damage classes. Two new classifier sets were defined as follows:
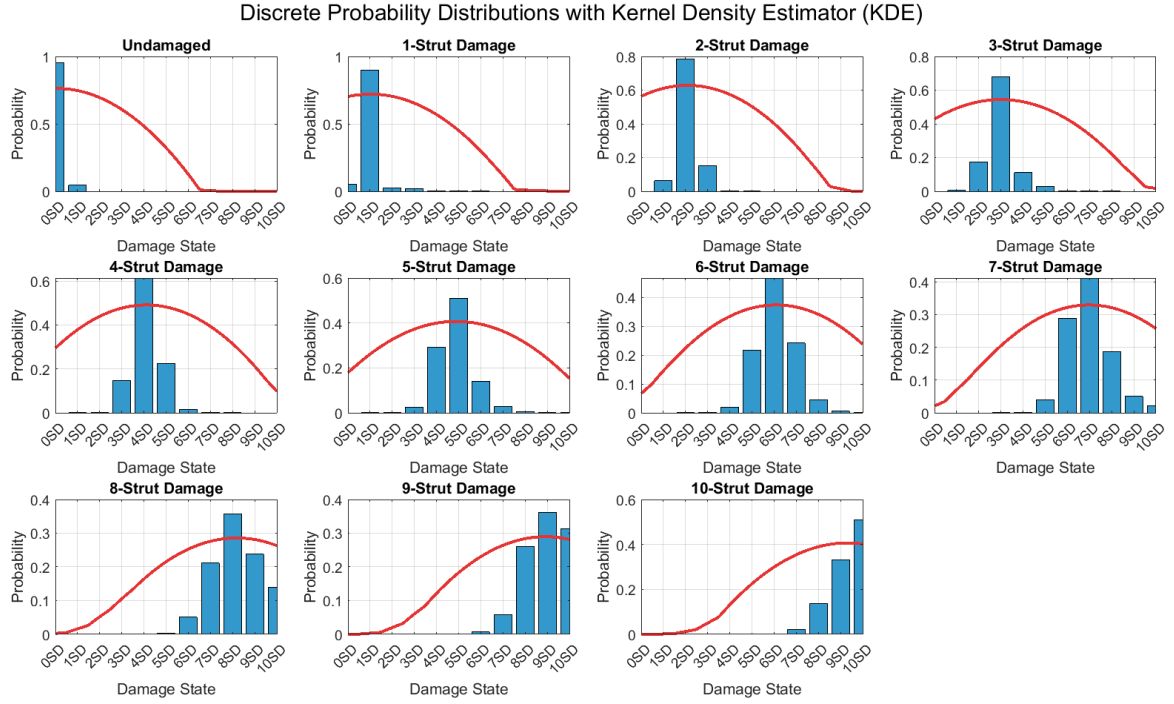
Figure 6.11: Probability distribution of classification scores for 11 classifiers. The density estimate illustrates the spread of predicted scores across neighboring classes, with higher damage states showing broader distributions, suggesting reduced confidence in predictions for these state

- In the first set of six classifiers, two damage states were combined to form one classifier (five classifiers for ten damage states) and one classifier was used for the undamaged state as shown in Table 6.4.

- In the second set, five classifiers were defined with lower damage cases having more classifiers than higher damage cases, as shown in Table 6.5. This was based on the findings of level 1 quantification, which showed better performance for lower damage cases.

Table 6.4: Class labels using six classifiers

Class definition	Old class labels	New class labels
Undamaged	0SD	0SD
One to two struts damage	1SD, 2SD	1-2SD
Three to four struts damage	3SD, 4SD	3-4SD
Five to six struts damage	5SD, 6SD	5-6SD
Seven to eight struts damage	7SD, 8SD	7-8SD
Nine to ten strut damage	9SD, 10SD	9-10SD

Training data

The data was trained based on the new set of class labels. Feature vectors were assigned new combined class labels and the classification model was trained accordingly.

Table 6.5: Class labels using five classifiers

Class definition	Old class labels	New class labels
Undamaged	0SD	0SD
One strut damage	1SD	1SD
Two to three struts damage	2SD, 3SD	2-3SD
Four to six struts damage	4SD, 5SD, 6SD	4-6SD
Seven to ten struts damage	7SD, 8SD, 9SD, 10SD	7-10SD

Results

The results for the level 2 quantification are now given. The confusion matrix for five and six classifiers is shown in Figures 6.13 and 6.12, respectively. The confusion of data with neighboring classifiers is much less in five classifiers than in six classifiers. Similarly, the classification scores for four damage cases (0SD, 3SD, 5SD, 7SD) are shown in Figure 6.14 for eleven, six, and five classifiers. The classification scores for the correct predictions are in the range of 0.3-0.4 for 11 classifiers, 0.6-0.7 for six classifiers, and 0.8-0.9 for five classifiers. These classification scores indicate high confidence levels for the model with five classifiers. Finally, the prediction accuracy for the five and six classifiers is given in Table 6.6. The prediction accuracy has significantly improved by grouping the classifiers with model having five classifiers greater than 90 percent accuracy. This is associated with the fact that this classification model has much higher classification scores for correct observation indicating high confidence levels.

Table 6.6: Comparison of prediction accuracy using five and six classifiers, showing improved performance with reduced classifier complexity.

	Prediction accuracy Using PCA	Prediction accuracy Using EFs
06 classifiers	84%	79%
05 classifiers	94%	92%
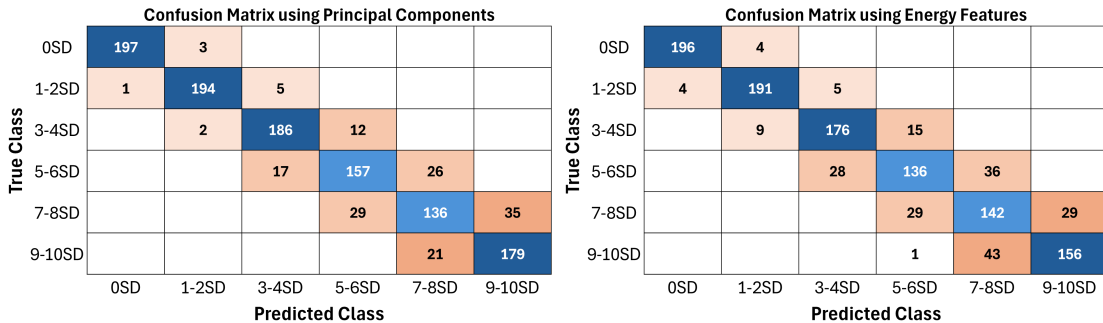
Figure 6.12: Confusion matrix for classification results using six classifiers, with (a) principal components and (b) energy features. The matrix demonstrates reduced confusion compared to 11 classifiers, especially for intermediate damage levels, indicating improved classification with fewer groups.
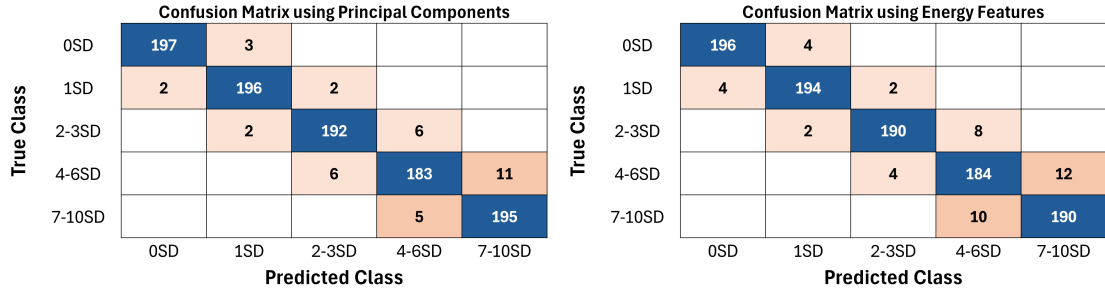
Figure 6.13: Confusion matrix for classification results using five classifiers, with (a) principal components and (b) energy features. The matrix reveals significantly better classification performance, particularly for higher damage levels, suggesting that grouping damage states enhances prediction accuracy.
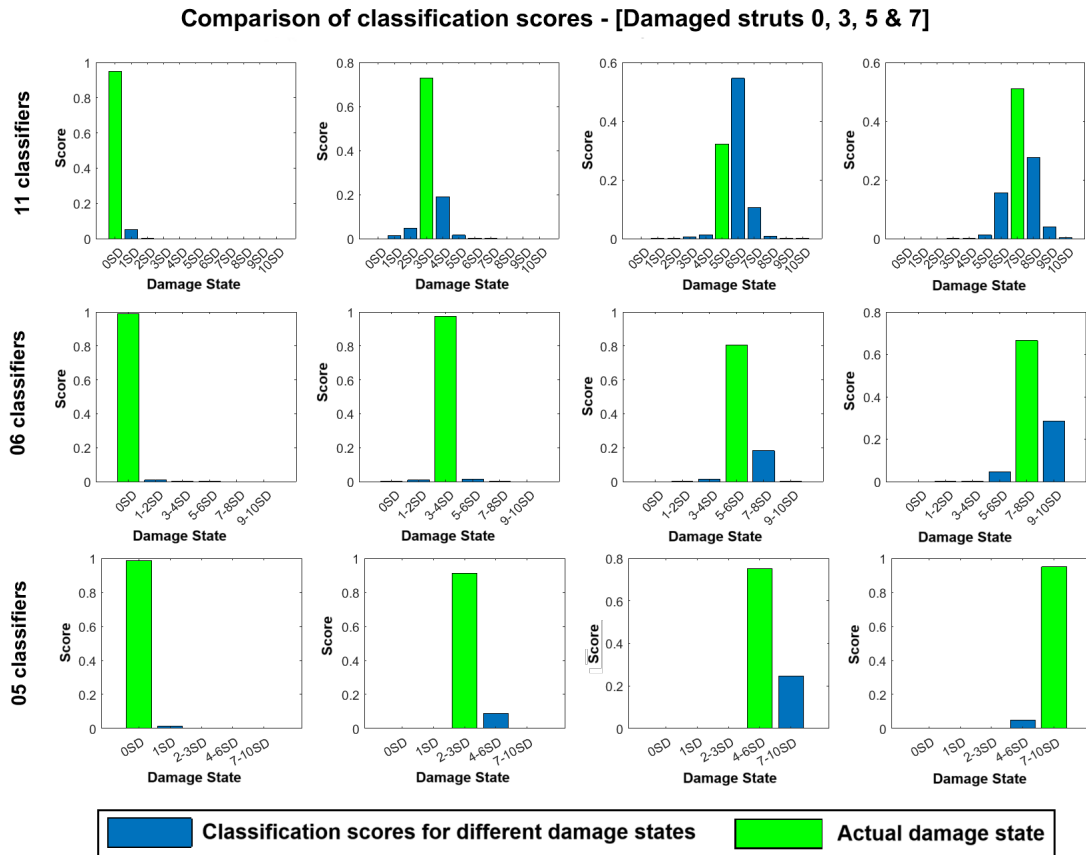
Figure 6.14: Comparison of classification scores for eleven, six, and five classifiers across selected damage cases. The scores show increasing confidence levels with fewer classifiers, as indicated by higher scores for correct predictions and reduced spread across neighboring classes.

Significance of quantifying group of damaged struts

In context of lattice structures, identifying a range of damaged struts makes an intuitive sense. This is because the lattice structures are formed with a large number of struts and it would be useful to identify a range of damaged struts which may drive a decision on the reliability of structure. For example, it would be useful to

know that four-to-six struts are damaged in the structure with high confidence than estimating the exact number of damage struts with low confidence. Quantifying a group of damaged struts may provide a reliable model for application on a variety of lattice structures and help implementation in real world application.

6.3.3 Level 3 quantification

Another important form of damage quantification in view of lattice structures can be to determine the number of damaged cells or zones in the structure. Lattice structures are formed by multiplication of its unit cell, and a typical lattice is formed by a large number of cells. It can serve a useful purpose to determine the number of damaged cells in the lattice based on which a decision regarding integrity of structure may be made.

With this application in mind, the lattice structure was divided into nine cells each containing four struts. The cell partitions are shown in Figure 6.15.
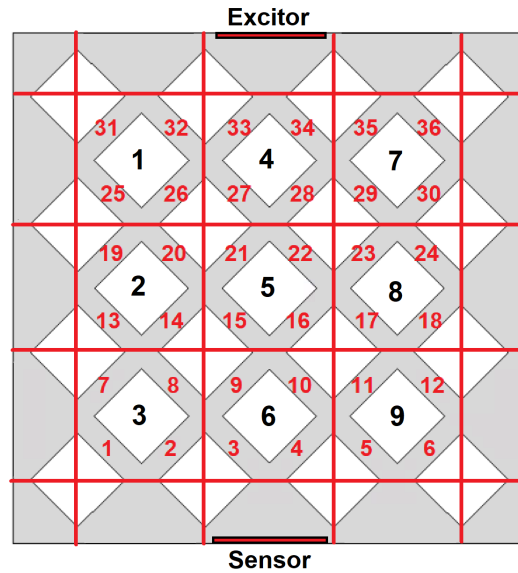
Figure 6.15: Partitioning of the lattice structure into nine cells, each containing four struts. This division provides a framework for damage quantification at the cellular level

Training data

A total of six classifiers were defined to quantify damaged cells. A label was assigned up to four cell damage (CD) and then a label was assigned for five or more cell damage, which would mean failure (F) of the structure. The class labels are shown in Table 6.7. Data from the 11,000 samples were assigned class labels based on the presence of damaged struts in the cells. If more than one strut is damaged in a cell, it would still be quantified as one damaged cell.

Table 6.7: Class labels for quantifying damaged cells

Class definition	Class label
Undamaged	0CD
One cell damage	1CD
Two cell damage	2CD
Three cell damage	3CD
Four cell damage	4CD
Five or more cell damage	F

Results

The classification scores for few damage cases are shown in Figure 6.16. The spread of classification scores indicates good performance of the classification model. The confusion matrix is shown in Figure 6.17. The prediction accuracy for quantifying damaged cells is 92 % using PCA and 89 % using EFs. Excellent prediction accuracy combined with high classification scores of the predictions indicated a reliable model for quantifying number of damaged cells in the structure.
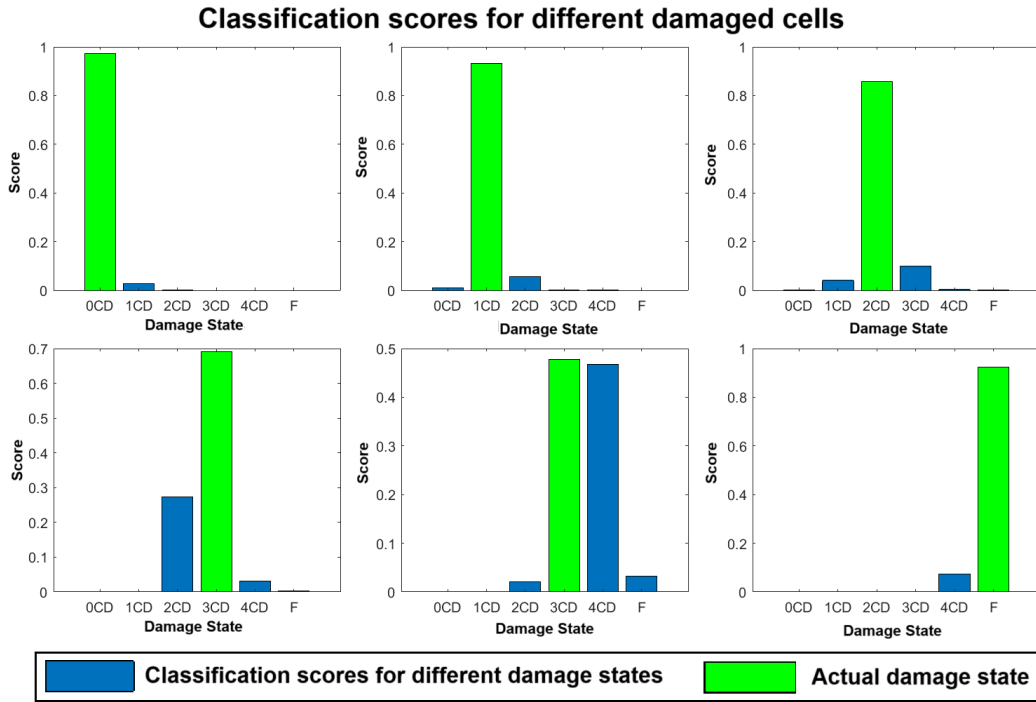
Figure 6.16: Classification scores for different number of damaged cells. The spread of scores demonstrates the model's ability to quantify damaged cells enhancing overall assessment reliability.

6.4 Numerical damage detection

The first aim of this study was to detect the presence of any damage in the structure. This is to distinguish between the healthy and damaged structures. In this case, a structure with any number of damaged struts will be considered as a damaged.

Confusion Matrix for Damaged Cells

True Class \ Predicted Class	0CD	1CD	2CD	3CD	4CD	F
0CD	192	6				
1CD	2	188	8	1		
2CD		6	183	9	3	
3CD			9	179	14	2
4CD				11	176	14
F					7	184

Figure 6.17: Confusion matrix for level 3 quantification using PCA. The matrix indicates strong classification performance, with minor misclassifications suggesting the model's potential for quantifying damaged cells.

For this, a binary classification model was trained on the numerical data with two classifiers i.e. damaged and undamaged. The prediction accuracy for detecting the presence of damage was very high in the range of 92-94 percent. This is also indicated in the confusion matrices of damage quantification as shown in Figures 6.10, 6.12 and 6.13 which shows high accuracy of predicting undamaged class. Furthermore, the classification scores for damage detection were also in the range of 0.8-0.9 indicating high confidence level of the predicted results.

6.5 Experimental model and results

To validate the numerical results, detailed experimental work was undertaken. The details of experimental apparatus, materials, and methods are already discussed in the Chapter 4.4. The numerical study has provided a good methodology for damage detection and quantification in which different quantification models were developed and tested. The experimental work is aimed to validate the applicability of the methodology of real structures. The numerical classification model was built using a large sample size which provides a robust trained classification model. This is a limitation with experimental work where only a limited number of samples can be tested. It is not feasible to build a standalone classification model using experimental data for the design space of the current problem having a large number of classifiers and damage cases. Therefore, a strategy was devised to test the experimental data on the numerical classification model. The strategy had following key aspects:

- To overcome the limitation of experimental data, yet have a methodology to validate the the numerical model.

- In the first step, the experimental data was scaled and normalized to the numerical data using methodology given in Chapter 4.7. The ensured consistent scales for both data sets.

- Features including PCs and EFs were extracted from the normalized experimental data and fitted to the numerical classification model.

- Performance of the model for the experimental data was calculated in terms of prediction accuracy for correct classifications.

Details of the experimental data collection, normalization and results are now presented.

6.5.1   Sample size and data collection

A total of 10 samples were manufactured for damage detection and quantification study. The manufactured lattice structure and the sequence of damage to the samples is given in the Figure 6.18. The response data from the samples were collected giving a total of 110 response signals.
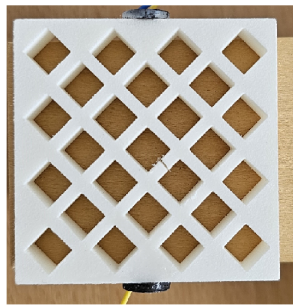
Sample	Damaged Strut No									
1	6	10	21	27	30	3	13	23	19	35
2	4	22	28	18	32	7	11	31	13	36
3	10	30	14	35	24	2	26	6	20	4
4	13	28	22	26	23	35	11	3	30	15
5	20	14	5	26	7	10	31	35	23	28
6	23	13	19	2	6	27	36	10	21	34
7	26	17	22	5	11	3	20	35	14	31
8	29	31	19	36	2	13	26	7	19	5
9	31	21	18	30	11	25	15	6	38	2
10	35	6	10	27	12	23	2	31	21	15

Figure 6.18: Sequence of damage progression across ten lattice samples, demonstrating increasing severity of damage from single-strut to multi-strut failures for experimental analysis.

6.5.2   Response signals and feature extraction

Some of the raw signals from experimental results are shown in Figure 6.19. Plot of two principal components and energy features extracted from experimental data are plotted in Figure 6.20 and 6.21 respectively showing the spread of damage clusters. The experimental data also shows a similar trend in the change of damage features as the damage progresses. The distinction between damage features starts to decrease for higher damage cases. The frequency response of the experimental data is shown in Figure 6.22 which is centered around the excitation frequency.

6.5.3   Normalizing experimental data

The experimental data was normalized to the numerical data using the equation given in section 4.6.4. The normalization process involved normalizing he amplitudes
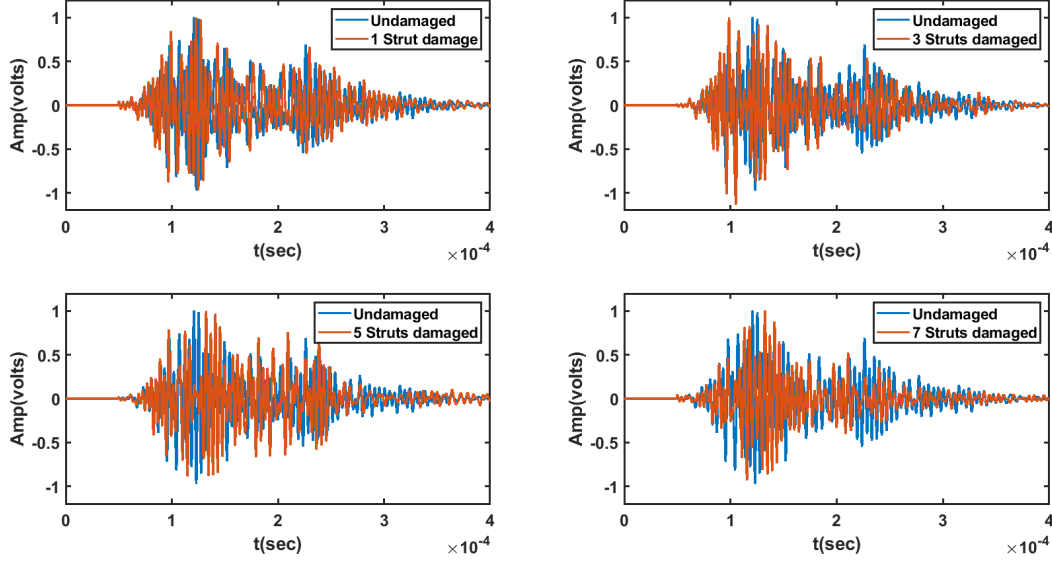
Figure 6.19: Time-domain response signals for four damage cases compared with the undamaged case, highlighting the progressive decrease in signal amplitude with increasing damage severity.
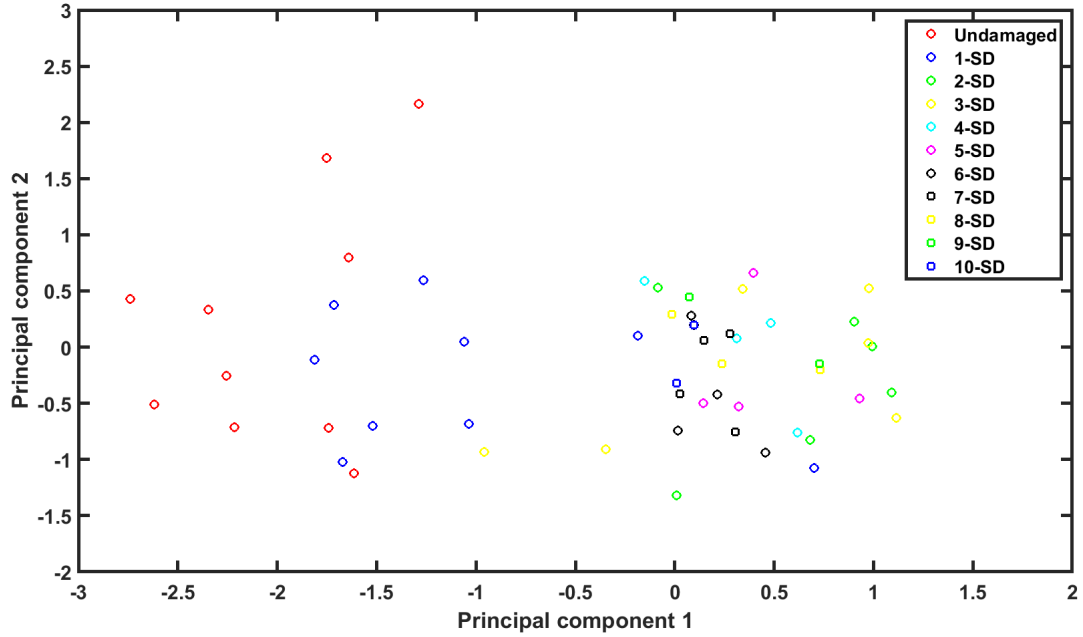
Figure 6.20: First two Principal Components (PCs) extracted from experimental data of ten lattice samples, showing clustering for different damage states.

of experimental data to the numerical response signals. Features were then extracted from the normalized experimental data and fitted to the numerical classification model.

6.5.4 Comparison of Numerical and Experimental Signals

To validate the accuracy of the developed numerical model, a comparison between the simulated and experimentally acquired ultrasonic response was performed. The
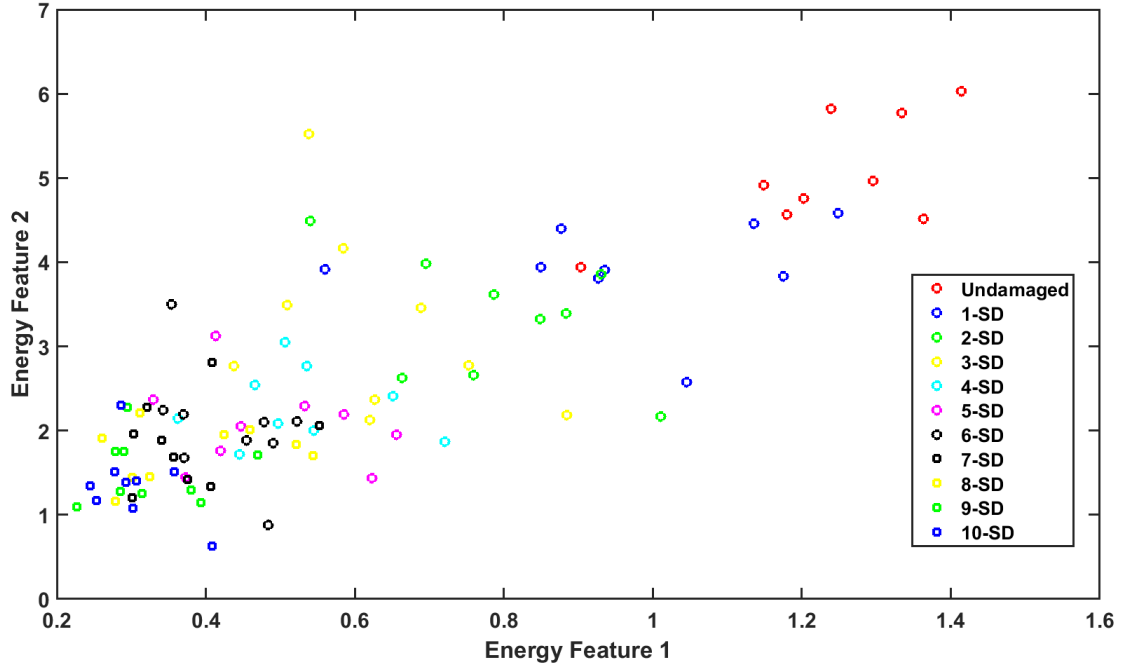
Figure 6.21: Two Energy Features (EFs) extracted from experimental data of ten lattice samples, showing clustering for different damage states.
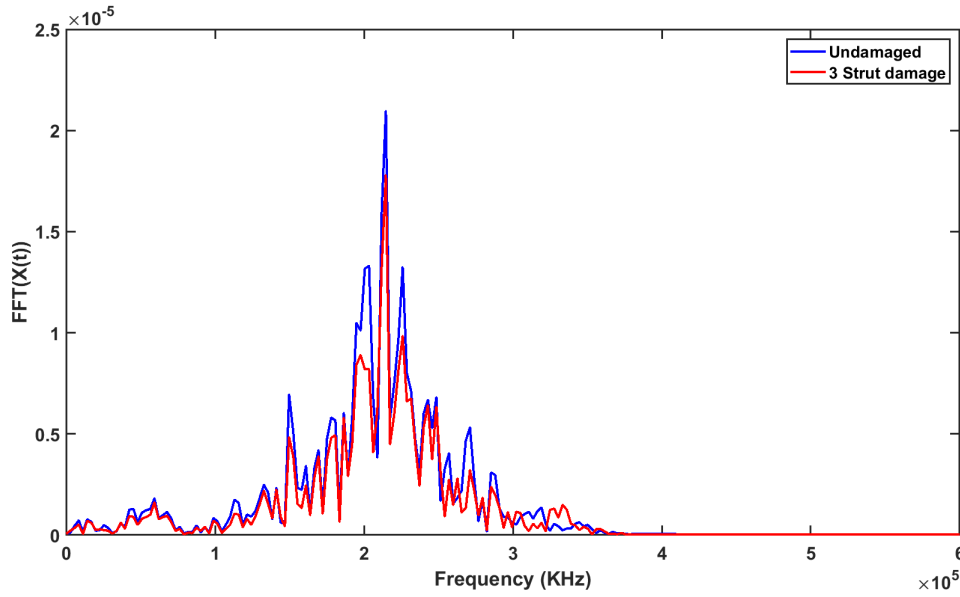
Figure 6.22: Frequency response of experimental data, illustrating the reduction in response magnitude with increasing damage.

experimental signal was normalized to match the amplitude scale of the numerical signal, ensuring a consistent basis for comparison. As shown in Figure 6.23, both signals exhibit good correlation in terms of waveform shape, amplitude evolution, and dominant frequency content. The arrival time of the initial wave packet, peak amplitudes, and subsequent decay patterns closely match between the two datasets. Minor deviations are observed in high-frequency components, which can be attributed to physical phenomena such as sensor noise, boundary imperfections,

and material inhomogeneity in the physical specimen, which are not fully captured in the idealized numerical model. Nonetheless, the degree of agreement between the two signals confirms that the numerical model accurately represents the wave propagation behavior in the lattice structure and is suitable for further parametric and damage characterization studies.
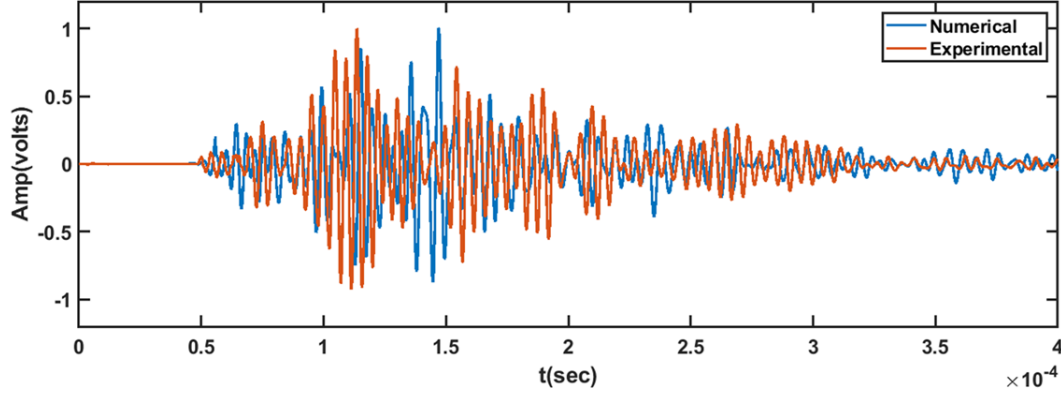
Figure 6.23: Comparison of normalized experimental and numerical signals

6.5.5 Results

The normalized experimental data was tested with the classification model trained over numerical data. The results of Level 2 & Level 3 quantification with the experimental data are shown in Figure 6.24 with the help of confusion matrix. The prediction accuracy of damage quantification for different cases for both PCA and EFs is given in Table 6.8. The prediction accuracy for damage detection with the normalized experimental data came out to be 83 percent.
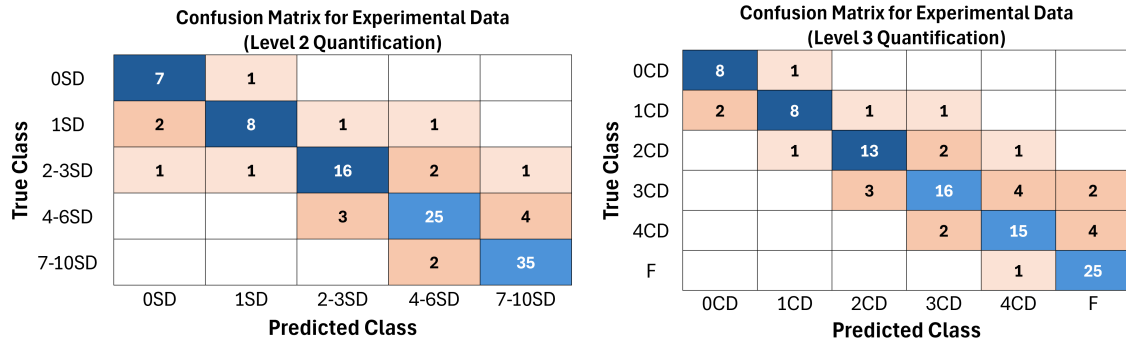
Figure 6.24: Results of the Normalized experimental data fitted to the numerical classification model. Confusion Matrix for Level 2 quantification depicts the performance of model for five classifiers combining different strut damages (SD-Strut damage). Confusion Matrix for Level 3 Quantification shows the performance of model for five cell classifiers (CD-Cell Damage)

Table 6.8: Prediction accuracy of normalized experimental data fitted to the numerical classification model, demonstrating the alignment between experimental and numerical results.

	Lev 1	Lev 2	Lev 2	Lev 3
	11 Classifiers	06 Classifiers	05 Classifiers	05 cell classifiers
PCA	28%	59%	74%	77%
Efs	32%	63%	82%	85%

6.6   Summary and Conclusions

This chapter presented a comprehensive methodology for damage detection and quantification in lattice structures using ultrasonic techniques. The approach involved numerical simulations to generate ultrasonic response signals for both undamaged and damaged lattice structures, followed by feature extraction using Principal Component Analysis (PCA) and energy-based metrics. A neural network classification model was developed to classify damage levels, and experimental data was normalized to validate the numerical methodology. This integrated approach bridges the gap between simulations and practical applications, enabling robust structural health monitoring of lattice structures.

Summary of Main Results

- **Numerical Simulations:** A nine-cell, 36-strut lattice structure was used to simulate various damage cases, generating 11,000 samples. Ultrasonic response signals exhibited distinct variations between undamaged and damaged states, providing a robust basis for feature extraction. PCA effectively reduced data dimensionality, enabling separation of damage states based on extracted features.

- **Damage Detection:** Binary classification achieved over 90% accuracy, reliably distinguishing between damaged and undamaged states. The high accuracy of damage detection confirms the robustness of ultrasonic signals for identifying the presence of damage.

- **Damage Quantification:** Neural network models for Level 1 quantification (11 classifiers) struggled with higher damage levels, showing increased misclassification. Simplified Level 2 (5 or 6 classifiers) and Level 3 (5 cell classifiers) quantification significantly improved accuracy, achieving over 90% prediction accuracy for numerical data. Classification scores indicated improved confidence and reduced uncertainty with simplified classifiers.

- **Experimental Validation:** Experimental data, normalized to fit the numerical model, achieved 78–84% accuracy for Level 2 and Level 3 quantifications. Classification scores ranged from 0.7 to 0.9, validating the consistency between experimental results and numerical predictions.

Conclusions

- This study demonstrates that ultrasonic testing, combined with PCA and neural network classification, provides a reliable and effective method for detecting and quantifying damage in lattice structures. The approach offers a strong foundation for structural health monitoring applications.

- Simplifying the classification process by reducing the number of classifiers significantly improves accuracy, particularly for higher damage levels, while also reducing computational demands. This makes the methodology practical and scalable for real-world use.

- The close agreement between numerical simulations and experimental validation highlights the robustness and adaptability of the developed approach. The ability to normalize experimental data to align with numerical models further enhances its practicality.

- Achieving over 90% accuracy in binary damage detection and reliable quantification across damage levels underscores the strength of the methodology. These results pave the way for applying this approach to more complex lattice geometries and advanced materials.

The methodologies and results from this chapter provide the foundation for Chapter 7, which explores damage localization in lattice structures. This next step applies advanced ultrasonic analysis to identify the spatial position of damage, further advancing the structural health monitoring framework.

Chapter 7

Damage Localization

7.1 Introduction

This chapter investigates the methodologies and results of damage localization within lattice structures, focusing on identifying the spatial location of damage. Damage localization is a key component of structural health monitoring as it enables precise identification of the affected areas, facilitating timely maintenance and reducing operational risks. Unlike damage detection and quantification, localization requires specialized techniques to map the position of damage within a structure accurately. The inherent complexity of AM lattice structures, due to their intricate geometries and extensive network of cells and struts, poses significant challenges for damage localization. To address these challenges, a systematic approach was developed using different localization models to improve the localization accuracy. Sensor triangulation methods were also employed to enhance localization accuracy by using spatial information.

This chapter is organized as follows:

- In Section 7.2, the details of lattice structure and model parameters are given.

- Section 7.3 outlines the numerical results of different localization models.

- Experimental results are given in Section 7.4

- Summary and conclusions are presented in Section 7.5

7.2 Lattice structure and model parameters

Two different lattice structures were tested during this study. One is a 16-strut lattice structure and the other is a 36-strut lattice structure. The methodology was first developed on the 16-strut lattice structure and later tested on the 36-strut lattice structure. A two-sensor configuration was used for acquiring the response signals, and subsequently, multiple sensors were also used for more effective damage localization. The lattice structures are shown in Figure 7.1.

7.2.1 Feature extraction and classification model

Both principal components and energy features were extracted and used for damage localization. The size of these features was used consistently in this study as already
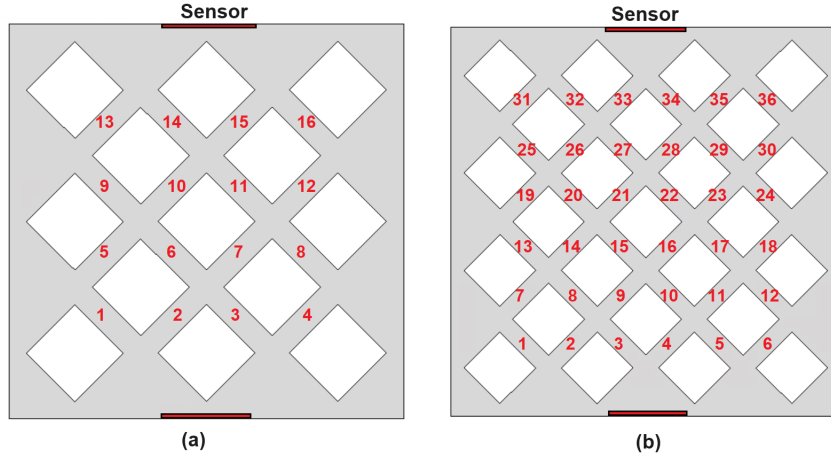
Figure 7.1: Lattice structure (a) 16 strut lattice structure (b) 36 strut lattice structure

optimized in the damage quantification study (refer to Section 6.2.7). These are reproduced again in Table 7.1.

Table 7.1: Number of features used for localization study

Feature	Size
Principal components	100
Energy features	50

The classification model used in the localization of the damage is the same as that used in the study of the detection and quantification of the damage. The following optimized parameters of the neural network were consistently used in this study as shown in Table 7.2.

Table 7.2: Parameters of classification model for localization

Parameter	Value
No of hidden layers	Two
Size of 1st hidden layer	100
Size of 2nd hidden layer	5
Loss function	Cross entropy
Optimization	Gradient descent

7.2.2 Localization Case Studies

Three different localization models were studied in this work. The localization models differed based on the area of the structure where damage is being localized. The three models are as given below:

- Localization Model A: In the model the predictions are made the location of individual damaged strut. Location of upto three damaged struts is studied in this model.

- Localization Model B: In this model the location of damaged cells is estimated.

- Localization Model C: This model uses spatial localization technique using multiple sensor pair to locate damage in different zones of the structure.

Now the numerical methodology and results for these three localization models will be discussed in detail.

7.3 Numerical Results

A detailed numerical study was first conducted to develop a methodology for damage localization. The details of numerical modeling of lattice structure are given in Section 4.3. Both 16 and 36 strut lattice structures were modeled in ABAQUS and simulated using explicit dynamics. A total of 500 samples were simulated for each damage case. Data from multiple sensors were recorded and localization problems for up to three strut damages were studied. The possible locations of damage for 36 and 16 strut structures are as given in Table 7.3.

Table 7.3: Possible damage locations for one, two and three strut damage

Damage	No of possible damage locations	
	36 strut structure	**16 strut structure**
1-strut damage	36	16
2-strut damage	630	120
3-strut damage	7140	560

There are three localization models which were developed and explored in this work. Each localization model is different in the approach and the area of the structure in which damage is localized. The results from the three localization models are now given in the following sections.

7.3.1 Localization Model A

In this localization model, a global localization technique was used to approximate the location of damaged struts. The data from a two-sensor configuration was used to train the classification model, and inferences were made on the location of the damaged struts. The localization model is represented in Figure 7.2.
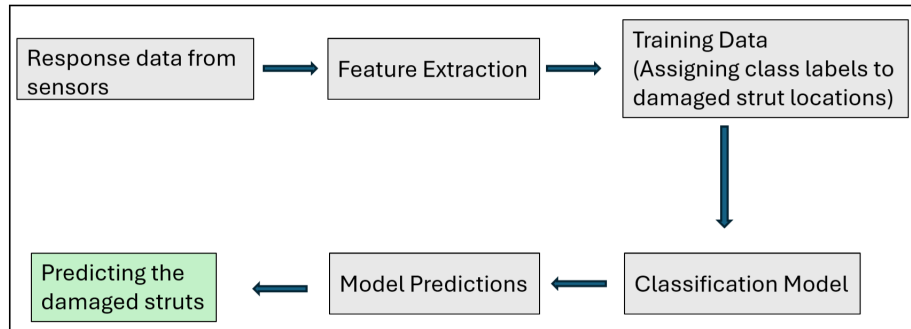
Figure 7.2: Flowchart of Localization Model A

Training data

Response data was measured from the two sensors. A total of 1000 data points were taken for each one, two, and three strut damage. The possible damage locations for both 16 and 36 strut lattices are quite large, especially for two and three strut damage, as shown in Table 7.3. This is particularly problematic in the localization study where each damage location is to be treated as a classifier corresponding to a

specific damage location. It is not practical to use such a large number of classifiers for the classification model. Instead, the features extracted from the data were assigned labels that corresponded to the location of the damaged struts. There are a total of 16 labels for the 16-strut lattice and 36 labels for the 36-strut lattice corresponding to the number of struts, respectively. One strut damage is assigned one label, two strut damage cases are assigned two labels corresponding to the individual location of each damaged strut, and similarly, for three strut damage, three labels are assigned. An example of assigning classification labels to the 36-strut lattice is shown in Table 7.4.

Table 7.4: Example of classification labels of 36-strut lattice for Localization Model A

Damage type	Damaged Strut No	Classification label for training data
1 Strut damage	6	Label - 6
2 Strut damage	11, 24	Label 1 - 11 Label 2 - 24
3 - Strut damage	4, 19, 32	Label 1 - 4 Label 2 - 19 Label 3 - 32

Classification scheme

The localization in this model was not based on hard classifications. Instead, the classifications were based on the posterior probabilities or classification scores. As an example, for three strut damage, the three labels with the highest classification scores correspond to the location of three broken struts, and prediction accuracy was measured based on how many of the first, second, and third labels were true. An example of classification scores for the 16 and 36 strut lattice is shown in Figure 7.3. The classification scores for each damaged strut location are given, and the green bars indicate the actual damaged strut. The classifiers with the highest classification scores were used to measure the prediction accuracy if they matched with the true location of the damage.

Results

The prediction accuracy for 16 and 36 lattice structures is given in Tables 7.5 and 7.6, respectively. The prediction accuracy for localizing a single damaged strut is good. However, correctly predicting the location of the second and third damaged struts has very low accuracy. Furthermore, it is seen that the classification scores are in the range of 0.2-0.3 for the 16 strut lattice and 0.1-0.2 for the 36 strut lattice. This signifies a low confidence level of the predictions; hence, this model is not robust enough to predict the locations of damaged struts with reasonable accuracy.
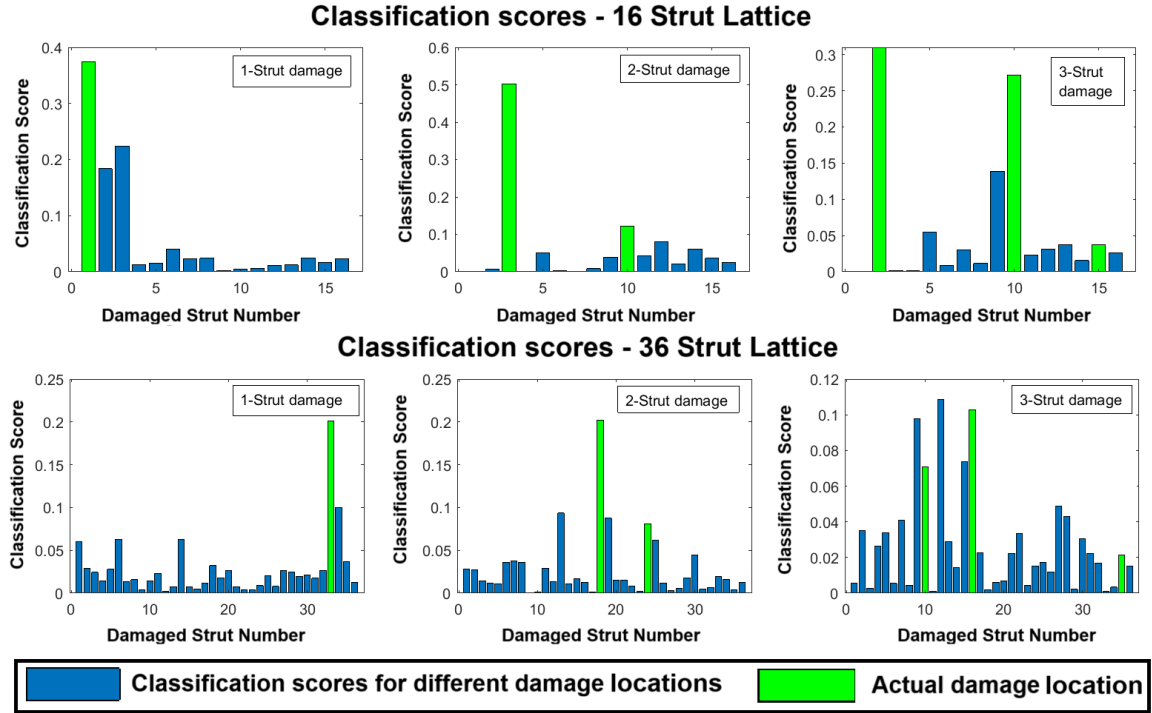
Figure 7.3: Bar graphs for classification scores from Localization Model A for damaged struts in the 16-strut and 36-strut lattices. True damaged struts are indicated by green bars, with neighboring bars showing model uncertainty for different damage levels. The results demonstrate good classification for single-strut damage but reveal challenges in handling overlapping scores for multiple struts.

Table 7.5: Classification accuracy of Localization model A - 16 strut lattice

Damage type	Classification output (based on classification scores)	Prediction accuracy (%)
1-Strut damage	One correct Label	84%
2- Strut damage	Atleast one correct label	64%
	Two correct label	52%
3-Strut damage	Atleast one correct label	62%
	Atlleast two correct labels	48%
	Three correct labels	24%

Table 7.6: Classification accuracy of Localization model A - 36 strut lattice

Damage type	Classification output (based on classification scores)	Prediction accuracy (%)
1-Strut damage	One correct Label	68%
2- Strut damage	Atleast one correct label	58%
	Two correct label	44%
3-Strut damage	Atleast one correct label	52%
	Atlleast two correct labels	38%
	Three correct labels	16%

7.3.2   Localization Model B

In this localization model, the aim was to determine the location of damaged zones or cells of the structure instead of finding the location of the exact broken strut. This was done to improve the prediction accuracy of the localization by reducing the design space of the problem and to develop a methodology for locating damaged cells or zones in a lattice structure. Locating a damaged cell may be particularly useful in the case of a lattice structure which is made up of a large number of cells, and isolating an area of damage may guide the decisions on the maintenance/repair and integrity of the structure. The model is represented in Figure 7.4. The structures were divided into multiple zones consisting of four struts. This significantly reduced the design space of the problem. The zones for 16 and 36 strut lattice are shown in Figure 7.5. There are a total of 4 zones for 16 strut lattice and 9 zones for 36 strut lattice.
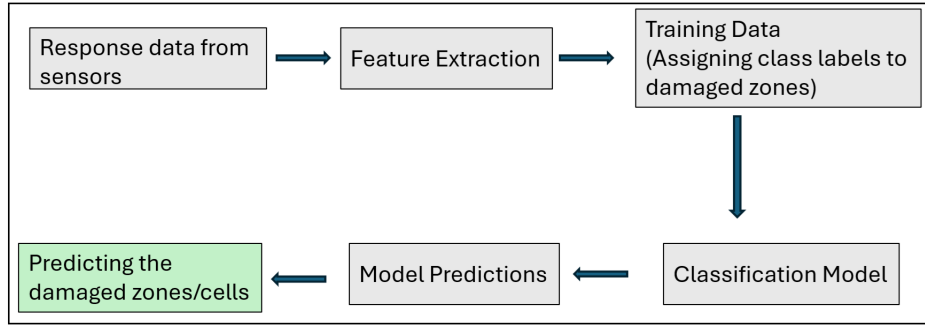
Figure 7.4: Flowchart for Localization Model B, which predicts damaged zones rather than individual struts.
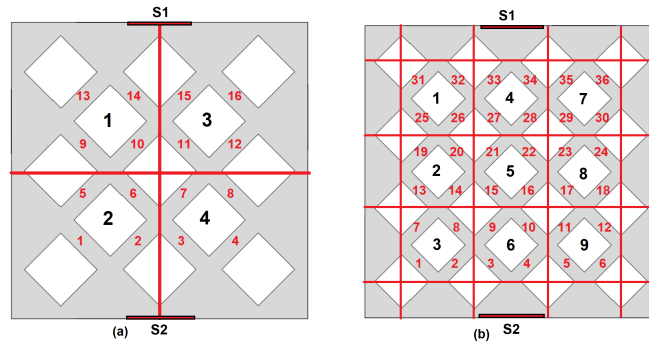
Figure 7.5: Zoning scheme applied to 16-strut and 36-strut lattices. The lattices are divided into zones to reduce complexity and improve damage localization accuracy.

Training data

Data labels were assigned to the damaged zones in this classification model. A zone was considered damaged if it contained one or more broken struts. Data labels were assigned based on the number of damaged zones in the structure. If a three-strut damaged structure had only two damaged zones, two data labels were assigned. Up to five strut damages were considered for this model and only those damage cases

that had three or fewer damaged zones were chosen. An example of this training data is given in Table 7.7.

Table 7.7: Example of classification labels for Localization Model B - 36 strut lattice

Damaged Struts	Class Labels
16	Zone-5
3,26	Zone 6, Zone 1
13,20	Zone-2
11,19,29	Zone 9, Zone 2, Zone 7
3,15,22	Zone-6, Zone-5
13,14,20	Zone-2
2,11,6,15,22	Zone-3, Zone-9, Zone-5

Classification scheme

The classification in this model reduced to finding the location of one, two, or three damaged zones in the structure. The training data was used to train the classification model, and outputs were received in the form of classification scores. The labels with the highest classification scores were used to determine the prediction accuracy of the model.

Results

The classification scores of 36 strut lattice structures for 9 zones are shown in Figure 7.6. The figure shows a much improved performance of the model with reduced design space. The classification of damage in the nine zones resulted in good prediction accuracy for localizing the damage. The prediction accuracy for 36 strut lattice structures is given in Table 7.8.

Table 7.8: Classification accuracy of Localization model B - 36 strut lattice

Damage type	Classification output (based on classification scores)	Prediction accuracy (%)
1 damaged zone	One correct Label	92%
2 damaged zones	Atleast one correct label	87%
	Two correct label	77%
3 damaged zones	Atleast one correct label	86%
	Atleast two correct labels	76%
	Three correct labels	64%
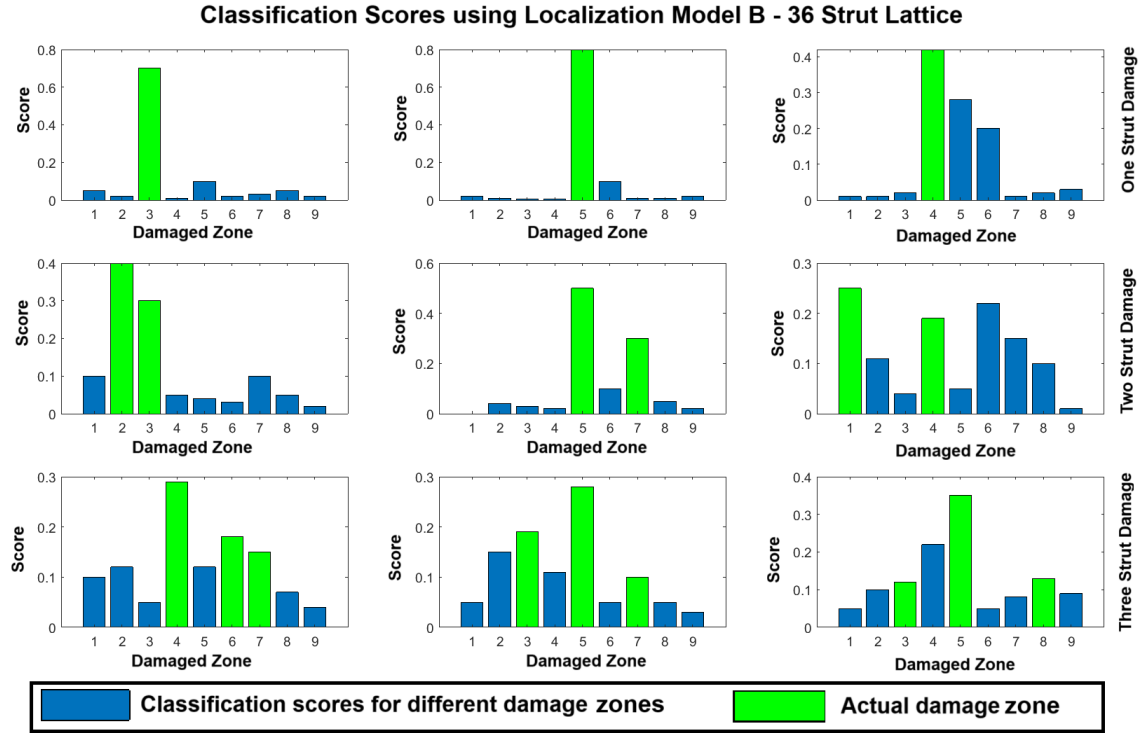
Figure 7.6: Classification scores for the 36-strut lattice using Localization Model B. This figure highlights the performance of the model in identifying damaged zones within the lattice structure. The results show improved prediction accuracy due to the reduced complexity of the design space.

7.3.3 Localization Model C

For this localization model, a spatial localization scheme was used. Using multiple sensor pairs, the location of damage is determined in different zones of the structure. Spatial information from different pairs of sensors is then merged to triangulate the location of damage in the structure. The model is represented in Figure 7.7.
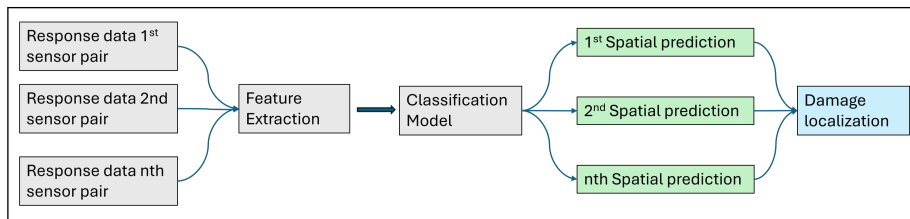
Figure 7.7: Flowchart illustrating Localization Model C, which incorporates spatial information from multiple sensors to triangulate damage locations.

Motivation behind spatial localization

So far, the two localization models that have been presented in the previous sections were based on the global response from one sensor pair. The data was used to train the classification model, which then made inferences about the damage location. There is no physical representation of how the damage locations affect the response

from the sensors. This approach provides a means to study how the spatial location of damage affects the sensor response. Furthermore, the spatial localization could lead to improved accuracy in predicting the location of damage.

Sensor arrangement and zoning of structure

A total of four sensors (two sensor pairs) were used for the 16-strut lattice, and eight sensors (four sensor pairs) are used for the 36-strut lattice. The physical representation of spatial zoning and sensor arrangement is shown in Figures 7.8 and 7.9 for the 16 and 36 strut lattices, respectively. For the 16-strut lattice, in Step 1, the sensor pair T1-B1 was used to isolate the damage in the left or right half of the structure marked as A and B. In Step 2, the sensor pair R1-L1 was used to isolate the damage in the upper and lower half of the structure marked C and D. Based on the results of Step 1 and 2, the localization in four zones (1, 2, 3 & 4) of the structure was carried out in Step 3. The localization of the 36-strut lattice involved three steps which are listed below.

1. Step 1 - Using sensor pair T1-B1 and T2-B2, isolate damage in zone A, B & C

2. Step 2 - Using sensor pair L1-R1 and L2-R2, isolate damage in zone D, E & F

3. Step 3 - Based on the results of Step 1 and 2, find the location of damage in zones 1-9
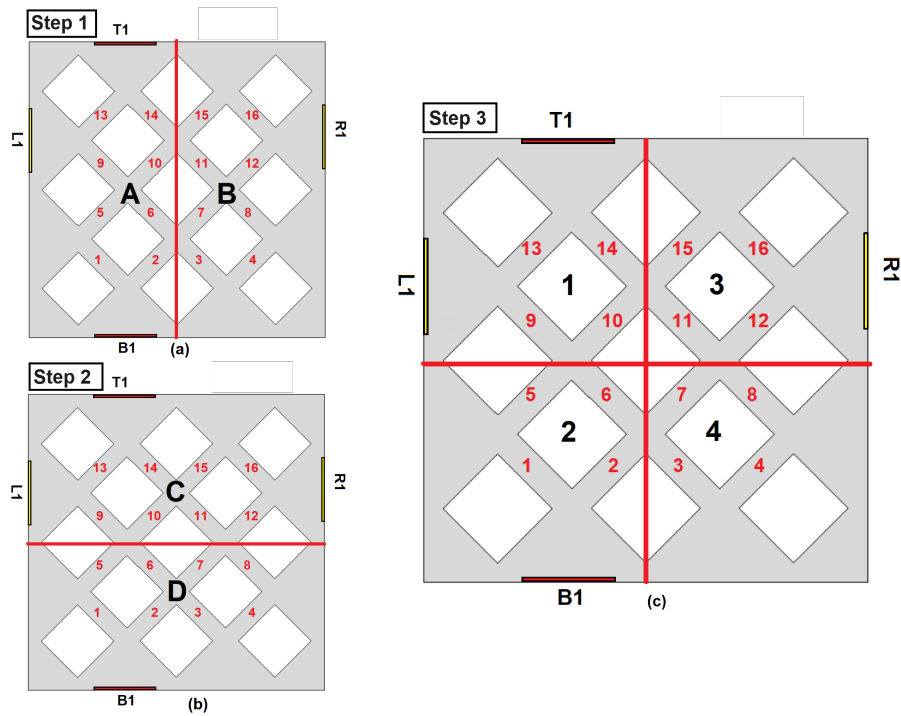
Figure 7.8: Spatial localization zones for the 16-strut lattice. The lattice is divided into four zones with a step-by-step process to identify the damaged area.
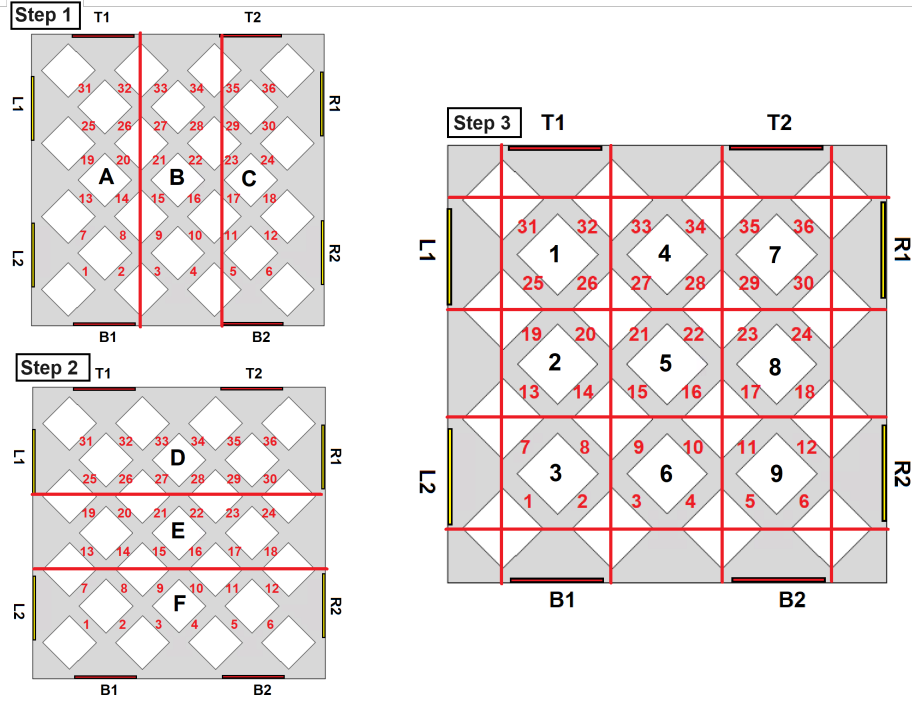
Figure 7.9: Spatial localization zones for the 36-strut lattice. This schematic divides the lattice into nine zones, enabling a systematic approach to isolating damage locations using sensor data.

Classification of 16 strut lattice

The classification matrix for 16 strut lattice is given in Figure 7.10. The results of Step 1 classify the damage in Zone A and B. As an example for three-strut damage, A-B-B in Step 1 means that out of three damaged struts, one lies in zone A and the other two in zone B. For zone A & B, there are two possibilities for 1-strut damage, three possible damage locations for 2-strut damage, and four possible damage locations for 3-strut damage. In Step 2, the location of the damage was isolated in zone C & D and the possible locations are shown in Figure 7.10. Based on the results of these first two steps, the final indices for the locations are determined in Step 3.

Classification of 36 strut lattice

In a manner similar to the 16-strut lattice, the classification matrix for the 36-strut lattice is shown in Figure 7.11. For each Step 1 and Step 2, there are three possible locations for 1-strut damage, six possible damage locations for 2-strut damage, and 10 possible locations for 3-strut damage. In Step 1, the damage was localized in zones A, B, and C, whereas in Step 2, damage was located in Zones D, E, and F. The location of damage in the nine zones based on the findings of Steps 1 and 2 was determined in Step 3.

Results

Before presenting these results, the effect of damage location in a particular zone on the response signal from different sensor pairs is shown. Figure 7.12 shows

	Step 1 Localization in Zone A, B	Step 2 Localization in Zone C, D	Step 3 Location of Damage in Zone 1, 2, 3, 4
1 Strut Damage	A	C	[1]
	A	D	[3]
	B	C	[2]
	B	D	[4]
2 Strut Damage	A-A	C-C	[1, 1]
	A-A	D-D	[3, 3]
	A-A	C-D	[1, 3]
	B-B	C-C	[2, 2]
	B-B	D-D	[4, 4]
	B-B	C-D	[2, 4]
	A-B	C-C	[1, 2]
	A-B	D-D	[3, 4]
	A-B	C-D	[1, 4] [2, 3]

	Step 1 Localization in Zone A, B	Step 2 Localization in Zone C, D	Step 3 Location of Damage in Zone 1, 2, 3, 4
3 Strut Damage	A-A-A	C-C-C	[1, 1, 1]
	A-A-A	D-D-D	[3, 3, 3]
	A-A-A	C-C-D	[1, 1, 3]
	A-A-A	C-D-D	[1, 3, 3]
	B-B-B	C-C-C	[2, 2, 2]
	B-B-B	D-D-D	[4, 4, 4]
	B-B-B	C-C-D	[2, 2, 4]
	B-B-B	C-D-D	[2, 4, 4]
	A-A-B	C-C-C	[1, 1, 2]
	A-A-B	D-D-D	[3, 3, 4]
	A-A-B	C-C-D	[1, 1, 4] [1, 3, 2]
	A-A-B	C-D-D	[1, 3, 4] [2, 3, 3]
	A-B-B	C-C-C	[1, 2, 2]
	A-B-B	D-D-D	[3, 4, 4]
	A-B-B	C-C-D	[1, 2, 4] [2, 2, 3]
	A-B-B	C-D-D	[1, 4, 4] [2, 3, 4]

Figure 7.10: Classification matrix for Localization Model C applied to the 16-strut lattice. The results show the accuracy of the model in isolating damage within specific zones.

the responses of the T1-B1 sensor pair for 16 strut lattice. The location of the T1-B1 sensor pair is in zone A, and the damages lying in zone A result in lower energy features than the damages in zone B. This was also seen for two and three strut damage. This difference in energy features for different sensor locations makes spatial localization more effective. Similar differences were also observed for the 36 strut lattice.

The results from this localization model are presented in the form of three case studies, one for 16-strut lattice and two for 36-strut lattice.

Case 1 - 16 Strut Lattice - Damage location [3-3-4]

The first case is for the 16-strut lattice. There are three damaged struts in this case, with struts 15, 12, and 7 damaged. The true location of these damaged struts in the zones is [A-A-B] for Step 1, [D-D-D-d] for Step 2 and [3,3,4] for Step 3. The results for three steps of localization based on the classification matrix are shown in Figure 7.13. The classification scores for steps 1 and 2 are high, meaning they provide a good prediction accuracy for the damage localization. Step-1 and Step-2 correctly predict the location indices for the damage in zones as A-A-B and D-D-D respectively. In Step-3, based on the results of Step-1 and Step-2, classification matrix in Figure 7.10 is used for predicting the location of damage as [3-3-4].

Case 2 - 36 Strut - Damage location [7-8]

The case 2 is a two strut damage case in the 36-strut lattice. The damaged struts are Strut 35 and Strut 17 corresponding to the zones [C-C], [D-E], and [7-8] in three steps respectively. The classification scores for step 1 and 2 are shown in Figure 7.14 resulting in the final prediction of correct damage location in zones as per the classification matrix of 36 strut lattice given in Figure 7.11.

1 Strut Damage

Step 1 Localization in Zone A, B, C	Step 2 Localization in Zone D, E, F	Step 3 Location of Damage in Zone 1-9
A	D	[1]
	E	[2]
	F	[3]
B	D	[4]
	E	[5]
	F	[6]
C	D	[7]
	E	[8]
	F	[9]

2 Strut Damage

Step 1 Localization in Zone A, B, C	Step 2 Localization in Zone D, E, F	Step 3 Location of Damage in Zone 1-9
A-A	D-D	[1,1]
	E-E	[2,2]
	F-F	[3,3]
	D-E	[1,2]
	E-F	[2,3]
	D-F	[1,3]
B-B	D-D	[4,4]
	E-E	[5,5]
	F-F	[6,6]
	D-E	[4,5]
	E-F	[5,6]
	D-F	[4,6]
C-C	D-D	[7,7]
	E-E	[8,8]
	F-F	[9,9]
	D-E	[7,8]
	E-F	[8,9]
	D-F	[7,9]

2 Strut Damage

Step 1 Localization in Zone A, B, C	Step 2 Localization in Zone D, E, F	Step 3 Location of Damage in Zone 1-9
A-B	D-D	[1,4]
	E-E	[2,5]
	F-F	[3,6]
	D-E	[1,5] [2,4[
	E-F	[2,6] [3,5]
	D-F	[1,6] [3,4]
B-C	D-D	[4,7]
	E-E	[5,8]
	F-F	[6,9]
	D-E	[4,8] [5,7]
	E-F	[6,8] [5,9]
	D-F	[4,9] [6,7]
A-C	D-D	[1,7]
	E-E	[2,8]
	F-F	[3,9]
	E-E	[1,8] [2,7]
	E-F	[2,9] [3,8]
	D-F	[1,9] [3,7]

3 Strut Damage

Step 1 Localization in Zone A, B, C	Step 2 Localization in Zone D, E, F	Step 3 Location of Damage in Zone 1-9
A-A-A	D-D-D	[1,1,1]
	E-E-E	[2,2,2]
	F-F-F	[3,3,3]
	D-D-E	[1,1,2]
	D-E-E	[1,2,2]
	D-D-F	[1,1,3]
	D-F-F	[1,3,3]
	D-E-F	[1,2,3]
	E-E-F	[3,2,2]
	E-F-F	[3,3,2]
B-B-B	D-D-D	[4,4,4]
	E-E-E	[5,5,5]
	F-F-F	[6,6,6]
	D-D-E	[4,4,5]
	D-E-E	[4,5,5]
	D-D-F	[4,4,6]
	D-F-F	[4,6,6]
	D-E-F	[4,5,6]
	E-E-F	[5,5,6]
	E-F-F	[5,6,6]
C-C-C	D-D-D	[7,7,7]
	E-E-E	[8,8,8]
	F-F-F	[9,9,9]
	D-D-E	[7,7,8]
	D-E-E	[7,8,8]
	D-D-F	[7,7,9]
	D-F-F	[7,9,9]
	D-E-F	[7,8,9]
	E-E-F	[8,8,9]
	E-F-F	[8,9,9]
A-A-B	D-D-D	[1,1,4]
	E-E-E	[2,2,5]
	F-F-F	[3,3,6]
	D-D-E	[1,1,5] [1,2,4]
	D-E-E	[1,2,5] [2,2,4]
	D-D-F	[3,1,4] [6,1,1]
	D-F-F	[1,3,6] [3,3,4]
	D-E-F	[1,2,6] [1,3,5] [2,3,4]
	E-E-F	[3,2,5] [2,2,6]
	E-F-F	[3,3,5] [6,3,2]

3 Strut Damage

Step 1 Localization in Zone A, B, C	Step 2 Localization in Zone D, E, F	Step 3 Location of Damage in Zone 1-9
A-B-C	D-D-D	[1,4,7]
	E-E-E	[2,5,8]
	F-F-F	[3,6,9]
	D-D-E	[2,4,7] [1,5,7] [1,4,8]
	D-E-E	[1,5,8] [2,4,8] [2,5,7]
	D-D-F	[3,4,7] [1,6,7] [1,4,9]
	D-F-F	[1,6,9] [3,4,9] [3,6,7]
	D-E-F	[1,5,9] [1,8,6] [2,4,9] [3,4,8] [3,5,7] [2,6,7]
	E-E-F	[3,5,8] [2,6,8] [2,5,9]
	E-F-F	[2,6,9] [3,5,9] [3,6,8]
B-B-C	D-D-D	[4,4,7]
	E-E-E	[5,5,8]
	F-F-F	[6,6,9]
	D-D-E	[4,4,8] [4,7,5]
	D-E-E	[4,5,8] [5,5,7]
	D-D-F	[4,4,9] [4,7,6]
	D-F-F	[6,6,7] [6,9,4]
	D-E-F	[4,6,8] [4,5,9] [5,6,7]
	E-E-F	[6,5,8] [9,5,5]
	E-F-F	[6,6,8] [6,9,5]
B-C-C	D-D-D	[7,7,4]
	E-E-E	[8,8,5]
	F-F-F	[9,9,6]
	D-D-E	[7,7,5] [7,4,8]
	D-E-E	[7,8,5] [8,8,4]
	D-D-F	[7,7,6] [7,4,9]
	D-F-F	[7,9,6] [4,9,9]
	D-E-F	[7,9,5] [7,8,6] [9,8,4]
	E-E-F	[6,8,8] [9,8,5]
	E-F-F	[8,9,6] [9,9,5]

3 Strut Damage

Step 1 Localization in Zone A, B, C	Step 2 Localization in Zone D, E, F	Step 3 Location of Damage in Zone 1-9
A-B-B	D-D-D	[1,4,4]
	E-E-E	[2,5,5]
	F-F-F	[3,6,6]
	D-D-E	[4,4,2] [1,4,5]
	D-E-E	[1,5,5] [4,5,2]
	D-D-F	[4,4,3] [1,4,6]
	D-F-F	[6,6,1] [3,6,4]
	D-E-F	[4,5,3] [6,5,1] [4,6,2]
	E-E-F	[5,5,3] [2,5,6]
	E-F-F	[6,6,2] [3,6,5]
A-A-C	D-D-D	[1,1,7]
	E-E-E	[2,2,8]
	F-F-F	[3,3,9]
	D-D-E	[1,1,8] [1,2,7]
	D-E-E	[1,2,8] [2,2,7]
	D-D-F	[3,1,7] [9,1,1]
	D-F-F	[1,3,9] [3,3,7]
	D-E-F	[1,2,9] [1,3,8] [2,3,7]
	E-E-F	[3,2,8] [2,2,9]
	E-F-F	[3,3,8] [9,3,2]
A-C-C	D-D-D	[1,7,7]
	E-E-E	[2,8,8]
	F-F-F	[3,9,9]
	D-D-E	[2,7,7] [1,7,8]
	D-E-E	[1,8,8] [2,7,8]
	D-D-F	[3,7,7] [1,7,9]
	D-F-F	[1,9,9] [3,7,9]
	D-E-F	[3,7,8] [1,8,9] [2,7,9]
	E-E-F	[3,8,8] [2,8,9]
	E-F-F	[9,9,2] [3,9,8]

Figure 7.11: Classification matrix for Localization Model C applied to the 36-strut lattice. This matrix presents the effectiveness of the spatial localization method in identifying damage across nine zones.

Case 3 - 36 Strut - Damage location [1-2-7]

Case 3 is a three strut damage case in a 36-strut lattice with damaged struts 26, 13, and 29 corresponding to the zones [A-A-C], [D-D-E], and [1-2-7] in three steps respectively. The classification scores shown in Figure 7.15 indicate a high accuracy of correct prediction for steps 1 and 2. The final prediction of the model corresponds to two possible damage locations, i.e. [1-2-1] or [1-1-8] as per the classification matrix given in Figure 7.11.
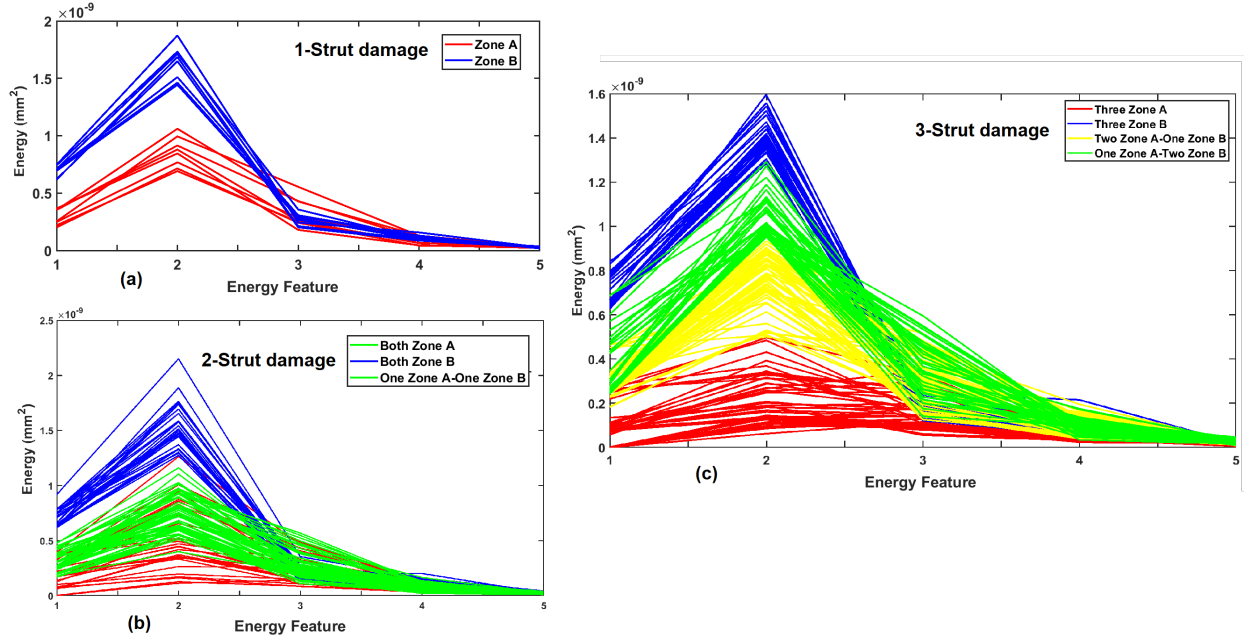
Figure 7.12: Energy feature response of the T1-B1 sensor pair (lying in zone A) for the 16-strut lattice, showing the variation in energy levels based on the zone of damage. Damages in Zone A yield lower energy features compared to damages in Zone B, supporting spatial differentiation for damage localization.
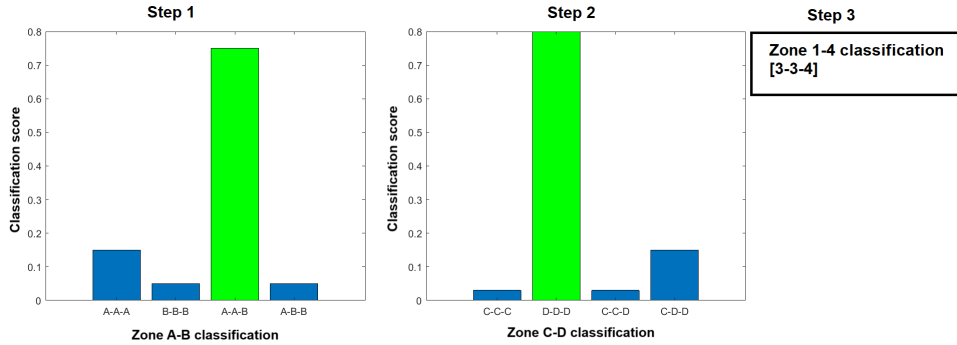
Figure 7.13: Case study results for Localization Model C applied to the 16-strut lattice, with damage [3, 3, 4] localized in correct zones . The stepwise classification scores show high accuracy for different steps, confirming the model's effectiveness for structured damage localization.

7.3.4 Generic Pseudo Code

The pseudo–algorithm in Algorithm 1 formalises the zone–based localisation workflow used in this study. It accepts an arbitrary sensor set and zoning resolution, concatenates the time-domain signals from every sensor pair, transforms them into a compact feature vector, and evaluates a trained multi-label classifier whose outputs are averaged to yield a probability for each zone. Because neither the number of sensors M nor the number of zones N is hard-coded, the routine scales naturally to larger lattice panels or finer grids, satisfying the examiner's request for a general and reproducible localisation method.
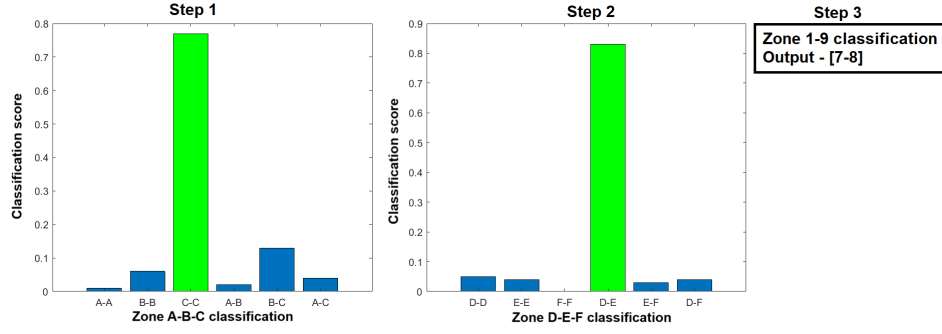
Figure 7.14: Classification scores for damage localization in the 36-strut lattice using Localization Model C (Case Study No. 2). The results show the model correctly predicting the zones of the damaged struts [7-8] in stepwise classification.
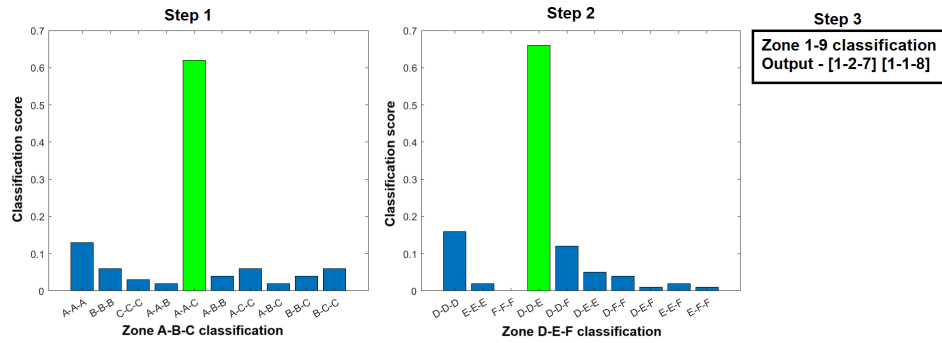
Figure 7.15: Classification scores for damage localization in the 36-strut lattice (Case Study No. 3). The results highlight predictions for damaged zones and reduced confidence for overlapping zones.

Algorithm 1 Generic Zone–Based Damage Localisation

Require: Sensor set $S = \{s_1, \ldots, s_M\}$ with known coordinates
    Zone set $Z = \{z_1, \ldots, z_N\}$ (arbitrary N)
    Feature extractor $f(\cdot)$ and trained classifier C ($|Z|$ outputs)
    Threshold T for zone decision (default 0.5) Raw time–domain signals $\{\text{sig}(s_m)\}_{m=1}^M$ Set of damaged zones $\mathcal{D}$ and probability vector $\mathbf{P}$
0: $\mathbf{P} \leftarrow \mathbf{0}_N$ // initialise accumulated probabilities
0: **for all** sensor pairs (s_i, s_j) with $i < j$ **do**
0:      signal $\leftarrow$ concatenate$\big(\text{sig}(s_i), \text{sig}(s_j)\big)$
0:      $\mathbf{x} \leftarrow f(\text{signal})$ // feature extraction
0:      $\mathbf{p} \leftarrow C.\text{predict}(\mathbf{x})$ // $\mathbf{p} \in [0,1]^N$
0:      $\mathbf{P} \leftarrow \mathbf{P} + \mathbf{p}$ // accumulate
0: **end for**
0: $\mathbf{P} \leftarrow \dfrac{\mathbf{P}}{\frac{M(M-1)}{2}}$ // average over all pairs
0: $\mathcal{D} \leftarrow \{\, z_k \in Z \mid P_k \geq T \,\}$
1: **return** $\big(\mathcal{D}, \mathbf{P}\big)$ =0

7.4 Experimental Results

The experimental samples used for the localization of the damage are shown in Figure 7.16. A total of five samples were manufactured for each 16 and 36-strut structure. Data from multiple sensor configurations were extracted from the installed sensors at different spatial locations. The data from the experimental results were normalized to the numerical data, and the corresponding performance of the model was measured. The results for damage localization are now presented.

(a)   **(b)**
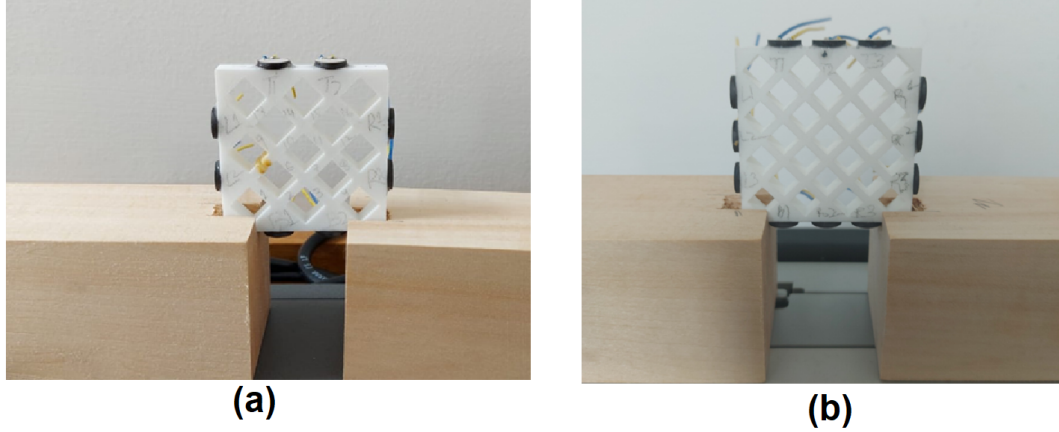
Figure 7.16: Experimental samples for damage localization showing (a) a 16-strut lattice and (b) a 36-strut lattice. These samples were used to validate the numerical results by normalizing experimental response data and fitting it to the trained numerical classification models.

7.4.1 Localization Model A & B

Localization model A estimates the location of individual damaged struts, whereas model B measures the locations of damaged zones in the structure. Experimental data on its own is not large enough to build a classification model. Instead, the experimental data is normalized to the numerical data (refer Section 4.7) and features are fitted to the trained numerical model. The performance of localization model A and model B is tabulated in Table 7.9 and Table 7.10 respectively. Localization model B, which predicts the locations of damaged cells, gives good performance, especially for isolating up to two damaged cells.

7.4.2 Localization Model C

The spatial response of the damage to different sensor locations was tested for the experimental data. Three cases are presented below which explain the spatial response of damage locations from experimental observations.

Case 1

The first case for the 16-strut lattice is shown in Figure 7.17. Strut-9 damage lies in Zone A, and the response of the T1-B1 sensor pair to this damage shows a significant

Table 7.9: Classification accuracy using experimental data for Localization Model A

Damage type	Classification output (based on classification scores)	Prediction accuracy-16 strut lattice	Prediction accuracy-36 strut lattice
1-strut damage	One correct Label	74%	58%
2-strut damage	Atleast one correct label	66%	54%
	Two correct label	48%	38%
3-strut damage	Atleast one correct label	64%	52%
	Atleast two correct labels	38%	32%
	Three correct labels	27%	18%

Table 7.10: Classification accuracy using experimental data for Localization Model B

Damage type	Classification output (based on classification scores)	Prediction accuracy-16 strut lattice	Prediction accuracy-36 strut lattice
1 damaged zone	One correct Label	83%	76%
2 damaged zones	Atleast one correct label	78%	73%
	Two correct label	71%	63%
3 damaged zones	Atleast one correct label	78%	74%
	Atleast two correct labels	63%	54%
	Three correct labels	52%	43%

change in the energy of the signal. Strut-12 damage lies in Zone B and its response signal for T1-B1 sensor pair shows very little change in energy features. This makes spatial localization of damage possible as was seen in the numerical localization study.

Case 2

The second case for 16-strut lattice is shown in Figure 7.18 for two strut damage. Strut-9 & 14 damage lies in Zone A and the response of T1-B1 sensor pair to this damage shows a significant change in energy of signal. Strut-12 & 15 damage lies in Zone B and its response signal for T1-B1 sensor pair shows very little change in energy features.
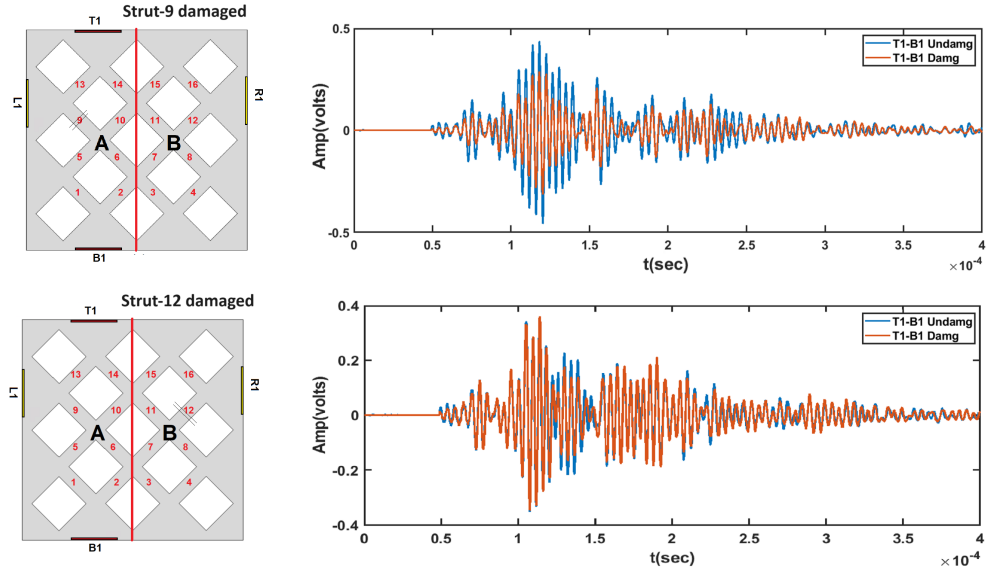
Figure 7.17: Spatial response of experimental data for a single-strut damage case in the 16-strut lattice (Case 1). The response shows significant energy changes in the zone containing the damaged strut, confirming the feasibility of spatial localization
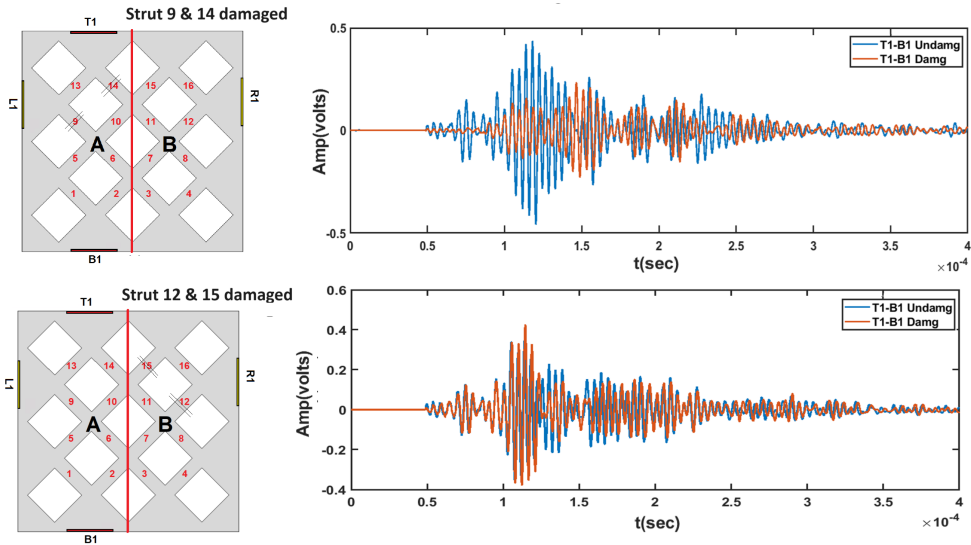
Figure 7.18: Spatial response of experimental data for a two-strut damage case in the 16-strut lattice (Case 2). Energy variations observed in sensor readings correlate with damage in different zones.

Case 3

The third case for 36-strut lattice is shown in Figure 7.19 for two strut damage. Strut-17 & 23 damage lies in Zone C and the responses of T1-B1 and T2-B2 sensor pairs to this damage are shown. The response of T1-B1 sensors which lies in Zone A shows very littled change in energy features whereas T2-B2 sensor pair which lies in Zone C shows appreciable changes in energy features.
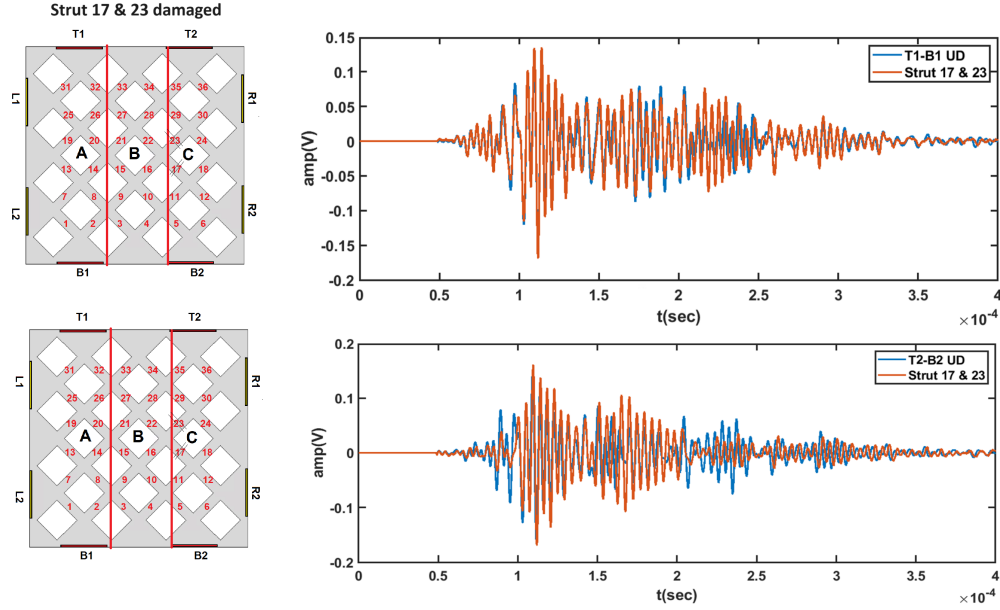
Figure 7.19: Spatial response of experimental data for a two-strut damage case in the 36-strut lattice (Case 3). The results emphasize the effectiveness of spatial localization in lattice structures. Sensors closer to damaged zones exhibit greater energy variations, aiding accurate localization

Interpretation of experimental observations

The experimental observations from different spatial sensors validate the methodology of spatial localization developed in the numerical study. There are marked differences between signal characteristics for damages present in different sensor zones as shown in the three cases above. Using this technique, location of damage in different regions of structures can be efficiently predicted. This methodology may be especially useful for bigger lattice structures having a large number of cells where spatial information from multiple sensors may be used to map the location of damage.

7.5   Summary and Conclusions

This chapter presented a comprehensive exploration of methodologies for damage localization in lattice structures, focusing on their utility in structural health monitoring (SHM). The study aimed to address the challenge of precisely identifying damage within complex lattice geometries, which are widely used in modern engineering applications.

The research developed and evaluated three localization models, each tailored to distinct scenarios of damage identification. **Localization** was designed to locate individual damaged struts and proved effective for single-strut damage. However, it faced difficulties in accurately identifying multi-strut damage due to overlapping classification outputs. **Localization Model B** introduced a zoning approach, targeting damaged regions/cells rather than individual struts, thereby simplifying the problem space. This model demonstrated improved prediction accuracy, particularly for scenarios involving multiple damaged zones. Lastly, **Localization Model**

C employed spatial triangulation using multiple sensors to refine localization precision further. By integrating spatial data, this model offered robust and accurate predictions, especially for higher damage classes.

The experimental validation reinforced the practical applicability of the proposed methodologies. By normalizing experimental data with numerical models, the study demonstrated alignment between experimental observations and simulated predictions. This validation was particularly significant for Localization Models B and C, which consistently achieved high prediction accuracy in identifying damaged zones and regions.

A key insight from the study was the realization that localizing damaged zones, rather than pinpointing individual damaged struts, is not only more efficient but also more applicable to large and intricate lattice structures. The zoning approach, coupled with spatial information from multiple sensors, provided a scalable and effective method for damage localization. Furthermore, the combination of energy features and principal component analysis (PCA) with neural network-based classification emerged as a powerful framework for accurate and reliable damage identification.

The major contribution of this chapter is a novel zone-based, multi-label classification approach, where the neural network predicts damage probabilities across defined regions as shown in Localization Model C. This architecture remains unchanged when the lattice topology or sensor layout is scaled, requiring only retraining on new data. To support generalization and practical deployment, a zone-agnostic pseudo–algorithm (Algorithm 1) was formalized. Experimental results validated the numerical predictions, with localization accuracies exceeding 88 %, thereby confirming the framework's robustness and applicability to real-world SHM scenarios.

7.5.1 Conclusions

In conclusion, the methodologies developed in this study offer an advancement in SHM for lattice structures. Among the models, Localization Model B and C stand out for their robustness and adaptability, particularly in addressing the challenges posed by multi-strut damage and intricate geometries. The experimental validation highlights the feasibility of implementing these techniques in real-world scenarios, providing a strong foundation for extending these methodologies to three-dimensional lattice structures. By developing an efficient damage localization methodology, this research paves the way for enhanced safety, maintenance practices, and operational reliability in applications involving additively manufactured components.

Building on the methodologies and findings of this chapter, the next chapter focuses on damage detection, quantification, and localization in three-dimensional lattice structures. The study expands the framework developed for 2D lattices to address the added complexities of 3D geometries, offering broader applicability to real-world scenarios.

Chapter 8

Analysis of 3D Lattice Structure

8.1 Introduction

The transition from two-dimensional (2D) to three-dimensional (3D) lattice structures introduces additional complexity in damage detection, quantification, and localization. While previous chapters have established robust methodologies for 2D lattices, the extension to 3D geometries is crucial for advancing structural health monitoring (SHM) in practical applications, particularly in additively manufactured components. The intricate geometry of 3D lattices, combined with complex wave propagation patterns, necessitates developing techniques to address these challenges effectively. While the methodologies developed in earlier chapters provided robust solutions for 2D lattices, extending these frameworks to 3D geometries requires addressing several key differences and complexities. The first major challenge lies in the spatial complexity of 3D lattices, where struts are interconnected in all three dimensions, leading to more intricate wave propagation patterns. Unlike 2D lattices, where wave propagation is constrained to a plane, 3D structures exhibit multi-directional wave behavior, increasing the difficulty of interpreting ultrasonic signals. Additionally, the expanded spatial domain introduces a larger design space for damage localization.

This chapter builds on the frameworks developed in Chapters 6 and 7, applying them to 3D lattice structures. Numerical simulations form the foundation of this study, with experimental validation used to confirm the applicability of the proposed methods. Damage detection is focused on identifying whether damage exists, quantification determines the extent of damage in terms of damaged struts and cells, and localization maps the exact regions or zones where damage has occurred.

The chapter is structured as follows: Section 8.2 introduces the 3D lattice structures and the damage scenarios studied. Section 8.3 outlines the methodology used for wave propagation analysis, feature extraction, and classification model. Numerical results for damage detection and quantification are presented in Sections 8.4 followed by experimental results in Section 8.5. Results of the damage localization study are given in Section 8.6. Finally, Section 8.7 concludes the chapter with a summary of the results and links to the overall conclusions of the thesis.

8.2   3D lattice structure

The 3D lattice structure designed for this study is shown in Figure. 8.1. It is an 8-cell lattice structure with the unit cell comprising 8 struts. The strut thickness is 2.5 mm and the strut length is 15 mm. The structure is made of 64 struts. A 2 mm thick surface is added at the top and bottom of the structure to facilitate the installation of sensors.
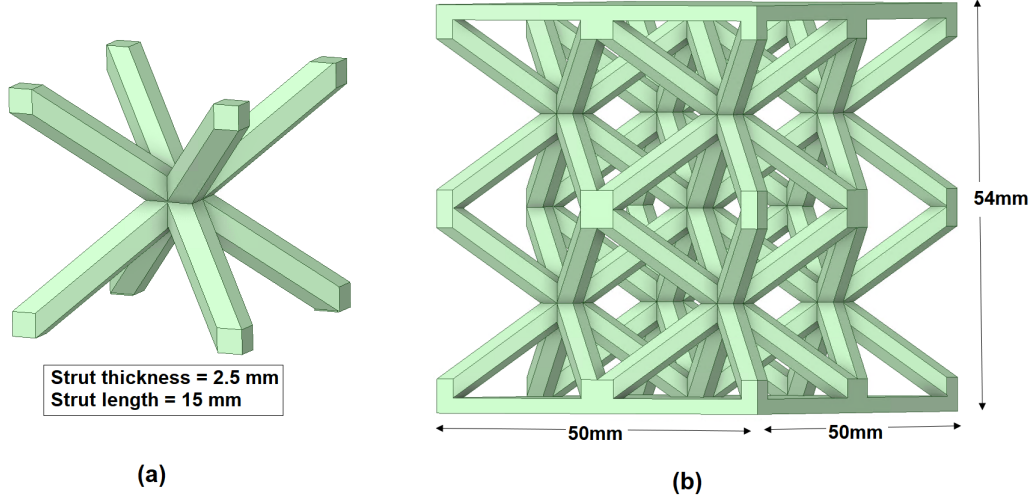
Figure 8.1: (a) An 8-strut unit cell of the 3D lattice structure. (b) Complete 8-cell lattice structure composed of 64 struts with added top and bottom surfaces for sensor placement.

Material properties

The material properties of the 3D lattice structure are the same as those used for the previous study. Nylon material is used for both numerical modeling and manufacturing of 3D samples. The material properties are given in detail in Section 4.2.

8.3   Modeling and Feature extraction

The numerical modeling of the 3D structure was done in ABAQUS. The details of the numerical modeling are already described in Section 4.3. The boundary and loading conditions, as well as the mesh for the numerical model, are shown in Figure 8.2. A sensor is modeled at the top and bottom of the structure. The Mesh was validated and Mesh convergence was achieved with a mesh size of 0.5 mm.

Numerical sample size

A total of 200 models were simulated for each damage case. One to ten strut damages were simulated, resulting in a total of 2200 unique simulated models, including the undamaged cases. The locations of damages were also recorded for the damage localization study.

(a)

(b)
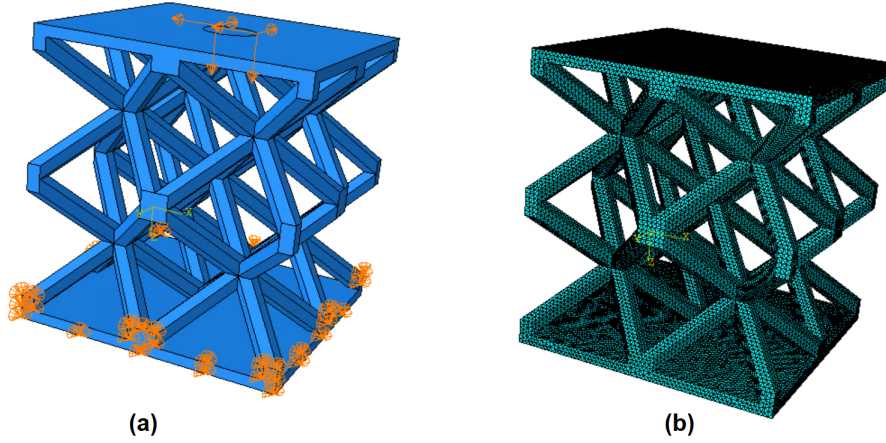
Figure 8.2: Numerical model of the 3D lattice structure showing (a) loads and boundary conditions applied for numerical simulations, and (b) the mesh used, optimized with a size of 0.5 mm for accuracy and computational efficiency.

8.3.1 Experimental Model

The experiments on the 3D lattice structure were also conducted. The experimental setup and manufacturing methods are already discussed in Section 4.4. The 3D lattice structure and experimental setup is shown in Figure. 8.3.

(a)

(b)
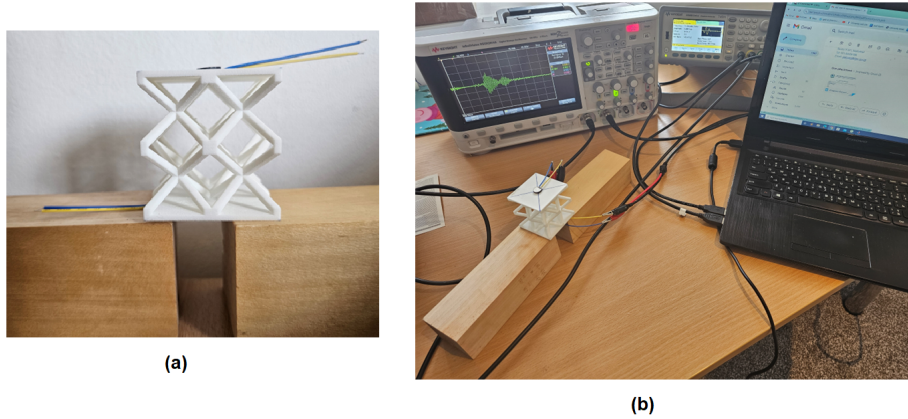
Figure 8.3: Experimental setup for the 3D lattice structure featuring (a) the fabricated 3D lattice and (b) the experimental arrangement, including sensor placement and data acquisition set-up for ultrasonic testing.

8.3.2 Feature extraction and classification model

Both PCA and energy features were extracted from the response signal and used for the classification of the data. The optimized number of these features is also discussed in later sections. The details of the classification model are already given in Section 4.6. The same classification model was used for the classification of damage in a 3D lattice structure. The optimized parameters of the model will also be discussed.

8.4 Damage detection and quantification

In this section, the numerical damage detection and quantification study for 3D lattice structure is given. The cell and lattice numbering for the numerical model is shown in Figure 8.4.

Cell No	Strut No
Cell 1	Strut 1-8
Cell 2	Strut 9-16
Cell 3	Strut 17-24
Cell 4	Strut 25-32
Cell 5	Strut 33-40
Cell 6	Strut 41-48
Cell 7	Strut 49-56
Cell 8	Strut 57-64
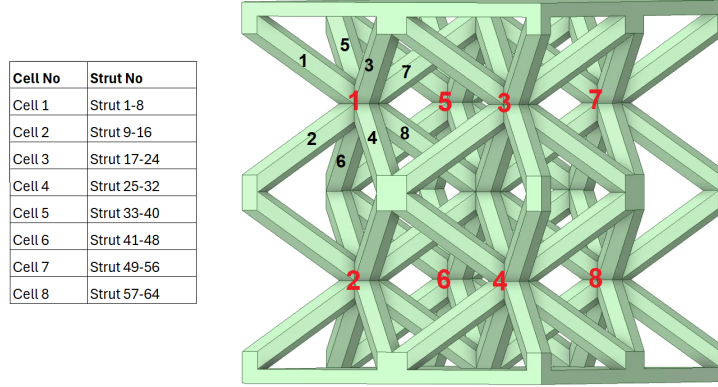
Figure 8.4: Cell and strut numbering of 3D lattice

8.4.1 Numerical data

The response signals from 2,200 simulated samples were extracted from the sensor data. The characteristics of the response signals are discussed as follows.

Response signals

The response signals from numerical simulations were first recorded. Some sample response signals for undamaged and damaged structures are shown in the Figure 8.5. Changes in the energy of the signal are seen for damaged structures.

Frequency response

The frequency response from the signals was also calculated using FFT. FFT response for damaged and undamaged signals is shown in Figure. 8.6. The central frequency of excitation is 215 KHz and the response is also centered around the central frequency. There is no phase shift observed.

Feature extraction

Both the energy features and principal components were extracted from the data. The plot of two EFs and PCs is given in Figure 8.7 and 8.8 respectively. The figures show a spread of the damage features across different classes of damage consistent with the findings of 2D lattice.

8.4.2 Results of Level 1 quantification

For Level 1 quantification, a total of 11 classifiers are used. Each classifier corresponds to one damage state, one classifier for undamaged, and 10 classifiers for
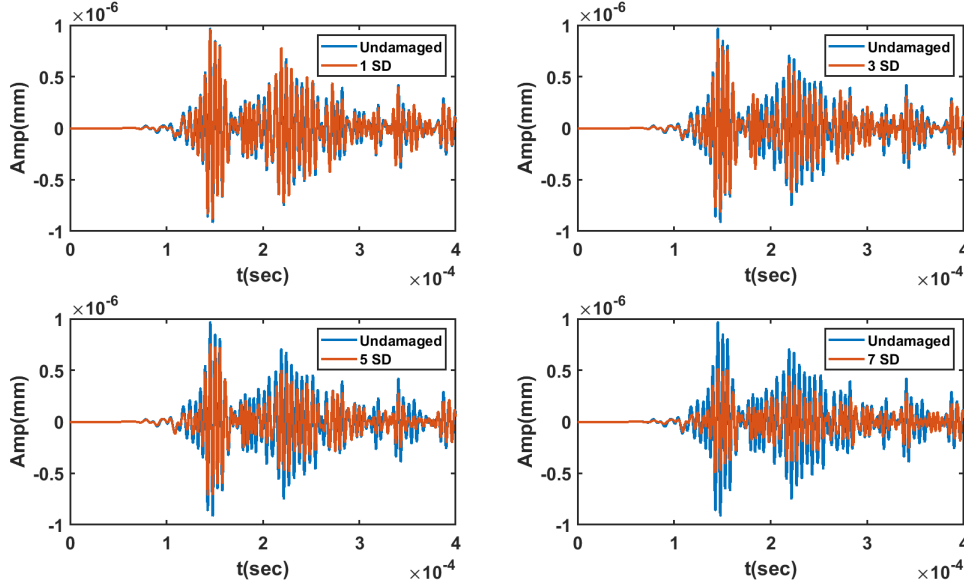
Figure 8.5: Numerical response signals for undamaged and damaged 3D lattice structures. The changes in signal energy highlight the effects of damage on the wave propagation characteristics.
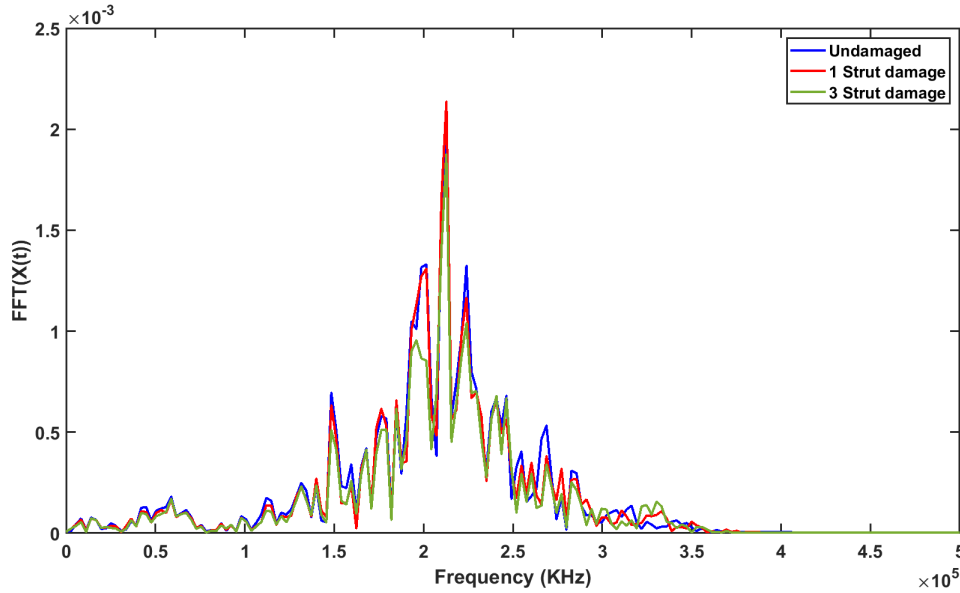
Figure 8.6: Frequency response (FFT) of numerical data for damaged and undamaged 3D lattice structures. The central frequency remains centered at 215 KHz, with no observed phase shift.

the number of damaged struts from one to ten. The output probability density for each classifier is given in Figure 8.10. The performance of lower damage classes is good; however, there is an increased probability distribution with the neighboring classes for higher damage classes. This was also observed in the 2D lattice structure response. The overall performance using 11 classifiers for the 3D lattice structure is 48 percent using energy features and 44 percent using Principal components.
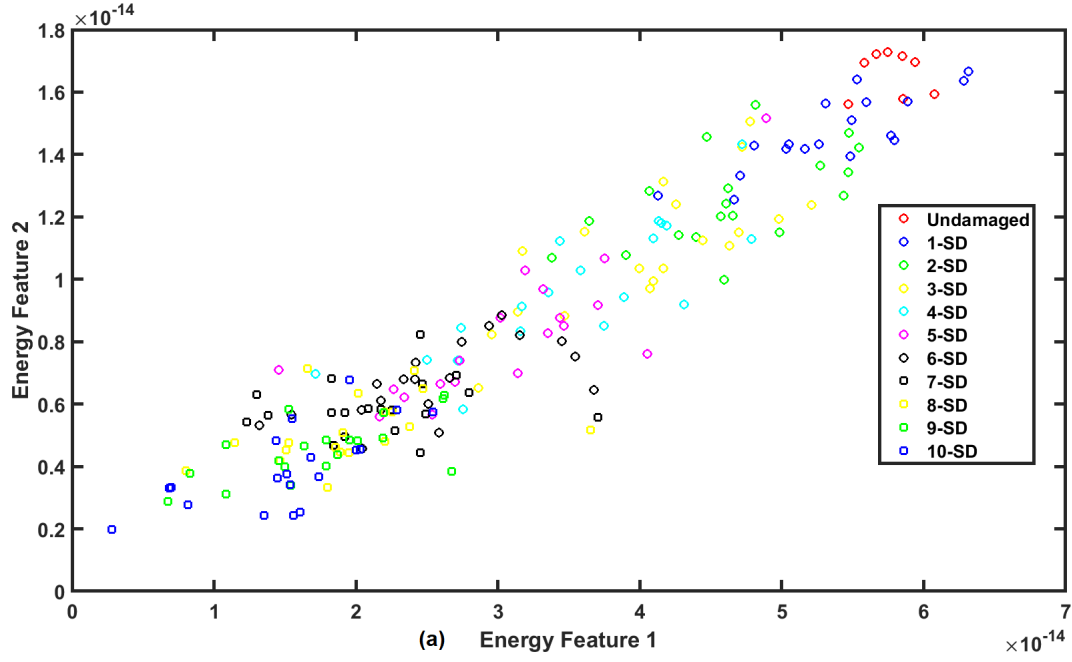
Figure 8.7: Features extracted from 3D numerical data, showing two energy features. The plots illustrate clusters of damage classes consistent with 2D structure.
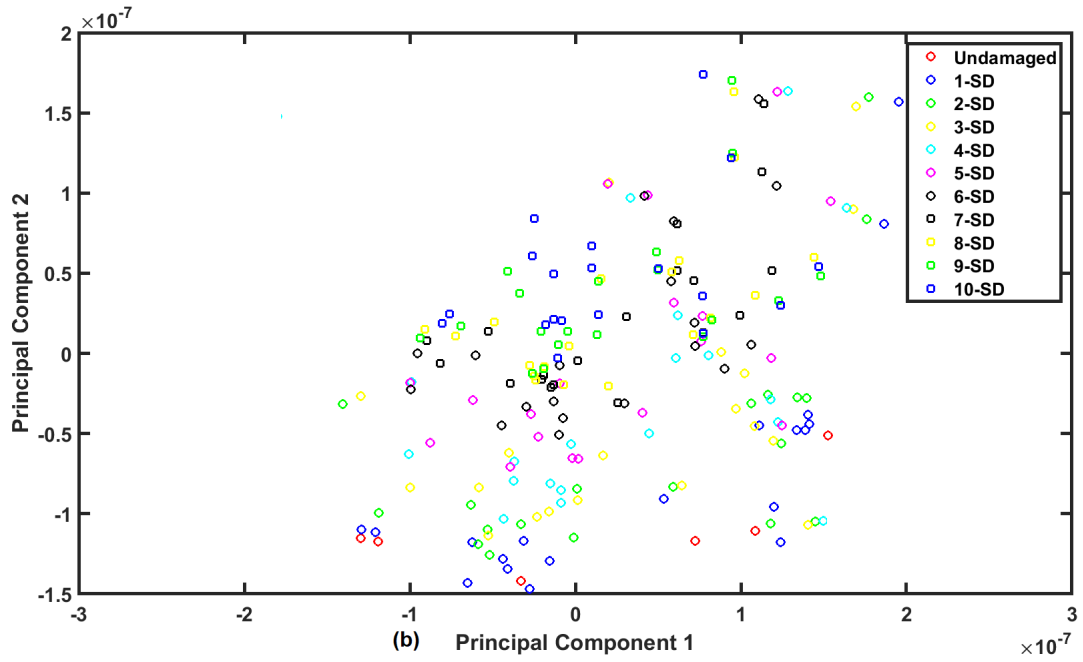
Figure 8.8: Features extracted from 3D numerical data, showing two principal components. The plots illustrate confused clusters of damage classes

8.4.3   Results of Level 2 quantification

The classifiers for Level 2 quantification are already explained in Chapter 6. The performance of 6 and 5 classifiers as probability density is shown in Figure 8.11 and 8.12 respectively. A significant improvement in the classification performance was seen compared to the 11 classifiers. The prediction accuracy for the level 2 quantification is given in Table 8.1.

8.4.4 Results of Level 3 quantification

The level 3 quantification is based on quantifying the number of damaged cells in the structure. There are a total of eight cells in the structure. A cell with one or more damaged struts was considered damaged. There are six classifiers for this level of quantification. The classifiers are the same as those used for the 2D lattice structure. Damage to five or more cells was assigned a single classifier marked as 'F' which signifies the failure of the structure. The prediction accuracy of this model is given in Table 8.1. The confusion matrix for level 3 quantification is shown in Figure 8.9 which shows a very good performance of the Level 3 quantification model.

Table 8.1: Prediction accuracy for three levels of damage quantification for 3D lattice

	Lev 1	Lev 2	Lev 2	Lev 3
	11 Classifiers	06 Classifiers	05 Classifiers	05 cell classifiers
PCA	44%	64%	78%	81%
Efs	46%	66%	82%	85%

Figure 8.9: Confusion matrix for Level 3 quantification of the 3D lattice. The matrix demonstrates good classification performance for quantifying damaged cells.

8.4.5 Damage detection

The damage detection is determining the presence of damage in the structure. For 3D lattice structure, any presence of damage was classified as damage. The damage could be one strut damage or more. The performance of measuring damage detection is very good for the 3D model as well, similar to the 2D lattice structure. The overall damage-detection accuracy using energy features is 91 percent, and using principal components, the accuracy is 87 percent.
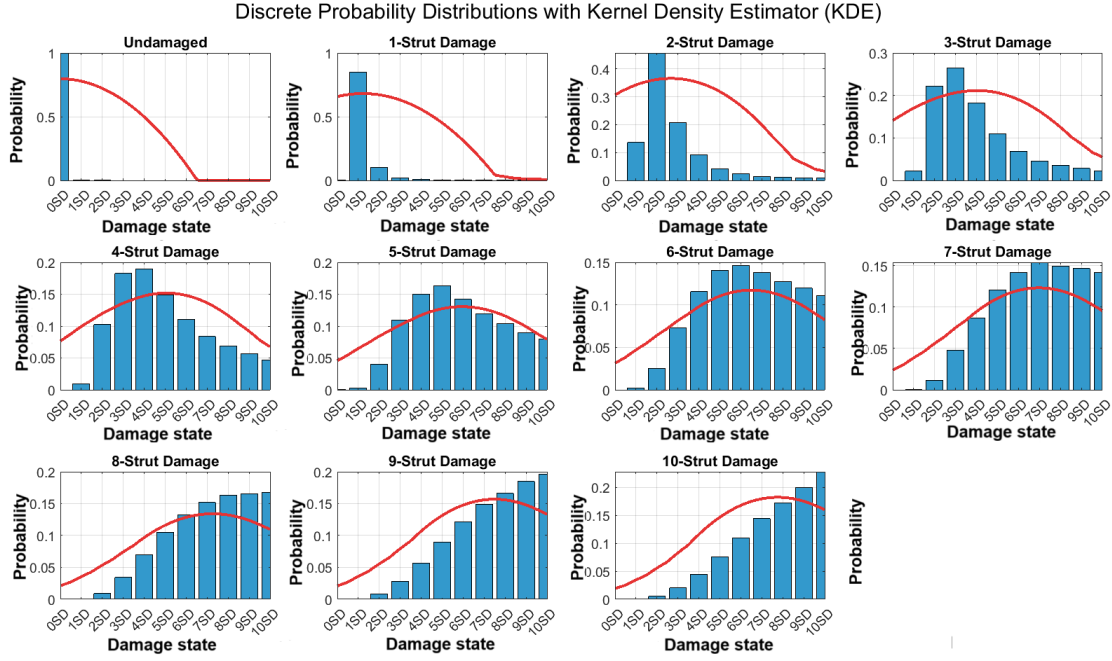
Figure 8.10: Probability distribution of 11 classifiers for Level 1 quantification of 3D numerical data. The distribution reflects increased uncertainty for higher damage states, consistent with prior observations in 2D lattices.
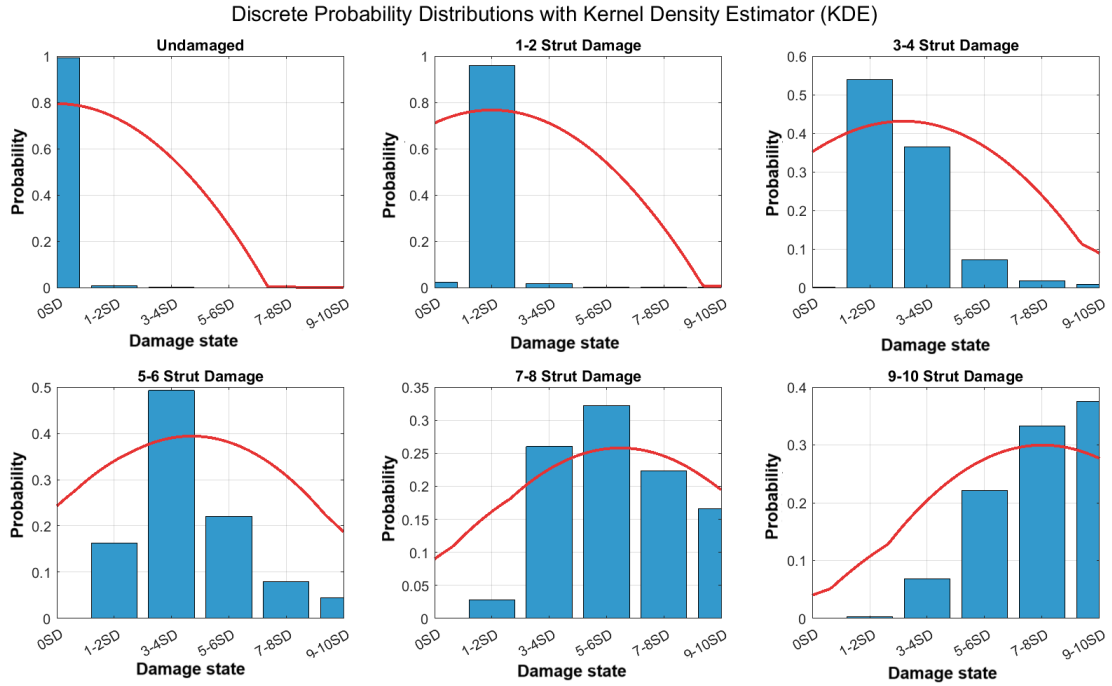
Figure 8.11: Probability distribution of six classifiers for Level 2 quantification of 3D numerical data. Reduced class overlap highlights improved accuracy compared to Level 1 quantification.
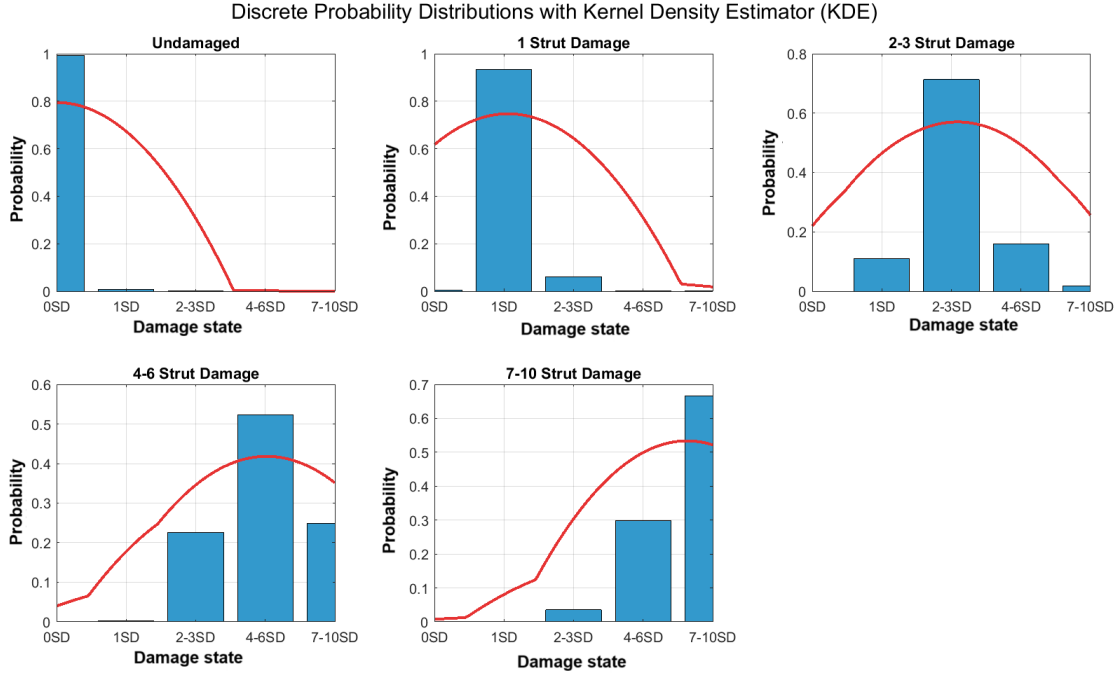
Figure 8.12: Probability distribution of five classifiers for Level 2 quantification. Improved separation between damage classes demonstrates the benefits of reduced classifier groups for quantification.

8.5 Experimental damage detection and quantification

The experimental results of damage detection and quantification for the 3D lattice structure are now presented. The experimental model and setup are shown in Figure 8.1.

Sample size and sensors

A total of 10 3D lattice samples were manufactured for experimental testing. Two different variations of sensors were used for testing (a) sensor with 10 mm diameter as was used for 2D lattice, (b) sensor with 20 mm diameter (Steminc SMD20T02F106412S PZT [146]). The central frequency of the 10 mm sensor is 215 KHz, and that of 20 mm sensor is 106 KHz. The sensors are shown in the Figure 8.13.

Response signals

The response signals for both damaged and undamaged signals were recorded. A sample of the response signal for the two different sensors is given in Figure 8.14. A change in the energy of signal is seen with the presence of damage.

Frequency response

The central frequency of the 20 mm sensor is 106 KHz, which was the excitation frequency used for this sensor. The center frequency of the 10 mm sensor is 215 KHz.

(a)　　　(b)
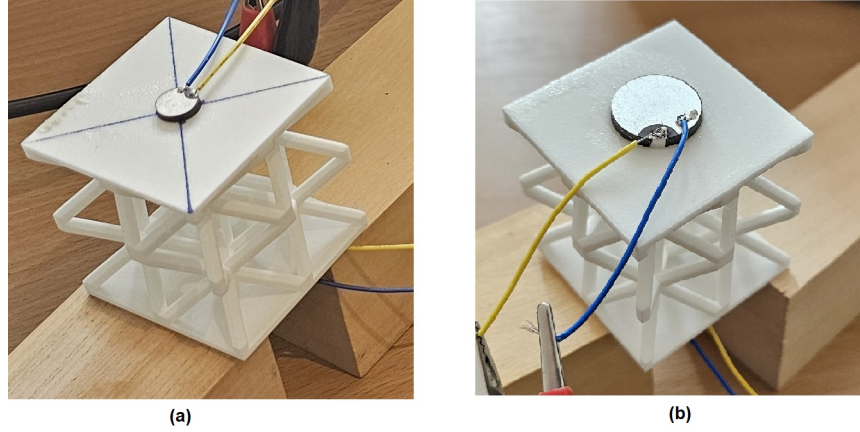
Figure 8.13: Two types of sensors used in 3D experimental studies: (a) a 10mm sensor with a central frequency of 215 KHz, and (b) a 20mm sensor with a central frequency of 106 KHz.
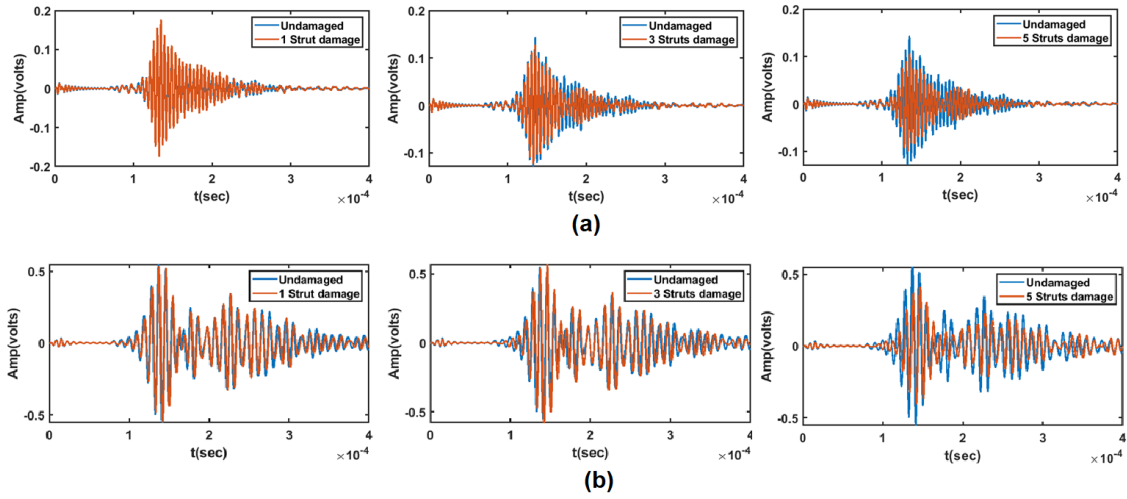
Figure 8.14: Response signals for damaged and undamaged 3D lattice structures, recorded using (a) the 10mm sensor and (b) the 20mm sensor. Changes in signal energy reflect damage severity.

FFT frequency response for both sensors is shown in Figure 8.15. The frequency response is centered around the central frequency of the sensors.

Experimental results

Response signals were recorded from the sensors installed on the 3D lattice. The response signals were normalized to the numerical response data. The features were extracted from the normalized response signals. The classification model trained with the numerical data was used to make inferences about the damage state of the structure and to measure the performance of the classification model. The best performance was achieved for level 3 quantification with a prediction accuracy of 67 %. One reason for low prediction accuracy is a great mismatch between numerical and experimental response signals. A better approach would be to gather a bigger sample size of experimental data and train a model using experimental

data. The prediction accuracy for the damage detection using experimental data was 74 percent.
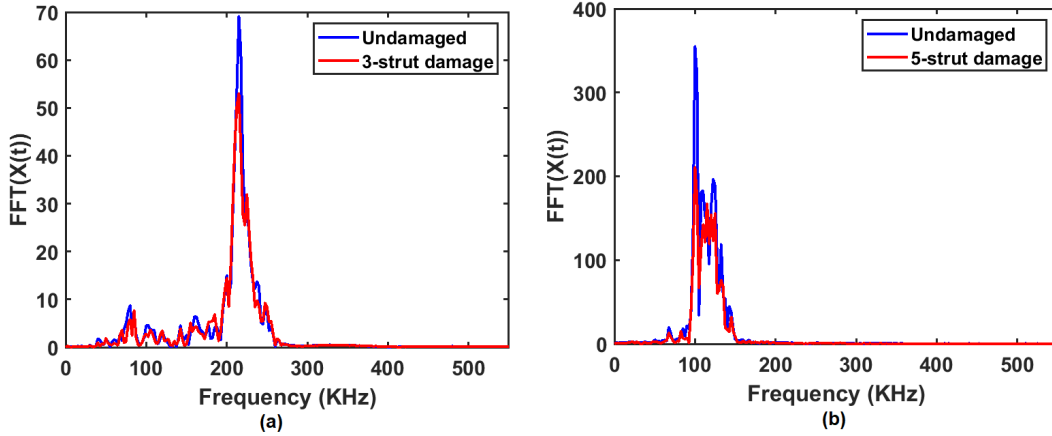
Figure 8.15: Frequency response of the 3D lattice recorded with (a) the 10mm sensor and (b) the 20mm sensor. Both responses align well with their respective excitation frequencies.

8.6 Damage localization study

Damage localization for the 3D lattice structure is conducted based on the similar methodology developed for 2D lattice structure. The purpose of the localization study is to approximate the location of the damage in the lattice structure. As discussed in the 2D localization study, the localization in the context of strut-based lattice structure could either be to localize the location or the identification number of the individual damaged strut. Another form of localization was defined as finding the location of the damaged cell. This is the similar scheme that was followed for the 2D lattice structure. Two localization models were tested for the 3D lattice structure as follows:

1. Localization Model A: To approximate the location of individual damaged strut

2. Localization Model B: To approximate the location of damaged cells in the structure

8.6.1 Numerical results

First, the numerical results for damage localization in the 3D lattice structure will be presented.

Localization Model A

There are a total of 8 cells in the lattice structure. Each cell has 8 struts, making a total of 64 struts in the lattice. The cell and strut numbering is shown in the Figure 8.4. The localization of up to 3 damaged struts was considered for this study. The possible damage locations for one, two, and three strut damage are given in Table

8.2. The number of possible damage locations for two and three strut damage is huge, making it impractical for the classification model. Instead, the location of damage was represented as the probability distribution over the 64 struts. The struts with higher classification scores indicated the probable locations of damage.

Table 8.2: Possible damage locations for 3D lattice

No of damaged struts	Possible location combinations in the 3D lattice
1	64
2	2016
3	41664

The data was trained with 64 labels. Each damage case was assigned labels based on the location of the damaged strut in it. The example of classification scores is shown in Figure 8.17 for one, two, and three damaged struts. There is a lot of spread in the classification scores, and the accuracy of predicting all correct labels is very low. The prediction accuracies are given in Table 8.3.
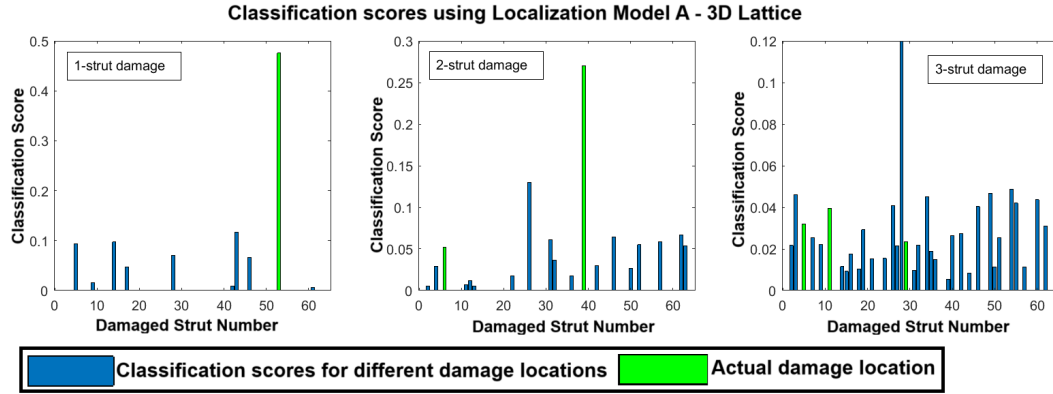
Figure 8.16: Classification scores for three damage cases using Localization Model A for the 3D lattice structure. The spread of scores across potential damage locations highlights the model's limitations in accurately predicting location of all damaged struts.

Localization Model B

In this localization model, the aim was to estimate the location of damaged cells. A cell was considered damaged if it had one or more damaged struts in it. There are a total of 8 cells in the structure. The cell and strut numbering is shown in the Figure 8.4. The localization of up to 3 damaged cells was studied. The data was trained with 8 labels corresponding to eight cells in the structure. The example of classification scores is shown in Figure 8.17 for one, two, and three damaged cells. The prediction accuracy for this localization model is much improved and provides a better estimate for the location of damage, especially for one and two cell damages. The prediction accuracy is given in Table 8.3.
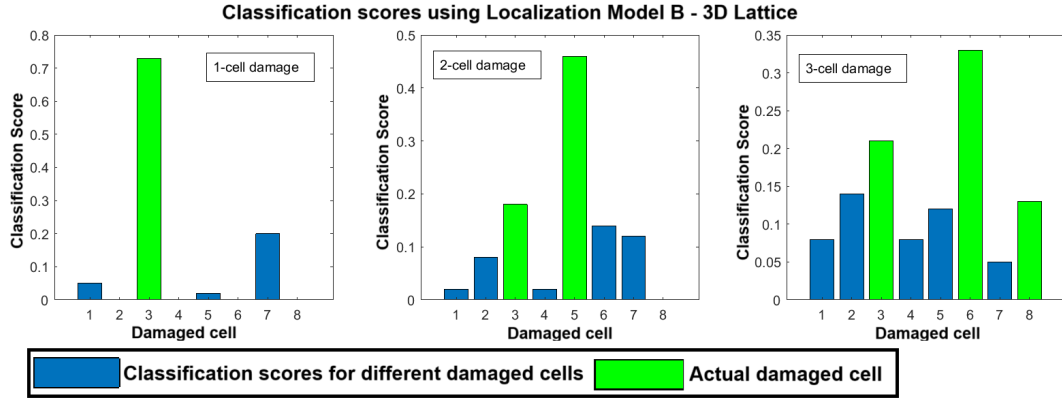
Figure 8.17: Classification scores for three damage cases using Localization Model B for the 3D lattice structure. The scores demonstrate improved prediction accuracy for single- and multi-cell damage cases compared to Model A.

Table 8.3: Prediction accuracy of numerical damage localization in 3D lattice

Damage type	Classification output (based on classification scores)	Prediction accuracy- Localization Model A	Prediction accuracy- Localization Model B
One damaged strut/cell	One correct Label	42%	83%
Two damaged struts/cells	Atleast one correct label	36%	77%
	Two correct label	22%	64%
Three damaged struts/cell	Atleast one correct label	33%	78%
	Atleast two correct labels	18%	64%
	Three correct labels	14%	48%

8.6.2   Experimental results of damage localization

The normalized experimental data was tested with the numerical classification mode to test the accuracy of damage localization. Since there is a greater mismatch between numerical and experimental response signals, the prediction accuracies are relatively low. The prediction accuracies of localization model A & B are given in Table 8.4.

Table 8.4: Prediction accuracy of experimental damage localization in 3D lattice

Damage type	Classification output (based on classification scores)	Prediction accuracy- Localization Model A	Prediction accuracy- Localization Model B
One damaged strut/cell	One correct Label	33%	62%
Two damaged struts/cells	Atleast one correct label	34%	57%
	Two correct label	18%	42%
Three damaged struts/cell	Atleast one correct label	33%	52%
	Atleast two correct labels	16%	37%
	Three correct labels	12%	26%

8.7   Summary and Conclusions

This chapter extended the methodologies developed for 2D lattice structures to the more complex realm of 3D lattice structures, focusing on damage detection, quantification, and localization. The study highlighted the challenges introduced by multi-directional wave propagation and the increased geometric intricacy inherent in 3D lattices.

The numerical simulations achieved a high degree of accuracy in damage detection, with energy features proving effective in distinguishing between damaged and undamaged states. Experimental validation, while slightly less accurate due to material inconsistencies and noise, demonstrated the applicability of the proposed methods. Damage quantification was assessed at three levels. Level 1 quantification, which employed 11 classifiers, faced challenges with feature overlap, especially at higher damage levels. By reducing the classifiers to six and then five in Level 2 quantification, significant improvements were achieved. Level 3 quantification, which focused on identifying damaged cells rather than individual struts, was the most effective, minimizing feature overlap and enhancing classification robustness.

Damage localization was studied using two models. Localization Model A, targeting individual struts, demonstrated moderate accuracy, especially for multiple-damage scenarios. Localization Model B, which focused on identifying damaged cells, significantly improved prediction accuracy by reducing complexity and broadening the applicability of the results.

The experimental results underscored the importance of addressing inconsistencies between numerical and experimental data, particularly for 3D lattice structures. The mismatch in response signals was a key challenge, suggesting the need for larger experimental datasets and more sophisticated normalization techniques.

Conclusion

The methodologies developed for 2D lattice structures were successfully adapted to the unique challenges posed by 3D lattice geometries. Among the quantification approaches, Level 3 quantification emerged as the most effective, achieving the highest accuracy in both numerical and experimental studies. Similarly, Localization Model B proved to be the most reliable for identifying damaged cells, offering a scalable

solution for complex 3D structures.

The study demonstrates the robustness of ultrasonic wave-based techniques, complemented by machine learning frameworks, in structural health monitoring for additively manufactured lattice structures. While the results are promising, the research also highlights the need for further refinement in experimental validation methods to better align with numerical models. This work provides a foundation for future advancements in non-destructive evaluation and monitoring of 3D lattice structures, with significant implications for safety, maintenance, and operational efficiency in real-world applications.

Chapter 9

Discussions, Future Work and Conclusions

9.1 Overview of Main Findings

This research developed and validated a structural health monitoring (SHM) framework for additively manufactured (AM) lattice structures using ultrasonic testing combined with machine learning (ML). It addresses critical challenges in detecting, quantifying, and localizing damage in these complex lattice geometries. In this context, damage refers to structural anomalies such as broken or fully fractured struts in the lattice (i.e. complete discontinuities in load-bearing members). Such damage significantly affects wave propagation and thus can be detected via ultrasonic methods. The main findings of this study include:

Effectiveness of Ultrasonic SHM

Ultrasonic wave propagation proved highly sensitive to internal defects in the lattice. Notably, the breaking of lattice struts caused measurable changes in the transmitted wave, particularly a clear attenuation of signal energy. These wave alterations allowed effective detection of structural anomalies that are not visible externally. This capability is especially valuable for non-invasive monitoring of intricate lattice architectures where direct visual inspection is impractical. The pronounced decrease in transmitted ultrasonic energy in the presence of damage confirmed that wave attenuation can serve as a primary indicator of structural health in lattice components.

Machine Learning Integration

ML models (notably an artificial neural network) were able to distinguish between healthy and damaged lattice states with high accuracy under the tested conditions. In numerical simulations, the classifier achieved around 90damage, demonstrating the promise of data-driven analysis for this application. The inclusion of Principal Component Analysis (PCA) as a feature reduction step significantly improved the efficiency and stability of the model by optimizing the feature set. By compressing the ultrasonic signal data into a few principal features, PCA helped the ML model focus on the most damage-sensitive information. As a result, the classification was both effective and computationally efficient. It should be noted, however,

that these accuracy levels were achieved in controlled experiments and simulations; performance may be lower in more complex or noisy real-world scenarios, so these results must be interpreted with appropriate caution.

Damage features

Damage features correspond to the characteristics of the response signal that are sensitive to the damage and provide good classification. Damage features serve to both reduce the dimensionality of the data as well as provide optimized information from the signal for damage classification. In this study, energy of the signal was seen to be progressively changing with the presence and severity of damage. Energy from different regions of the signal was effectively used for classification of damage state. PCA was also used to reduce the dimensionality of data and extract features for damage classification. These damage features provided a compact and informative representation of the structural state. They enabled the ML classifier to be trained effectively, improving damage detection and characterization performance. In summary, the progressive reduction in signal energy due to damage (and its capture through features) was a key finding that underpins the classification approach.

Damage Quantification and Localization

Beyond simply detecting damage, the features extracted from ultrasonic signals carried information about the extent and location of damage. In this work, a zone-based classification strategy was employed for damage quantification and localization. Instead of trying to count every broken strut exactly (which proved difficult due to overlapping signal effects), the methodology classified damage into categories by severity and by region. For quantification, the framework could distinguish between different levels of damage (i.e. or one damaged cell vs. multiple damaged cells) with reasonable accuracy, even if identifying the precise number of broken struts was challenging. This approach of grouping damage severity was more reliable than attempting a one-to-one mapping of signal changes to each broken strut. For localization, the lattice structure was conceptually divided into zones (for example, grouping struts into cells or sections), and multiple sensor pairs were deployed to detect damage in those zones. This spatial classification approach enabled the identification of which region of the lattice was affected by damage. The results demonstrated that for relatively simple damage cases (e.g. one to three damaged cells), the method correctly identified the damaged zone in a majority of instances. This is a valuable capability given the complexity of wave propagation in lattices. However, the precision of localization was limited: as the number of damaged elements increased or if damage was more distributed, the accuracy of pinpointing exact zones decreased. In summary, the developed method can localize defects within 2D and 3D lattice structures to a regional extent, offering a practical way to narrow down inspection areas.

Scalability to 3D Lattices

The SHM methodology was successfully extended from two-dimensional (2D) lattices to more complex three-dimensional (3D) lattice structures. Adapting the approach to 3D required addressing additional challenges such as multi-axial wave

propagation paths and a larger number of potential damage sites. The core techniques (ultrasonic excitation/measurement, feature extraction, and classification) remained applicable and effective in 3D, demonstrating the approach's adaptability. Consistent trends were observed between 2D and 3D cases – for example, the presence of damage led to attenuated signals and the ML classifier could detect and categorize damage in both geometries. The study showed that even in an 8-cell 3D lattice with complex connectivity, the framework could identify damaged vs. healthy states and perform zone-based localization of damage. Achieving this scalability is a noteworthy result; it indicates that the method can be applied to real lattice components (which are inherently 3D) beyond the simplified 2D prototypes.

Collectively, these findings demonstrate the potential viability of the proposed ultrasonic-ML SHM approach for monitoring lattice structures. The research established a foundational framework that is both scalable (applicable to various lattice sizes and dimensions) and shows promise in terms of reliability for detecting internal damage. At the same time, the results highlight certain limitations (such as reduced localization precision in complex scenarios and the need for calibration between simulation and experiment) which temper the claims of immediate real-world readiness. Overall, the study provides strong evidence that ultrasonic waves and machine learning can be combined to detect and characterize damage in intricate lattice geometries, supporting the feasibility of this SHM methodology for future practical use with further refinement.

9.2 Evaluation of Aims, Objectives, and Hypotheses

This section evaluates how well the research met its stated aims and objectives (as defined in Chapter 1), and revisits the initial hypotheses in light of the findings. The primary goal was to develop a reliable methodology for damage characterization in AM lattice structures using ultrasonics and ML. Four specific objectives were set to achieve this goal, each of which is discussed below along with the outcomes:

Understanding Wave Propagation in Lattice Geometries

Through an analytical study on ultrasonic transmission in lattice structure, the research provided detailed insights into how ultrasonic waves interact with the unique lattice geometries and defect types of lattice structures. The analytical study enabled the calculations of transmission efficiencies of lattice unit cells which were then calculated for complete structures. Changes in ultrasonic transmissions for a healthy and damaged structure were measured and a qualitative analysis of the same was carried out. The qualitative analysis revealed attenuation of wave transmissions due to the presence of damage. This attenuation acts as the primary feature for damage characterization in this study. Thus analytical study not only helped to further the understanding of ultrasonic transmission in lattice structures but also served as a proof of concept of developing a methodology for damage detection and quantification. The analytical study also provides a quick and efficient method for calculating transmission efficiency in various forms of lattice structures.

Developing a methodology for damage detection and quantification

A comprehensive methodology for damage detection and quantification was developed. The methodology involved numerical simulations of a large sample set of a 2D lattice structure to generate response data for undamaged and damaged structures. A neural network classification model was trained using the known class labels of the simulated data and validated through test data. The best accuracy of more than 90% was achieved when quantifying a range of damaged struts. The methodology was validated using experimental testing. Due to limited experimental data, a standalone classification model was not generated for the experimental data. Instead, the experimental data was normalized to the numerical response data and tested on the classification model trained with numerical data. Good accuracies were seen for the experimental data tested on the classification model.The methodology was then tested on a 3D lattice structure and similar results were seen.

Establishing a Damage Localization Methodology

A detailed damage localization study was conducted on two different 2D lattice structures with a varying number of cells. Three different localization models were tested in this study. In Localization Model A, the aim was to approximate the location of exact damaged strut in the structure. This methodology did not perform well when locating more than one damaged struts. In Localization model B, the aim was to measure the location of damaged cells instead of individual struts. Locations of upto three damaged cells were approximated with good accuracy in this model. Finally, in Localization Model C, a spatial localization technique using multiple sensors and zoning of the structure was used to determine the location of damaged struts in different zones of the structure. Localization model C provided the best accuracy for the localization of damage. The experimental testing of localization methodology was also carried out which validated the findings of spatial localization in numerical testing. Finally, the localization scheme was also validated for a 3D lattice structure using first two localization models.

Incorporating Machine Learning for Enhanced SHM

Application of ML formed the core of this study. A robust classification model was developed using a trained Neural network, the parameters of which were optimized. The ML learning model was tested again the statistical models and ML models results in better classification accuracy. Moreover, ML classification was able to handle complex dataset involving overlapping damage states. This study highlights the possible applications of Machine learning in SHM applications.

Evaluating Scalability and Applicability

The methodologies developed for 2D models were tested on a 3D lattice structures. The results indicated the scalability of the proposed model to 3D structures and real world applications.

These achievements confirm the research's success in addressing its primary aim while establishing a robust foundation for future studies in SHM for AM components.

9.2.1 Validation of Hypotheses

This research was guided by four key hypotheses, each addressing critical aspects of structural health monitoring (SHM) in additively manufactured (AM) lattice structures. The results obtained through numerical simulations, experimental studies, and machine learning (ML) integration confirm these hypotheses:

Hypothesis 1: Defects in lattice structures significantly alter ultrasonic wave properties

The numerical results along with experimental findings confirmed that the breaking of struts, a key form of damage in lattice structures, led to significant changes in the ultrasonic wave properties. A measurable change in wave attenuation and scattering properties were seen after interaction with the damage. This was also validated through analytical calculations of wave propagation in a lattice structure. The presence of damage altered the transmitted wave to the sensor.

Hypothesis 2: The difference between the response of healthy and damaged structures can provide a baseline for damage characterization

The study developed a baseline dataset of ultrasonic wave responses for undamaged lattices, which was compared with responses from damaged structures. Feature extraction techniques highlighted separations between healthy and damaged states, providing a robust basis for classification. Establishing this baseline is critical for quantifying damage and serves as a foundation for ML-driven damage characterization.

Hypothesis 3: Advanced signal processing techniques and machine learning algorithms can be used for the detection and quantification of damage in lattice structures

Principal Component Analysis (PCA) and neural networks were employed to process ultrasonic signal data. The ML model achieved over 90% classification accuracy for damage detection and quantification, proving the hypothesis correct. This result highlights the potential for integrating ML into SHM frameworks, enabling accurate, automated, and scalable damage assessment.

Hypothesis 4: A systematic approach combining experimental data and numerical simulations can enhance the accuracy of damage quantification and localization in lattice structures

The neural network classification model was trained using the numerically simulated data of the lattice structures. The numerical models also included the material and sensor placement uncertainties incorporated to match closely with real-world applications. The experimental data was normalized to the numerical data and tested with the classification model. Good accuracy of prediction was seen for the experimental data, boosting confidence in the developed methodology. By further improving the normalization techniques, this will also enable developing a trained classification model for a variety of lattice structures using numerical simulations and then using those models for classifying damage in real-world applications.

9.3 Key Contributions of the Research

This research makes several noteworthy contributions to the state of the art in structural health monitoring and non-destructive evaluation of lattice structures. The contributions span theoretical insights, methodological innovations, and practical implications. In one sentence, the core contribution of this thesis is the development and demonstration of an integrated ultrasonic and-ML framework for detecting, quantifying, and localizing internal damage in complex AM lattice structures. Building on this overarching achievement, the key specific contributions are outlined below:

- **Enhanced understanding of ultrasonic wave behavior** The thesis provides a deeper theoretical and experimental insight into how high-frequency stress waves travel through and interact with the complex geometry of strut-based lattices. By systematically analyzing wave transmission and reflection in both healthy and damaged lattice cells, the study identified wave attenuation as a robust indicator of damage. This is a significant academic contribution: previous works have studied ultrasonic propagation in simpler structures, but this work extends that understanding to architected lattice materials. It highlights the critical parameters (such as transmitted wave amplitude and energy loss) that correlate strongly with structural damage. This new knowledge lays the groundwork for ultrasonic-based inspection techniques tailored to lattices, a domain that had not been thoroughly explored before. Essentially, the research bridges a gap by explaining how and why a broken strut in a lattice can be detected via changes in an ultrasonic signal, thus advancing the theoretical foundation for SHM in architected materials.

- **Development of an integrated SHM methodology** A major contribution of this work is the creation of a novel SHM framework that combines ultrasonic testing with machine learning to automatically detect damage in AM lattice structures. While machine learning has been applied in SHM of conventional structures, this thesis is among the first to tailor and validate such an approach for the unique context of lattice geometries produced by additive manufacturing. The methodology covers the entire process: sensing (using piezoelectric transducers to excite and capture waves), signal processing (feature extraction and PCA), and automated damage classification (via neural networks). This integrated approach proved capable of distinguishing damaged versus undamaged lattices with high accuracy and could even classify damage severity levels. The contribution here is twofold: (1) a practical framework/algorithm that researchers and engineers can build upon for monitoring lattice-based components, and (2) evidence that data-driven models can overcome the complexities of lattice signals (which are typically difficult to interpret with traditional methods). By demonstrating an effective use of ML in this scenario, the work pushes the boundary of SHM practice – showing that even highly complex, periodic structures can be monitored using intelligent algorithms. This contribution is expected to inspire further studies on applying and refining ML techniques for SHM in other complex geometries and advanced materials.

- **Innovative approach to damage quantification and localization in lattices** The thesis introduces and validates a spatial classification strategy for dealing with damage quantification and localization, which is a new way to handle these challenges in a lattice structure. Instead of relying on direct physics inversion or dense sensor networks, the approach segments the structure into logical zones and trains classifiers to recognize damage in those zones or within certain severity ranges. This zone-based damage localization method is an important contribution because traditional SHM methods struggle to pinpoint damage in complex lattices using global signals. By breaking the problem into smaller sub-regions and focusing on pattern recognition within signals, the research achieved a level of localization that was not previously attainable in lattices with a simple two-sensor setup. Furthermore, the concept of using multiple simplified classifiers for different levels of damage (the multi-level classification scheme for quantification) proved effective – this strategy improved accuracy by reducing the confusion that arises when one tries to discriminate too many damage cases at once. Collectively, these methodological innovations (zonal localization and multi-level damage classification) are contributions that make SHM of complex structures more feasible.

- **Extension of SHM to 3D lattice structures,** The research successfully scaled and tested the damage detection methodology on 3D lattice specimens, thereby demonstrating scalability and adaptability of the SHM approach. Many prior studies in SHM focus on simple or planar structures; in contrast, this work tackled the more complex 3D lattice which is closer to real engineering components (e.g., lattice infills in aerospace or biomedical parts). Adapting the techniques to a full 3D lattice (with multiple layers of cells) required overcoming challenges like more complicated wave paths and increased signal attenuation, and the thesis showed that this can be done.

- **Simulation-experiment integration** An additional technical contribution of the thesis is the demonstrated approach for combining numerical simulations with experimental measurements to develop data-driven SHM models. The study showed how normalizing and aligning data from different sources can overcome the scarcity of experimental data when training machine learning models. In essence, the numerical simulations were used to train initial damage classification models, and a calibration procedure then allowed those models to interpret real experimental signals correctly.

Collectively, these contributions advance the field of SHM for additively manufactured structures on multiple fronts. Academically, the work enriches the understanding of wave-damage interaction in lattices and introduces new techniques for damage evaluation. Practically, it offers a prototype SHM system that, with further development, could be deployed to monitor critical lattice components in service. The findings and methods from this thesis thus pave the way for more reliable and efficient monitoring strategies tailored to the unique challenges of AM lattice structures. They also provide a foundation upon which future researchers can build – whether it is by refining the ultrasonic/ML algorithms, exploring other sensor types, or extending the approach to different types of lattice geometries and materials.

9.4 Challenges and Future Work

While this research achieved its primary objectives, it also revealed several challenges and limitations that provide avenues for future improvement. It is important to critically assess these issues to understand the scope and honesty of the contributions. Addressing these challenges in future work will be crucial for translating the proposed SHM framework into a robust real-world application.

- **Material and modeling uncertainties:** One challenge lies in the uncertainties associated with the material properties and manufacturing quality of the lattices, which can affect the accuracy of both numerical models and experimental results. Additively manufactured lattice structures often exhibit variability such as micro-porosity, residual stresses, or slight geometric deviations (e.g., strut thickness variations) from the ideal design. These factors can influence ultrasonic wave propagation in ways that are hard to predict with simplified models. Future work should investigate more robust modeling techniques that account for material and manufacturing uncertainties. Furthermore, the mass of sensors has not been modeled in the current study which may have impacted the accuracy of the prediction model. It is suggested that future work should cater for the mass of the sensors.

- **Limited data and machine learning generalization:** Another significant challenge is the limitation of the available data, especially experimental data, for training and validating the machine learning models. In this project, thousands of simulated signals were available, but the experimental dataset was relatively small (restricted by the number of specimens and tests that could be practically carried out). Consequently, the ML classifier's ability to generalize to new situations (for instance, a lattice of a different design or a slightly different damage scenario) is not yet proven. The current classification models rely on the assumption that the damage patterns seen in training cover those that will be seen in practice. Future studies should focus on greatly expanding the dataset, including a wider range of damage types, severities, and lattice configurations. This could involve generating more numerical data for different lattice designs (to see if the same features and models work) and, importantly, gathering more experimental data.

  Additionally, advanced machine learning techniques could be explored to improve generalization. For example, transfer learning or domain adaptation algorithms might allow a model trained on one type of lattice or simulation data to adapt to another type. More sophisticated neural network architectures (such as convolutional or recurrent networks that might better capture signal patterns) could also be tested for improved performance.

- **Damage definition and detection scope:** The scope of damage considered in this thesis was limited to complete breaking of struts (full discontinuities). This is a logical starting point, as broken struts cause a pronounced effect on ultrasonic waves. However, in real structures, damage can be more subtle – for instance, a strut could develop a crack that only partially reduces its stiffness, or there could be a weak bonded joint or some localized plastic deformation. These kinds of minor or incipient damages do not completely sever the load

path but still represent damage that could grow over time. In the current approach, such small-scale damage might not produce as large or as clear a change in the ultrasonic signal as a fully broken strut, and thus might go undetected or be hard to distinguish from noise. Future research should broaden the types of damage studied to include these partial damages or degradation states.

- **Alternate sensing techniques:** The current SHM setup used a pair of piezoelectric transducers in a pitch-catch arrangement (one transmitter, one receiver) for most tests, with additional sensors for localization in certain cases. Future work could explore more complex sensor arrays and optimize sensor placement to improve coverage of the structure. Moreover, alternative types of sensors could be investigated. The exclusive use of piezoelectric transducers means we focused on ultrasonic wave transmission; however, other modalities like accelerometers or strain gauges could pick up vibrational or static strain changes due to damage. Incorporating an accelerometer array might allow vibration-based SHM in conjunction with ultrasonics – a hybrid approach that could catch a wider range of damage types. For instance, low-frequency vibrations might be more sensitive to global stiffness loss from partial damage, complementing the local sensitivity of high-frequency ultrasound. Additionally, optical methods (like fiber Bragg grating sensors) could be considered for high-resolution strain monitoring in critical struts. In future implementations, a multisensor, multi-modal SHM system might provide the best coverage: ultrasonics for detecting internal cracks or breaks, and vibration/strain monitoring for detecting slight stiffness changes and confirming global structural integrity. The challenge of limited sensor representation identified by the examiners can thus be addressed by broadening the sensing strategy in subsequent research.

- **Complexity of 3D geometries and advanced localization methods:** As the study showed, moving to 3D lattices increases the complexity of the SHM task. Wave propagation in 3D is inherently more complicated (waves can take many paths and modes), and the number of potential damage sites grows. The zone-based localization method worked to an extent for the tested 3D case, but its performance may decline as the structure size or complexity further increases. A challenge for future work is to maintain or improve localization accuracy in larger or more intricate lattices. One promising direction is to employ more advanced computational methods for localization, such as inverse problem solving or machine-learning-based regression that directly predicts damage location coordinates from signals. In the current approach, we simplified the localization by classification (zones), but another approach could train a model to output a probable damage location (perhaps formulated as coordinates or an image of the structure with highlighted damage).

9.5   Future Research Directions

In light of the challenges identified, the following future research directions are particularly recommended to build upon this thesis:

- **Broader damage scenarios:** Expand the investigation to include different damage forms (e.g., gradual cracks, debonded joints, material fatigue damage) beyond the complete strut fractures studied here. This will test the method's sensitivity and possibly require new features or techniques for detecting smaller-scale damage.

- **Larger and varied lattice configurations:** Apply the methodology to a wider range of lattice designs (different cell topology, size, and material) to evaluate its adaptability. This will help ensure the approach is robust across different use cases and not over-fitted to one geometry. It will also provide insight into how lattice parameters (such as cell size, complexity, or base material properties) affect SHM performance.

- **Advanced signal processing and ML models:** Investigate alternative feature extraction methods (such as wavelet transforms or nonlinear time-series analyses) and cutting-edge ML algorithms (including deep learning models) for potentially improved accuracy. For instance, a deep neural network might automatically learn complex features from raw waveforms, which could outperform manually crafted features like energy metrics, especially for detecting subtle damages. Any new model should be tested for its ability to generalize and for interpretability in the context of physical wave behavior.

- **Improved experimental validation:** Conduct more extensive experimental testing, including long-term monitoring scenarios if possible. For example, one could subject a lattice to cyclic loading to introduce fatigue cracks and attempt to detect them with the SHM system *in situ*. Such experiments would validate the system's real-world applicability and help identify any reliability issues (e.g., sensor durability, repeatability of results over time, false alarm rates) that need to be addressed.

- **Hybrid SHM approaches:** Explore combining the ultrasonic-ML framework with other complementary SHM approaches. As mentioned, integrating vibrational monitoring could be beneficial. One could develop a hybrid model that takes both ultrasonic features and vibrational frequency changes as inputs to a unified classifier or decision engine. This multi-faceted monitoring might greatly enhance confidence in detection and also provide redundancy (so that if one method misses a damage, another might catch it).

- **Sensor network optimization:** Research optimal sensor placement and minimal sensor requirements for lattice SHM. Using simulation tools, one could perform a sensitivity analysis to see which sensor locations yield the most information about certain damage locations, then use optimization algorithms to suggest the best sensor layout for a given lattice structure. The outcome would guide practical implementations in terms of where to mount sensors on a part and how many are needed to achieve a desired level of diagnostic capability.

By addressing these future directions, the limitations identified in the current work can be mitigated step by step. Progress in these areas will ensure that the SHM framework becomes more robust, accurate, and broadly applicable. Ultimately, the

goal of future research inspired by this thesis is to develop a comprehensive SHM system for AM lattice structures that is reliable under real operating conditions, capable of detecting even minor damage early, and straightforward to deploy on actual components.

9.6   Concluding Remarks

In this chapter, we discussed the outcomes of the research in the context of the original aims, examined the contributions and limitations, and outlined paths for future work. It is evident from the discussion that the project has achieved its primary objectives and has made a meaningful contribution to the field of structural health monitoring for advanced lightweight structures. The developed ultrasonic-ML framework was shown to be effective in detecting and characterizing internal damage in lattice structures, thereby confirming the central hypotheses of the study. The integration of ultrasonic testing with machine learning proved to be a viable approach to handle the complexity of lattice geometries, something that traditional methods alone could not easily accomplish.

A key achievement of this research is that it establishes a proof of concept for monitoring AM lattice structures in a way that is both non-invasive and automated. The ability to identify not only the presence of damage but also an estimate of its severity and location is a step forward for SHM of intricate architectures. This work thus provides a foundation for future SHM systems that could be used to ensure the integrity of components made by additive manufacturing. By validating the approach on real printed specimens (albeit at laboratory scale), the thesis moves the theoretical concept closer to practical realization.

It is important to emphasize the novelty and context of these contributions: while structural health monitoring and even the use of ML in SHM are not new by themselves, their application to the specific domain of periodic lattice materials fills a gap in the current literature and practice. Lattice structures are increasingly employed in high-performance engineering applications (such as lightweight aerospace components, biomedical implants with lattice scaffolds, and energy-absorbing automotive parts). Ensuring the safety and reliability of such components is critical. However, their complex geometry makes conventional inspection difficult. The methods developed in this thesis — using ultrasonic waves that can penetrate complex internal geometry, and intelligent algorithms to interpret the signals — offer a solution tailored to this need. In academic terms, the thesis contributes new knowledge about how damage in these novel structures can be detected and assessed. In industrial terms, it suggests a pathway to real-time in-service monitoring of AM lattice components, which could significantly enhance maintenance strategies and safety margins.

At the same time, the research has been careful to identify its own limitations. The performance metrics achieved (for example, classification accuracy and localization precision) are encouraging but not yet at a level where one would simply deploy the system on an aircraft wing or an implanted medical device without further development. There is room for improvement in terms of reliability, generality, and resolution. By openly discussing these aspects, the thesis provides a realistic assessment and avoids overstating the readiness of the technology. This honesty is important for guiding future efforts; it ensures that subsequent researchers focus on the most pressing issues (such as those outlined in Section 9.5) to advance the

method from a promising prototype to a mature tool.

In conclusion, this thesis has demonstrated that ultrasonic-based SHM augmented with machine learning is a promising approach for the detection and characterization of damage in additively manufactured lattice structures. The work bridges the gap between theoretical wave propagation analysis and practical damage detection through a data-driven framework, contributing to both domains. With further refinement – including better models, more extensive data, and broader validation – the approach developed here has the potential to become a reliable technique for monitoring complex structures in real time. Such a capability would be highly valuable: it could enable engineers to detect incipient damage in critical components before it leads to failure, thus improving the safety, performance, and lifespan of next-generation lightweight structures. The contributions of this research, therefore, have significance not only in advancing scientific understanding but also in pointing the way toward safer and more efficient use of advanced manufactured materials in industry. The hope is that this work will spur continued research at the intersection of ultrasonics, machine learning, and advanced materials engineering, ultimately leading to smart structures that can monitor their own health throughout their service life.

Appendix A

Appendix

Bibliography

[1] Material extrusion. https://www.lboro.ac.uk/research/amrg/about/the7categoriesofadditivemanufacturing/materialextrusion. Accessed: 2024-09-30.

[2] Powder bed fusion. https://www.lboro.ac.uk/research/amrg/about/the7categoriesofadditivemanufacturing/powderbedfusion/. Accessed: 2024-09-30.

[3] Powder bed fusion. https://www.lboro.ac.uk/research/amrg/about/the7categoriesofadditivemanufacturing/directedenergydeposition/. Accessed: 2024-09-30.

[4] Powder bed fusion. https://www.lboro.ac.uk/research/amrg/about/the7categoriesofadditivemanufacturing/vatphotopolymerisation/. Accessed: 2024-09-30.

[5] Powder bed fusion. https://www.lboro.ac.uk/research/amrg/about/the7categoriesofadditivemanufacturing/binderjetting/. Accessed: 2024-09-30.

[6] Powder bed fusion. https://www.lboro.ac.uk/research/amrg/about/the7categoriesofadditivemanufacturing/sheetlamination/. Accessed: 2024-09-30.

[7] Haijun Gong. Generation and detection of defects in metallic parts fabricated by selective laser melting and electron beam melting and their effects on mechanical properties. 2013.

[8] Thabiso Hopewell Sibisi, Mxolisi Brendon Shongwe, Lerato C Tshabalala, and Ipfi Mathoho. Lam additive manufacturing: A fundamental review on mechanical properties, common defects, dominant processing variables, and its applications. *The International Journal of Advanced Manufacturing Technology*, 128(7-8):2847–2861, 2023.

[9] Renishaw. Residual stresses. https://www.metal-am.com/articles/how-residual-stress-can-cause-major-build-failures-in-3d-printing/. Accessed: 2024-09-30.

[10] R Rodrigues, P Lopes, Luis Oliveira, L Santana, and J Lino Alves. Design parameters to develop porous structures: Case study applied to dlp 3d printing. In *International conference on flexible automation and intelligent manufacturing*, pages 319–327. Springer, 2023.

[11] Ajit Panesar, Meisam Abdi, Duncan Hickman, and Ian Ashcroft. Strategies for functionally graded lattice structures derived using topology optimisation for additive manufacturing. *Additive Manufacturing*, 19:81–94, 2018.

[12] Steminc. Pzt-5h datasheet smd10t2r111wl. Product datasheet, 2024.

[13] C. R. Farrar and K. Worden. *Structural Health Monitoring: A Machine Learning Perspective*. Wiley, 2012.

[14] P. Chang et al. A review of structural health monitoring 2000–2021. *Sensors*, 22:1234, 2022.

[15] Wohlers Associates. Wohlers report 2024. Industry report, 2024.

[16] I. Gibson and D. Rosen. Additive manufacturing research trends 2014–2023. *Addit. Manuf.*, 67:102838, 2023.

[17] Airbus. World's first 3d-printed bionic partition for a320. Press release, 2017.

[18] GE Aviation. 3d-printed leap fuel nozzle. Web article, 2018.

[19] Oxford Performance Materials. Peek and ti lattice implants. White paper, 2022.

[20] S. Leuders et al. Fatigue crack growth in slm ti–6al–4v lattices. *Int. J. Fatigue*, 126:136–145, 2019.

[21] W. Yan et al. Porosity-induced failure of additively manufactured lattices. *Addit. Manuf.*, 59:103088, 2022.

[22] P. Shull. Nde and shm: convergence and divergence. *Mater. Eval.*, 75:614–628, 2017.

[23] J. L. Rose. Guided waves in structural health monitoring. *Ultrasonics*, 108:106227, 2020.

[24] J. Jia and Y. Li. Deep learning for ultrasonic shm: challenges and trends. *Sensors*, 23:8824, 2023.

[25] C. S. N. Pathirage et al. Autoencoder neural networks for damage identification. *Eng. Struct.*, 172:13–28, 2018.

[26] F. Rios et al. Mechanical performance and inspection of additively manufactured lattices: a review. *Prog. Mater. Sci.*, 139:101157, 2024.

[27] Y. Qi and J. L. Rose. Guided wave damage detection in honeycomb sandwich panels. *NDTE Int.*, 116:102356, 2020.

[28] Kumar Kanishka and Bappa Acherjee. Revolutionizing manufacturing: A comprehensive overview of additive manufacturing processes, materials, developments, and challenges. *Journal of Manufacturing Processes*, 107:574–619, 2023.

[29] Nurhalida Shahrubudin, Te Chuan Lee, and RJPM Ramlan. An overview on 3d printing technology: Technological, materials, and applications. *Procedia manufacturing*, 35:1286–1296, 2019.

[30] Ian Gibson, David W Rosen, Brent Stucker, and Mahyar Khorasani. *Additive manufacturing technologies*, volume 17. Springer, 2021.

[31] Julien Gardan. Additive manufacturing technologies: state of the art and trends. *Additive Manufacturing Handbook*, pages 149–168, 2017.

[32] Brian N. Turner, Robert Strong, and Scott A. Gold. A review of melt extrusion additive manufacturing processes: I. process design and modeling. *Rapid Prototyping Journal*, 2014.

[33] Helena N. Chia and Benjamin M. Wu. Recent advances in 3d printing of biomaterials. *Journal of Biological Engineering*, 2015.

[34] Ian Gibson, David W. Rosen, and Brent Stucker. *Additive Manufacturing Technologies*. Springer, 2010.

[35] Daniel Herzog, Vito Seyda, Eric Wycisk, and Claus Emmelmann. Additive manufacturing of metals. *Acta Materialia*, 2016.

[36] M. J. Bermingham, S. D. McDonald, and D. H. StJohn. Application of laser-based additive manufacturing techniques. *Journal of Materials Science*, 2012.

[37] R. Singh et al. Additive manufacturing of functionally graded materials: A review. *Materials Today: Proceedings*, 2017.

[38] T. D. Ngo, Alireza Kashani, Giuseppe Imbalzano, Kate T. Q. Nguyen, and David Hui. Additive manufacturing (3d printing): A review of materials, methods, applications and challenges. *Composites Part B: Engineering*, 2018.

[39] Ferry P.W. Melchels, Marco A.N. Domingos, Travis J. Klein, Jos Malda, Paulo J. Bartolo, and Dietmar W. Hutmacher. Review: Additive manufacturing of tissues and organs. *Progress in Polymer Science*, 2010.

[40] Brian Derby. Inkjet printing of functional and structural materials: Fluid property requirements, feature stability, and resolution. *Annual Review of Materials Research*, 2010.

[41] Yang Bai and Christopher B. Williams. Binder jetting additive manufacturing with a particle-free metal ink as a binder precursor. *Additive Manufacturing*, 2017.

[42] David R. White et al. Sheet lamination processes for rapid manufacturing. *Procedia CIRP*, 2016.

[43] Charles W. Schick. Ultrasonic additive manufacturing: Enhancing metal fabrication. *Welding Journal*, 2013.

[44] Salvatore Greco et al. Porosity and defect detection in metal additive manufacturing: A review. *Journal of Manufacturing Processes*, 2019.

[45] Ching Y. Leung and William Y. Tam. Effect of porosity on fatigue life of additively manufactured ti-6al-4v. *Additive Manufacturing*, 2022.

[46] Hossein Taheri, Mohammad Rashid Bin Mohammad Shoaib, Lucas W Koester, Timothy A Bigelow, Peter C Collins, and Leonard J Bond. Powder-based additive manufacturing-a review of types of defects, generation mechanisms, detection, property evaluation and metrology. *International Journal of Additive and Subtractive Materials Manufacturing*, 1(2):172–209, 2017.

[47] Wayne E. King et al. Observation of keyhole-mode laser melting in laser powder-bed fusion additive manufacturing. *Journal of Materials Processing Technology*, 2015.

[48] T. Mukherjee and T. DebRoy. Residual stresses in additive manufactured components. *Additive Manufacturing*, 2017.

[49] P. Mercelis and J.-P. Kruth. Residual stresses in selective laser sintering and selective laser melting. *Rapid Prototyping Journal*, 2006.

[50] L. Parry et al. Understanding the effect of laser scan strategy on residual stress in selective laser melting. *Additive Manufacturing*, 2016.

[51] G. Strano et al. The role of surface roughness in fatigue of additively manufactured metals. *Procedia Engineering*, 2013.

[52] Beichen Song et al. Surface roughness in metal additive manufacturing: A review. *Journal of Materials Processing Technology*, 2020.

[53] T. DebRoy et al. Additive manufacturing of metallic components – process, structure and properties. *Progress in Materials Science*, 2018.

[54] C. Yan et al. Review of powder-based electron beam additive manufacturing technology. *Materials & Design*, 2018.

[55] Niloofar Sanaei and Ali Fatemi. Defects in additive manufactured metals and their effect on fatigue performance: A state-of-the-art review. *Progress in Materials Science*, 117:100724, 2021.

[56] MC Brennan, JS Keist, and TA Palmer. Defects in metal additive manufacturing processes, 2021.

[57] D. de Baere, M. Strantza, M. Hinderdael, W. Devesse, and P. Guillaume. Effective structural health monitoring with additive manufacturing. In *7th European Workshop on Structural Health Monitoring (EWSHM 2014)*. NDT.net, 2014.

[58] Khalil Khanafer, Junqian Cao, and Hussein Kokash. Condition monitoring in additive manufacturing: A critical review of different approaches. *Journal of Manufacturing and Materials Processing*, 8(3):95, 2024.

[59] Lorna J. Gibson and Michael F. Ashby. *Cellular Solids: Structure and Properties*. Cambridge University Press, 2nd edition, 1999.

[60] Michael F. Ashby, Anthony G. Evans, Norman A. Fleck, John W. Hutchinson, and Haydn N. G. Wadley. *Metal Foams: A Design Guide*. Butterworth-Heinemann, 2005.

[61] I. Maskery, N. T. Aboulkhair, C. J. Tuck, I. A. Ashcroft, R. D. Wildman, and R. J. M. Hague. Local mechanical properties of lattice structures manufactured using selective laser melting. *Materials Science and Engineering A*, 670:264–274, 2016.

[62] M. Leary, M. Mazur, and et al. Gyroid structures: A new paradigm for heat exchanger design. *Materials & Design*, 95:344–354, 2016.

[63] Y. Li, X. Guo, and Y. Zhang. Mechanical behavior of lattice structures fabricated by additive manufacturing. *Materials Science and Engineering A*, 651:361–370, 2016.

[64] Ifeanyichukwu Echeta, Xiaobing Feng, Ben Dutton, Richard Leach, and Samanta Piano. Review of defects in lattice structures manufactured by powder bed fusion. *The International Journal of Advanced Manufacturing Technology*, 106(5):2649–2668, 2020.

[65] Vikram S. Deshpande, Norman A. Fleck, and Michael F. Ashby. Foam topology: bending versus stretching dominated architectures. *Acta Materialia*, 49(6):1035–1040, 2001.

[66] Lorna J. Gibson and Michael F. Ashby. *Cellular Solids: Structure and Properties*. Cambridge University Press, 2nd edition, 1997.

[67] Charles R Farrar and Keith Worden. An introduction to structural health monitoring. *Philosophical Transactions of the Royal Society A: Mathematical, Physical and Engineering Sciences*, 365(1851):303–315, 2007.

[68] Yongrae Roh, Gyuhae Park, and Daniel J Inman. Novelty detection in structural health monitoring through local outlier factor approach. *Journal of Intelligent Material Systems and Structures*, 22(9):1021–1032, 2011.

[69] Joseph L. Rose. *Ultrasonic Guided Waves in Solid Media*. Cambridge University Press, 2014.

[70] Keith Worden and Graeme Manson. Principal component analysis for damage location in structures. *Mechanical Systems and Signal Processing*, 21(6):2461–2481, 2007.

[71] Mohsen Mousavi, Mohammad Sadegh Taskhiri, Damien Holloway, JC Olivier, and Paul Turner. Feature extraction of wood-hole defects using empirical mode decomposition of ultrasonic signals. *NDT & E International*, 114:102282, 2020.

[72] Diego A Tibaduiza, Luis Eduardo Mujica, and Jose Rodellar. Damage classification in structural health monitoring using principal component analysis and self-organizing maps. *Structural control and health monitoring*, 20(10):1303–1316, 2013.

[73] Peng Yang and Qiufeng Li. Wavelet transform-based feature extraction for ultrasonic flaw signal classification. *Neural Computing and Applications*, 24(3):817–826, 2014.

[74] N Cheraghi, GP Zou, and F Taheri. Piezoelectric-based degradation assessment of a pipe using fourier and wavelet analyses. *Computer-Aided Civil and Infrastructure Engineering*, 20(5):369–382, 2005.

[75] JP Dron, F Bolaers, et al. Improvement of the sensitivity of the scalar indicators (crest factor, kurtosis) using a de-noising method by spectral subtraction: application to the detection of defects in ball bearings. *Journal of Sound and Vibration*, 270(1-2):61–73, 2004.

[76] Stefan Pittner and Sagar V. Kamarthi. Feature extraction from wavelet coefficients for pattern recognition tasks. *IEEE Transactions on pattern analysis and machine intelligence*, 21(1):83–88, 1999.

[77] Anders Rytter. Vibrational based inspection of civil engineering structures. 1993.

[78] Charles R Farrar and Keith Worden. *Structural health monitoring: a machine learning perspective.* John Wiley & Sons, 2012.

[79] Keith Worden, Wieslaw J Staszewski, and James J Hensman. Natural computing for mechanical systems research: A tutorial overview. *Mechanical Systems and Signal Processing*, 25(1):4–111, 2011.

[80] Deepam Goyal and BS Pabla. The vibration monitoring methods and signal processing techniques for structural health monitoring: a review. *Archives of Computational Methods in Engineering*, 23:585–594, 2016.

[81] Diogo Montalvao, Nuno Manuel Mendes Maia, and António Manuel Relógio Ribeiro. A review of vibration-based structural health monitoring with special emphasis on composite materials. *Shock and vibration digest*, 38(4):295–324, 2006.

[82] Pengcheng Jiao, King-James I Egbe, Yiwei Xie, Ali Matin Nazar, and Amir H Alavi. Piezoelectric sensing techniques in structural health monitoring: A state-of-the-art review. *Sensors*, 20(13):3730, 2020.

[83] K Diamanti and C Soutis. Structural health monitoring techniques for aircraft composite structures. *Progress in Aerospace Sciences*, 46(8):342–352, 2010.

[84] Hoon Sohn. Effects of environmental and operational variability on structural health monitoring. *Philosophical Transactions of the Royal Society A: Mathematical, Physical and Engineering Sciences*, 365(1851):539–560, 2007.

[85] C Pachaud, R Salvetat, and C Fray. Crest factor and kurtosis contributions to identify defects inducing periodical impulsive forces. *Mechanical systems and signal processing*, 11(6):903–916, 1997.

[86] Jennifer E Michaels. Detection, localization and characterization of damage in plates with an in situ array of spatially distributed ultrasonic sensors. *Smart Materials and Structures*, 17(3):035035, 2008.

[87] Yinghui Lu and Jennifer E Michaels. Feature extraction and sensor fusion for ultrasonic structural health monitoring under changing environmental conditions. *IEEE Sensors Journal*, 9(11):1462–1471, 2009.

[88] Jennifer E Michaels and Thomas E Michaels. An integrated strategy for detection and imaging of damage using a spatially distributed array of piezoelectric sensors. In *Health Monitoring of Structural and Biological Systems 2007*, volume 6532, page 653203. International Society for Optics and Photonics, 2007.

[89] Shahab Torkamani, Samit Roy, Mark E Barkey, Edward Sazonov, Susan Burkett, and Sushma Kotru. A novel damage index for damage identification using guided waves with application in laminated composites. *Smart Materials and Structures*, 23(9):095015, 2014.

[90] Ye Lu, Lin Ye, Dong Wang, and Zhaorui Zhong. Time-domain analyses and correlations of lamb wave signals for damage detection in a composite panel of multiple stiffeners. *Journal of composite materials*, 43(26):3211–3230, 2009.

[91] Jennifer E Michaels and Thomas E Michaels. Detection of structural damage from the local temporal coherence of diffuse ultrasonic signals. *IEEE transactions on ultrasonics, ferroelectrics, and frequency control*, 52(10):1769–1782, 2005.

[92] William H Press, Saul A Teukolsky, William T Vetterling, and Brian P Flannery. Numerical recipes in c++. *The art of scientific computing*, 2:1002, 1992.

[93] Shie Qian and Dapang Chen. *Joint time-frequency analysis: methods and applications*. Prentice-Hall, Inc., 1996.

[94] Shengyuan Zhang, Chun Min Li, and Wenjing Ye. Damage localization in plate-like structures using time-varying feature and one-dimensional convolutional neural network. *Mechanical Systems and Signal Processing*, 147:107107, 2021.

[95] Nader Cheraghi and Farid Taheri. A damage index for structural health monitoring based on the empirical mode decomposition. *Journal of Mechanics of Materials and Structures*, 2(1):43–61, 2007.

[96] Yanhua Zhang, Lu Yang, and Jianping Fan. Study on feature extraction and classification of ultrasonic flaw signals. *WSEAS Transactions on Mathmatics*, 9(7):529–538, 2010.

[97] Piervincenzo Rizzo and Francesco Lanza di Scalea. Feature extraction for defect detection in strands by guided ultrasonic waves. *Structural Health Monitoring*, 5(3):297–308, 2006.

[98] Subhash Sharma. *Applied multivariate techniques*. John Wiley & Sons, Inc., 1995.

[99] Ling Yu, Jun-hua Zhu, and Liu-jie Cheri. Parametric study on pca-based algorithm for structural health monitoring. In *2010 Prognostics and System Health Management Conference*, pages 1–6. IEEE, 2010.

[100] Xinlin P Qing, Hian-Leng Chan, Shawn J Beard, and Amrita Kumar. An active diagnostic system for structural health monitoring of rocket engines. *Journal of intelligent material systems and structures*, 17(7):619–628, 2006.

[101] Ryan Watkins and Ratneshwar Jha. A modified time reversal method for lamb wave based diagnostics of composite structures. *Mechanical Systems and Signal Processing*, 31:345–354, 2012.

[102] Angelo De Fenza, Assunta Sorrentino, and Pasquale Vitiello. Application of artificial neural networks and probability ellipse methods for damage detection using lamb waves. *Composite Structures*, 133:390–403, 2015.

[103] Zhanjun Wu, Xinlin P Qing, Kumar Ghosh, Vistasp Karbhar, and Fu-Kuo Chang. Health monitoring of bonded composite repair in bridge rehabilitation. *Smart Materials and Structures*, 17(4):045014, 2008.

[104] D.J. Inman, C.R. Farrar, V. Lopes, and V. Steffen. *Damage Prognosis: for Aerospace, Civil and Mechanical Systems*. John Wiley & Sons, 2005.

[105] X. Maldague. *Theory and Practice of Infrared Technology for Nondestructive Testing*. John Wiley & Sons, 2001.

[106] I. Gibson, D.W. Rosen, and B. Stucker. *Additive Manufacturing Technologies*. Springer, 2 edition, 2015.

[107] K.V. Wong and A. Hernandez. A review of additive manufacturing. *ISRN Mechanical Engineering*, 2012:1–10, 2012.

[108] Keith Worden and Janice M Dulieu-Barton. An overview of intelligent fault detection in systems and structures. *Structural Health Monitoring*, 3(1):85–98, 2004.

[109] L. Tarassenko. A guide to neural computing applications. *Electronics & Communication Engineering Journal*, 10(4):185–193, 1998.

[110] I. Goodfellow, Y. Bengio, and A. Courville. *Deep Learning*. MIT Press, 2016.

[111] C.M. Bishop. *Pattern Recognition and Machine Learning*. Springer, 2006.

[112] J.L. Beck and L.S. Katafygiotis. Updating models and their uncertainties: Bayesian statistical framework. *Journal of Engineering Mechanics*, 124(4):455–461, 1998.

[113] D.C. Montgomery, E.A. Peck, and G.G. Vining. *Introduction to Linear Regression Analysis*. John Wiley & Sons, 5 edition, 2012.

[114] C. Cortes and V. Vapnik. Support-vector networks. *Machine Learning*, 20(3):273–297, 1995.

[115] J. Schmidhuber. Deep learning in neural networks: An overview. *Neural Networks*, 61:85–117, 2015.

[116] D.E. Rumelhart, G.E. Hinton, and R.J. Williams. Learning representations by back-propagating errors. *Nature*, 323(6088):533–536, 1986.

[117] Lionel Tarassenko, Alexandre Nairac, N Townsend, I Buxton, and Peter Cowley. Novelty detection for the identification of abnormalities. *International Journal of Systems Science*, 31(11):1427–1439, 2000.

[118] Ceena Modarres, Nicolas Astorga, Enrique Lopez Droguett, and Viviana Meruane. Convolutional neural networks for automated damage recognition and damage type identification. *Structural Control and Health Monitoring*, 25(10):e2230, 2018.

[119] Chathurdara Sri Nadith Pathirage, Jun Li, Ling Li, Hong Hao, Wanquan Liu, and Pinghe Ni. Structural damage identification based on autoencoder neural networks and deep learning. *Engineering structures*, 172:13–28, 2018.

[120] Lionel Tarassenko, Alexandre Nairac, N. Townsend, I. Buxton, and Peter Cowley. Novelty detection for the identification of abnormalities. *International Journal of Systems Science*, 31(11):1427–1439, 2000.

[121] Ceena Modarres, Nicolas Astorga, Enrique Lopez Droguett, and Viviana Meruane. Convolutional neural networks for automated damage recognition and damage type identification. *Structural Control and Health Monitoring*, 25(10):e2230, 2018.

[122] Ian Goodfellow, Yoshua Bengio, and Aaron Courville. *Deep Learning*. MIT Press, 2016.

[123] Jing Jia and Ying Li. Deep learning for structural health monitoring: Data, algorithms, applications, challenges, and trends. *Sensors*, 23(21):8824, 2023.

[124] M. Jameel, A. Aziz, A. Ghaffar, S. Z. H. Shah, S. Sultana, M. Hassan, and H. Li. Machine learning techniques for structural health monitoring using sensor data: A review. *Sensors*, 21(22):7663, 2021.

[125] Charles R. Farrar and Keith Worden. An introduction to structural health monitoring. *Philosophical Transactions of the Royal Society A*, 365(1851):303–315, 2007.

[126] Victor Giurgiutiu. *Structural Health Monitoring of Aerospace Composites*. Academic Press, 2015.

[127] Joseph L. Rose. Ultrasonic guided waves in structural health monitoring. In *Key Engineering Materials*, volume 270, pages 14–21. Trans Tech Publications, 2004.

[128] Yuting Yang, Wei Huang, Yu-E Ma, Shengnan Wang, Xianmin Chen, and Yifei Meng. Mechanical properties and failure modes of additively manufactured ti6al4v lattice structures under quasi-static compressive loading. *International Journal of Applied Mechanics*, 14(09):2250081, 2022.

[129] Forge Labs. Nylon PA12 – Strong, Flexible, Durable, n.d. Accessed: 2025-05-03.

[130] ASTM International. ASTM D638-22: Standard Test Method for Tensile Properties of Plastics. https://www.astm.org/d0638-22.html, 2022. Accessed: 2025-05-03.

[131] Joseph L Rose. Ultrasonic guided waves in structural health monitoring. In *Key Engineering Materials*, volume 270, pages 14–21. Trans Tech Publ, 2004.

[132] Nikola Marković and Dragoslav Stojić. Numerical modeling of ultrasonic wave propagation using explicit fem in abaqus. *ResearchGate*, 2018. Available at: https://www.researchgate.net/publication/325873278_Numerical_modeling_of_ultrasonic_wave_propagation_-_by_using_of_explicit_FEM_in_ABAQUS [Accessed 3 May 2025].

[133] Cara A. C. Leckey and F. R. Parker. 3d guided wave motion analysis on laminated composites. Technical Report NASA/TP–2014-217676, NASA Langley Research Center, 2014. Available at: https://ntrs.nasa.gov/api/citations/20140002793/downloads/20140002793.pdf [Accessed 3 May 2025].

[134] A. Raghavan and C. E. S. Cesnik. Guided-wave signal processing using the wavelet transform for structural health monitoring. *Smart Materials and Structures*, 16(2):355–366, 2007.

[135] H. Sohn, C. R. Farrar, N. F. Hunter, and K. Worden. Structural health monitoring using statistical pattern recognition techniques. *Journal of Dynamic Systems, Measurement, and Control*, 123(4):706–711, 2000.

[136] Dong C. Liu and Jorge Nocedal. On the limited memory bfgs method for large scale optimization. *Mathematical Programming*, 45(1):503–528, 1989.

[137] Sashank J. Reddi, Satyen Kale, and Sanjiv Kumar. On the convergence of adam and beyond. *International Conference on Learning Representations (ICLR)*, 2019.

[138] Sebastian Ruder. An overview of gradient descent optimization algorithms. *arXiv preprint arXiv:1609.04747*, 2016.

[139] Lothar Cremer and Manfred Heckl. *Structure-borne sound: structural vibrations and sound radiation at audio frequencies*. Springer Science & Business Media, 2013.

[140] Karl F. Graff. *Wave Motion in Elastic Solids*. Clarendon Press, Oxford, 1975.

[141] Bertram A. Auld. *Acoustic Fields and Waves in Solids*, volume 1–2. John Wiley & Sons, New York, 1973.

[142] Lawrence E. Kinsler, Austin R. Frey, Alan B. Coppens, and James V. Sanders. *Fundamentals of Acoustics*. John Wiley & Sons, New York, 4th edition, 2000.

[143] Xavier P. Maldague. *Theory and Practice of Infrared Technology for Nondestructive Testing.* Wiley, 2001.

[144] Anton Du Plessis, Ina Yadroitsava, and Igor Yadroitsev. X-ray microcomputed tomography in additive manufacturing: a review. *Measurement Science and Technology*, 29(7):072001, 2018.

[145] Jon C Helton and Freddie Joe Davis. Latin hypercube sampling and the propagation of uncertainty in analyses of complex systems. *Reliability Engineering & System Safety*, 81(1):23–69, 2003.

[146] STEMINC. Piezo Ceramic Disc 20x0.2mm S 106 KHz (SMD20T02F106412S). https://www.steminc.com/PZT/en/piezo-ceramic-disc-20x02mm-s-106-khz, 2025. Accessed: 2025-05-26.